University of California
Los Angeles

Sensor Network Data Faults and Their Detection Using Bayesian Methods

A dissertation submitted in partial satisfaction
of the requirements for the degree
Doctor of Philosophy in Electrical Engineering

by

Kevin Song-Kai Ni

2008

The dissertation of Kevin Song-Kai Ni is approved.

Mark Hansen

Kung Yao

Mani B. Srivastava

Gregory J. Pottie, Committee Chair

University of California, Los Angeles

2008

To my parents.

Table of Contents

List of Figures

List of Tables

Acknowledgments

I would like to thank several people whose help and guidance were instrumental in writing this thesis. First and foremost, I would like to thank my advisor, Professor Greg Pottie. He has given me the opportunity and support for this to happen. I thank him for the faith and trust he put in me. His guidance and insightful advice has been invaluable to my success. With his patience and understanding nature, he created an environment within which I was able to learn and grow.

I would also like to thank Professors Mark Hansen, Mani Srivastava, and Kung Yao for their time and effort to be on my committee. Through classes, workshops, or just one-on-one conversations, each one has provided advice and direction for my work. Their influence cannot be understated in providing me the background and basis upon which this thesis is based. I thank Professor Hansen for his energetic guidance and direction for the statistical underpinnings of my work. I thank Professor Srivastava for his insightful tips and directions during meetings and workshops that helped to shape the direction of my work. I also thank Professor Yao whose teachings and guidance during my coursework was vital for several sections of my thesis.

Additionally, I'd like to thank everyone involved with the Data Integrity group. Most notably, Laura Balzano, Nabil Hajj Chehade, Sheela Nair, Nithya Ramanathan, and Sadaf Zahedi. Their assistance and input was important in helping me get to this point.

Finally, I'd like to thank Tom Harmon, Robert Gilbert, Henry Pai, Tom Schoellhammer, Eric Graham, Gaurav Sukhatme, Bin Zhang, and Abishek Sharma. They helped in providing me all of the data upon which all of this work is based.

Vita

1982	Born, San Diego, California, USA
2004	B.S. (Electrical Engineering), UCLA, Los Angeles, California.
2004	Intern, Intel Corporation, Santa Clara, California.
2005	M.S. (Electrical Engineering), UCLA, Los Angeles, California.
2008	Teaching Assistant, Electrical Engineering Department, UCLA, Los Angeles, California.
2005-present	Graduate Student Researcher, UCLA, Los Angeles, California.

Publications

Ni, K. and Pottie, G. (June 2007). Bayesian Selection of Non-Faulty Sensors. IEEE International Symposium on Information Theory (ISIT2007).

Ni, K., Ramanathan, N., Hajj Chehade, M.N., Balzano, L., Nair, S., Zahedi, S., Pottie, G., Hansen, M., and Srivastava, M. (2008). Sensor Network Data Fault Types. Accepted to ACM Transactions on Sensor Networks.

Abstract of the Dissertation

Sensor Network Data Faults and Their Detection Using Bayesian Methods

by

Kevin Song-Kai Ni

Doctor of Philosophy in Electrical Engineering

University of California, Los Angeles, 2008

Professor Gregory J. Pottie, Chair

The identification of unreliable sensor network data is important in ensuring the quality of scientific inferences based upon this data. Current sensor network technology for use in the environmental monitoring application frequently delivers faulty data due to a lack of an extensive testing and validation phase. Identification of data faults is difficult due to a lack of understanding of the faults and good models of the phenomenon.

Aided by of the large amounts of data currently available, we present a detailed study of the most common sensor faults that occur in deployed sensor networks. We develop a set of features useful in detecting and diagnosing sensor faults in order to systematically define these sensor faults.

We then present a system to detect these sensor network data faults. First we introduce a Bayesian maximum a posteriori probability method of selecting a subset of agreeing sensors upon which we model the expected behavior of all other sensors using first-order linear auto-regressive modeling. This method successfully selects sensors that are not faulty, but it has limited success in actual fault detection due to poor modeling of the phenomenon.

Then we explore the benefits of using hierarchical Bayesian space-time modeling over linear auto-regressive modeling in sensor network data fault detection. While this approach is more complex, it is much more accurate and more robust to unmodeled dynamics than linear auto-regressive modeling.

Finally we pair our method of selecting an agreeing subset of sensors with hierarchical Bayesian space-time modeling to detect faults. While this end-to-end Bayesian system requires a carefully defined model for the phenomenon, it is very capable of detecting sensor faults with a low false detection rate.

CHAPTER 1

Introduction

A sensor network is a connected network of sensing nodes distributed spatially to measure and monitor a physical phenomenon. Usually these sensors are networked via wireless communications and have limited processing, storage, and communication abilities [CES04] [PK00] [EGP01].

Sensor networks have enabled new ways of observing the environment. Scientists are now able to access vast amounts of data to draw inferences about environmental behaviors [CYH07]. But, as sensor networks mature, the focus on data quality has also increased. Since the sensor equipment is left exposed to the sometimes harsh environment, they may fail or malfunction during a deployment, leading to faulty data and bad inferences. Thus, it is important to ensure data integrity and identify when data is faulty.

There has been a large effort in ensuring the integrity of data communications in large distributed ad-hoc networks, e.g. [DPK04] [SP04] [Vog04]. However, none of these focus on the problem of the integrity of the data itself.

Many deployment experiences show that this is a major issue that needs to be addressed. For example, with the goal of creating a simple to use sensor network application, [BGH05] observes the difficulty of obtaining accurate sensor data. Following a test deployment, they note that failures can occur in unexpected ways and that calibration is a difficult task. Using this system, the authors of

[TPS05] deployed a sensor network with the goal of examining the micro-climate over the volume of a redwood tree. The authors discovered that there were many data anomalies that needed to be discarded post deployment. Only 49% of the collected data could be used for meaningful interpretation. Also, in a deployment at Great Duck Island, [SMP04] classified 3% to 60% of data from each sensor as faulty.

With such high data fault rates, it is difficult to draw meaningful scientific inferences. In addition, any scientific conclusion would have an elevated uncertainty associated with it due to the high rate of sensor data faults. Therefore, to reduce this uncertainty and to aid scientists, we have studied the most common faults and how they behave. With this understanding we then developed an effective system to detect these faults.

1.1 Background concepts

Before we delve into sensor network data faults, we first discuss some important background concepts that are the basis of our fault detection methods. Much of our work is based upon the application and use of Bayes' rule and the derivation of the posterior distribution. We also focus extensively on detection theory including the maximum a posteriori and Neyman-Pearson criteria. Finally, we frequently use linear autoregressive modeling as a general modeling approach.

1.1.1 Bayes' Rule

Our detection and modeling systems are based upon Bayesian inference and the use of Bayes' rule. We will summarize the important points that are used in this thesis, and a detailed presentation of Bayesian inference can be found in [GCS04].

To make an inference about a certain parameter θ given some observed data y, Bayes' rule is as follows:

$$p(\theta|y) = \frac{p(\theta)p(y|\theta)}{p(y)}$$

$p(\theta|y)$ is the posterior distribution for the parameter θ. This is the distribution from which we can make inferences regarding θ. The term $p(\theta)$ defined as the prior distribution for θ, and $p(y|\theta)$ is the likelihood. The normalizing term $p(y)$ can be computed by $p(y) = \sum_\theta p(\theta)p(y|\theta)$ for a discrete θ.

If we omit the normalizing term $p(y)$ which does not depend on the parameter θ, then we have the unnormalized posterior density:

$$p(\theta|y) \propto p(\theta)p(y|\theta)$$

The unnormalized posterior density is frequently used because it is easier to work with when deriving distributions.

The primary draw to using Bayesian analysis is the inclusion of prior distributions $p(\theta)$. This allows for systems to favor certain hypotheses over others. Or in our case, if a sensor is known to be faulty, it will have less weight in the prior distribution, thus decreasing the chances that it will be selected as being correct.

1.1.2 Posterior distribution simulation

The key to Bayesian inference is using the posterior probability distributions, $p(\theta|y)$, to draw conclusions about the parameter(s) of interest, θ. However, it is frequently very difficult to determine this distribution analytically, especially when θ is a high-dimensional parameter vector. Thus, computational simulation is the most feasible method of obtaining samples from the posterior distribution. We provide an introduction to this material for the purposes in this thesis, in depth information on MCMC and other methods of posterior distribution simu-

lation can be found in [GCS04].

In the cases where the posterior distribution is complicated and θ is a multi-dimensional parameter vector, we use Markov chain Monte Carlo (MCMC) simulation methods. The basic concept behind this method is that we draw values of θ from an approximate distribution. Based off of these draws, new samples are generated that better approximate the target posterior distribution.

One of the most popular types of MCMC algorithms is the Gibbs sampler which we use extensively. We divide the parameter vector θ into subvectors or subcomponents $\theta = (\theta_1, \ldots, \theta_N)$. For each iteration the Gibbs sampler draws a random sample for θ_i conditional on the most recent values of $\theta_1, \ldots, \theta_{i-1}, \theta_{i+1}, \ldots, \theta_N$. That is, at iteration t, we draw from the conditional distribution that is easy to derive and easy to sample from:

$$p(\theta_i^t | \theta_1^t, \ldots, \theta_{i-1}^t, \theta_{i+1}^{t-1}, \ldots, \theta_N^{t-1}, y)$$

After a number of initial iterations, the samples for each component of θ converge to the true distribution. Thus, after an initial period, each draw of the elements of θ is from the true distribution of $p(\theta|y)$. Selecting initial starting points of θ^0 may be difficult. To ensure accuracy, it is necessary that one choose several test starting points for θ^0 and check to see that the different samples for each starting point all converge to the same final distribution. A simple example of this is presented in chapter 11 of [GCS04].

1.1.3 Detection theory

In order to classify certain data as faulty or not, we use detection theory as the basis of our systems. Detection, or hypothesis testing, is the theory of determining the correct distribution from which given data is derived given a set of possible

probability distributions. We will provide an overview of this theory as it pertains to our problem. Detailed information can be found in [MW95].

The basic problem in detection theory is to determine at a receiver which one of two signals, s_0 or s_1, was sent by a transmitter. That is, if we observed a value x that is either $s_0 + n$ with probability p_0 or $s_1 + n$ with probability p_1 where n represents noise, how do we determine the original signal?

There are many approaches to the problem of detection, but we focus on two in particular. The first approach is to use the *maximum a posteriori probability* (MAP) criterion. Given the noise probability distribution, then we can calculate the probability distributions for $p(x|s_0)$ and $p(x|s_1)$. For example, if n is additive normal noise with variance σ^2, which we use frequently throughout this thesis, then $p(x|s_0)$ is a normal distribution with mean s_0 and variance σ^2. According to the MAP criterion, we decide that the original signal was s_1 if:

$$p(s_1|x) \geq p(s_0|x)$$

and we choose s_0 if:

$$p(s_1|x) < p(s_0|x)$$

We arbitrarily assign ties to favor s_1. One can use Bayes' rule to determine the posterior probabilities, $p(s_1|x)$ and $p(s_0|x)$, e.g.

$$p(s_1|x) = \frac{p(x|s_1)p_1}{p(x)}$$

When we correctly determine $x = s_1 + n$ when s_1 was sent, we call this a *detection* event. When we incorrectly determine that $x = s_1 + n$ when s_0 was sent, then we call this a *false alarm* event.

The second approach is to use the *Neyman-Pearson* criterion. The goal of this criterion is to maximize the probability of a detection event, P_D, while keeping

the probability of a false alarm event, P_{FA} below a predefined value, α. That is, we maximize P_D such that $P_{FA} < \alpha$. Given the noise distribution, we can work to determine a range of values for x to be decided as $s_1 + n$ that meets this goal.

Both of these methods rely on the assumption that the original signals s_1 and s_0 are known. However, in the field of sensor network data fault detection, one does not have access to the true original values. Without the true original values, the distributions from which we are deciding amongst are unknown. This lack of knowledge makes fault detection difficult. As we will see in the following chapters, the expected values for the phenomenon value can only be determined by a model. Unless artificially inserted, faults will never have a given expected value. In our detection systems, we will seek only to determine whether the measurement matches with our expected phenomenon value s_0, while labeling anything else as a fault, or s_1.

1.1.4 Linear Regression

Throughout this thesis, we use linear regression as a means of modeling data. This problem is also known more generally as a linear least squares problem. Detailed information on the formulation and methods of solving this type of problem are in [Lau05].

The linear regression problem as it pertains to our work here can be summarized as follows. Given a series of data points $(t_1, y_1), \ldots, (t_n, y_n)$, we want to fit the best line $y = at + b$ as defined by parameters a and b. The best line is defined by the best $\tilde{a}$ and $\tilde{b}$ that minimizes the sum of the square distances from the data points. That is we want to choose a and b that minimizes:

$$\sum_{i=1}^{n} (y_i - (at_i + b_i))^2$$

We can restate this problem into vector format where we define $y = \begin{bmatrix} y_1 \\ \vdots \\ y_n \end{bmatrix}$, $\mathbf{A} = \begin{bmatrix} t_1 & 1 \\ \vdots & \vdots \\ t_n & 1 \end{bmatrix}$, and $x = \begin{bmatrix} a \\ b \end{bmatrix}$. Then the problem becomes $y = Ax$, and to solve this we want to select the best x such that:

$$\min_x (Ax - y)^T (Ax - y)$$

There are many standard computational packages that can capably solve this problem efficiently. We use MATLAB's least squares solver in our work.

1.2 Contributions and Organization of Thesis

We make several contributions to the sensor network community.

- We provide a detailed study of sensor network data fault types and their underlying causes and features.
- We develop a maximum a posterior method for selecting a subset of non-faulty sensors.
- We introduce a new application of a Bayesian data modeling method to the field of fault detection.
- We develop an effective end-to-end Bayesian system to detect faulty sensor data.

This thesis is structured as follows. In chapter 2, we first present a detailed study of sensor faults that occur in deployed sensor networks and a systematic ap-

proach to model these faults. We begin by reviewing the fault detection literature for sensor networks in section 2.2. We discuss major system assumptions and issues facing fault detection system designers in section 2.3. We draw from current literature, personal experience, and data collected from scientific deployments to develop a set of commonly used features useful in detecting and diagnosing sensor faults presented in section 2.4. In section 2.5, we use this feature set to systematically define commonly observed faults, and provide examples of each of these faults from sensor data collected at recent deployments.

Chapter 3 presents a detection based method of identifying faulty and non-faulty sensors from a given set of sensors that are expected to behave similarly. We use a Bayesian MAP detection approach to select a subset of sensors which give the best probability of being correct given the data in section 3.3. This gives us a model from which we can determine whether sensors readings fall out of a reasonable range for the sensor set. In section 3.5, we apply our method to simulated data and real temperature data from a deployment at James Reserve in California and get mixed results.

In chapter 4, we resolve the modeling shortcomings of the method in chapter 3. After some preliminaries in section 4.2, we apply the hierarchical Bayesian space-time (HBST) modeling framework presented in [WBC98] to data fault detection in sensor networks in section 4.3. To show the effectiveness of HBST modeling, we develop a rudimentary tagging system to mark data that does not fit with given models in section 4.5. Using this, we compare HBST modeling against first order linear autoregressive (AR) modeling, which is used in chapter 3, by applying it to three sets of data in section 4.6. We show that while HBST is more complex, it is much more accurate than linear AR modeling as evidenced in greatly reduced false detection rates while maintaining similar, if not better

detection rates.

In chapter 5, we pair the HBST modeling technique with the subset selection process of chapter 3. First, in section 5.2 we refine and alter the assumptions on the system and the phenomenon made in previous chapters. We then detail the two phase end-to-end Bayesian approach to detecting sensor data faults in section 5.3. In the same section, we discuss many of the issues resolved by pairing the sensor subset selection method of chapter 3 with HBST modeling. Applying this end-to-end Bayesian system to the same data in as in section 4.6, we see much better gains in false detection while maintaining fault detection performance.

In chapter 6, we present our conclusions and suggestions for future research.

CHAPTER 2

Sensor Network Data Fault Types

2.1 Introduction

In order to make meaningful conclusions with sensor data, the quality of the data received must be ensured. While the use of sensor networks in embedded sensing applications has been accelerating, data integrity tools have not kept pace with this growth. One root cause of this is a lack of in-depth understanding of the types of faults and features associated with faults that can occur in sensor networks. Without a good model of faults in a sensor network, one cannot design an effective fault detection process.

In this chapter, we provide a systematically characterized taxonomy of common sensor data faults. We define a data fault to be data reported by a sensor that is inconsistent with the phenomenon of interest's true behavior. As discussed in chapter 1, faults are very common in sensor network deployments, and this impacts the ability of scientists to make meaningful conclusions. Examining the large amounts of data from sensor network deployments available at the Center for Embedded Networked Sensing (CENS) as well as other institutions, we have selected datasets that represent the most common faults observed in a deployment. We use these datasets as examples to support the selection and characterization of the faults.

By providing a list of the most commonly seen faults, the material presented

here can be utilized in several ways to make a sensor network more robust to faults. In the initial design stage of a sensor network system, the designer could account for and anticipate such faults so that negative impact of a fault can be reduced. When testing a fault detection system, because the faults presented here are the most common, they should be the first to be used in testing by injecting them into either simulated or real datasets. For a system that has been deployed, this list can be used as a first step to screen data for common faults and possibly fix sensors. Finally this list can be used to establish a standardized method of evaluating fault detection and diagnosis algorithms for embedded networked sensing systems.

In order to systematically define faults, we also present a list of the most commonly used features in practice to model both data and faults. We use the term *features* to generally describe characteristics of the data, system, or environment that can cause faults or be used for detection and be modeled. The models based upon these features describe either the expected behavior of the data or the typical behavior of a fault along a set of feature axes. We do not provide a full algorithm for use in detecting any particular fault. However, to show the utility of certain features, we will provide simple examples where they have proved to be useful in practice.

2.2 Prior and Related Work

Sensor faults have been studied extensively in process control [Ise05]. Tolerating and modeling sensor failures was studied in [Mar90]. However, studying faults in wireless sensing systems differs from faults in process control in a few ways that make the problem more difficult. The first issue is that sensor networks may involve many more sensors over larger areas. Also, for a sensor network the

phenomenon being observed is often not well defined and modeled resulting in higher uncertainty when modeling sensor behavior and sensor faults. Finally, in process control, the inputs to the system are controlled or measured, whereas in sensing natural phenomena this is not the case.

As sensor networks mature, the focus on data quality has also increased. As discussed in chapter 1, there are many deployment experiences that show that this is a major issue that needs to be addressed. Several works such as [BGH05], [TPS05], and [SMP04] have indicated the high rate of sensor faults. In addition, [WLJ06] takes a "science-centric" view and attempt to evaluate effectiveness of a sensor network being used as a scientific instrument with high data quality requirements. They evaluate a sensor network based upon two criteria, yield and data fidelity, and determine that sensor networks must still improve.

Now we examine several existing fault detection methods; we discuss the major assumptions and the fault models upon which the detection methods are focused. We also discuss some areas which may benefit from having a systematic fault definition. We see several features for specific faults that are defined that we will incorporate when defining our fault taxonomy.

[EN03] identifies two main sources of errors, systematic errors creating a bias, and random errors from noise, but focus on the latter. Identifying several sources of noise, they attempt to reduce the uncertainty associated with noisy data using a Bayesian approach to clean the data. The sensor noise model assumed is a zero mean normal distribution, and prior knowledge comes in the form of a noise model on the true data. With a more accurate real world sensor model, the sensor noise model and the prior noise model may be improved.

[DGM04] uses models of real-world processes based on sensor readings to answer queries to a sensor network for data. Using time-varying multivariate

Gaussians to model data, the authors respond to a predetermined set of query types, treating the sensor network like a database. To some extent this shields the user from faulty sensors. However, the authors point out that more complex models should be used to detect faulty sensors and give reliable data in the presence of faults.

Many of the recent fault detection algorithms have either vaguely defined fault models or an overly general fault definition. [KPS03b] briefly lists selected faults and develops a cross validation method for online fault detection based on very broad fault definitions. Briefly describing certain faults, the authors of [MPD04] target transient, "soft" failures, using linear auto-regressive models to characterize data for error correction. The errors are modeled as inversions of random bits which become the focus of local error correction. In [JAF06], the authors attempt to take advantage of both spatial and temporal relations in order to correct faulty or missing data. By defining temporal and spatial "granules," the authors require the assumption that all data within each granule are homogeneous. Readings not attributable to noise are considered faults.

Additionally, [EN04], [NP07], and [KI04] exploit spatial and temporal relations in order to detect faults using Bayesian methods. [EN04] introduces a method of learning spatio-temporal correlations to learn contextual information statistically. They use Markov models and assume only short range dependencies in time and space, i.e. the distribution of sensor readings is specified jointly with the readings of immediate neighbors and its own previous reading. The Bayesian approach is also evident in [KI04]. However, their sensor network model assumption of having massively over-deployed sensor networks is not applicable in the type of sensing applications we target. Also their fault model assumes any value exceeding a high value threshold is a fault, which may not always be the case.

In [NP07], it is assumed that sensors only need to be correlated and have similar trends, and a detection system based upon this assumption is developed. The authors use regression models to develop the expected behavior combined with Bayesian updates to select a subset of trusted sensors to which other sensors are compared. There is limited success in modeling mainly due to the lack of a good fault model and a good way of modeling sensor data.

An experiment involving sensors deployed in Bangladesh to detect the presence of arsenic in groundwater cites the importance of detecting and addressing faults immediately [RBB06]. The authors develop a fault remediation system for determining faults and suggesting solutions using rule-based methods and static thresholds.

A key source of error in sensor networks is calibration error. Sensors throughout their deployed lifetimes may drift, and it is important to correct for this in some manner. In [BGH05], calibration is performed offline before and after a sensor network deployment. The authors determine that calibration is a difficult challenge for future development. Both [BME03] and [BN07] suggest methods to perform calibration online while the sensor network is deployed without the benefit of any ground truth readings.

The initial work of [BME03] uses a dense sensor deployment with the assumption that all neighboring sensors should have similar readings. However, sensor networks in use do not have the type of dense deployment assumed in the paper. [BN07] removes this assumption and use the correlation between sensors to determine the calibration parameters of an assumed linear model. While both of these works have moderate success in applying their algorithms to actual data, they recognize that the lack of good knowledge of true sensor values is a major handicap.

Focusing on a single fault type, [SLM07] seeks to detect global outliers over data collected by all sensors. They estimate a data distribution from a histogram to judge distance based outliers. The authors have a well defined fault model based on distance between points.

[CKS06] uses a sensor network model that consists of a large, dense randomly deployed sensor network. The authors focus on three types of sensor faults: calibration systematic error, random noise error, and a complete malfunction.

Looking beyond fault detection and correction techniques, there has been relevant work that frames our thrust to provide a fault taxonomy.

Following sensor network deployments, both [SPM04] and [RSE06] explore likely causes for errors in data and node failures for their specific deployment context. While [SPM04] focuses mainly on communication losses, the authors also cite causes for abnormal behavior by certain types of sensors. [RSE06] focus on the specific case of a soil deployment where sensors are embedded at various depths in the soil monitoring chemical concentrations. The authors determine the specific hardware issues that caused the faulty data. Both of these works focus on the causes of abnormal data patterns in their respective applications but do not systematically characterize the resultant fault behavior.

Features for use in assessing data quality are explained in [MB02] and exploited in an urban drainage application in [BBM03]. The focus of these works is data validation using their defined features. We will expand on these ideas and move beyond their specific application in order to model all types of faults.

[SGG07] focuses on a small set of possible sensor faults observed in real deployments. Three types of faults are briefly defined, and different methods of detecting faults are examined. Then, three collected data sets from sensor deployments are analyzed to determine the efficacy of these fault detection methods.

We will more clearly define the faults presented and will generalize their definitions to more application contexts.

2.3 Data Modeling and Fault Detection

We first discuss some fundamentals of sensor network design and data modeling to put into context where one can utilize this fault taxonomy. There are two basic applications of sensor networks: environmental monitoring and event detection. In environmental monitoring, which is our primary focus, data is constantly collected and utilized in scientific or other applications. However, in event detection, one is only interested in detecting the occurrence a specific or an "interesting" event [GBT07].

While our primary focus is on environmental monitoring and the data collection involved, these faults and our framework are still applicable to event detection sensor networks. In the environmental monitoring application, a fault is anomalous data that exceeds normal expected behavior. In event detection, both events and faults present themselves as anomalous data that exceeds normal expected behavior. Thus, what is defined as a fault on our list, may characterize an event. To differentiate between a fault and and event, a training phase may be utilized to determine a model of a specific interesting event. Without such a model for events it is impossible to determine whether anomalous behavior is a fault or an event without human intervention.

In either application, better hardware and software can potentially reduce faults, but at greater financial or computational costs. Even when better hardware is available, this hardware will still likely produce faulty data if only because it can now be used in more challenging environments to answer more difficult

questions. For example, section 2.5.2.4 presents an example of a costly ISUS nitrate sensor in a controlled calibration environment that will produce unreliable data at higher nitrate concentrations.

2.3.1 System Assumptions

There are a wide variety of assumptions made on both the sensor network and the data for the fault detection algorithms in the presented literature. However, there are a few common assumptions to most of the systems that we will also make. The first assumption is that all sensor data is forwarded to a central location where the data processing occurs. This is conceptually simple and convenient because we do not require any type of distributed computing algorithm for statistical computations.

We recognize that local processing may occur to reduce overall communication costs. However, by the data processing inequality [CT91], with more local processing it is likely that less information is available at the fusion center, which may likely result in lowered confidence in fault decisions. Therefore, our discussion represents a best-case scenario, and we will not address the trade-off between decentralization and data quality loss.

The next assumption we make is that all data received by the fusion center is not corrupted by any communication fault. In order to keep things simple, missing data, which may be due to a communication error or not, is simply treated as data not collected and not as a sign of fault.

The alternate view of missing data as a sign of a sensor fault has merit in some cases. For example, when data is expected at regular intervals such as the heartbeat messages in [WLJ06], missing data can be a sign of a fault. However, as we are only concerned with data faults and since our datasets do not have any

instances of large gaps of missing data, we do not assume that missing data is a fault.

Finally, we also assume that we do not have malicious attacks on the sensor network system. While there has been much work on the security of sensor networks [SP04], this is beyond the scope of this work.

2.3.2 Sensor Network Modeling

Modeling data is the basis for all fault detection methods, and we emphasize its role here. All the work presented here on fault detection techniques employs models, and this is either explicitly stated or generally assumed. We define a model to be a concise mathematical representation of expected behavior for both faulty and non-faulty sensor data. A model may define a range within which data is expected to be, or it may be a well-defined formulaic model. A formulaic model should be able to generate simulated data and faults that behave similarly to the expected true phenomenon.

Data modeling is vital because, in the likely absence of ground truth, faults can only be defined relative to the expected model. By developing a set of models with which data is to be compared, data can be classified as either good data or as belonging to a particular type of fault. As we will see in section 2.3.3 and noted in [EN03], the models developed are heavily dependent on the sensor network deployment context and the phenomenon of interest as they can alter the interpretation and importance of certain faults.

Human input is a necessary component in modeling and system design, providing vital contextual knowledge for modeling expected behavior and faults. By selecting the features of importance to the application, humans are better able to incorporate contextual information into models than any automated algorithm.

If models do not fit the data within a given confidence level, human input can be used to create new fault models, validate unusual measurements, and/or update the accuracy of the models. The initial set of models may be incomplete; models may not be complex enough to capture features that humans did not notice before. However, as we learn more about the phenomena at the scales at which we are measuring, our models will be updated and improved. As such, the need for human involvement should decrease, but never disappear, as the system develops.

2.3.3 Fault Detection System Design

This list of faults can be utilized in several ways when designing a fault detection system as they serve as a basis of what to expect in a real deployment. These faults and features can be incorporated into a fault detection system to more accurately identify faulty data. To test the efficacy of a detection system, faults may be injected into a test data set. As our list provides for the most common faults in a sensor network, the listed faults can be the first ones to be tested.

When analyzing data from a deployed sensor network, anomalous data can be first checked against this list of faults in an automated manner to eliminate the simple cases and simple causes. This reduces the workload for data users by leaving unclassified anomalous data for analysis, e.g. in updating the fault models.

The application for which the sensor network is being used and types of sensors used play an important role in the design of a fault detection algorithm. Assumptions for one application or sensor may not hold true in another, e.g. the day to day variations for soil CO_2 concentrations of figure 2.7 are not expected to be the same as the light intensity of figure 2.12. Because of this, there is generally

no single module that can detect a particular fault regardless of sensor type.

The most common major classes of sensors that have been used extensively in environmental monitoring deployments are temperature, humidity, light (including photosynthetically active solar radiation sensors), and chemical. There are other sensor types that are used more for event detection that are not covered here, e.g. seismic and acoustic sensors. The faults listed are very generalizable to different classes of sensors because each fault can potentially occur on any sensor type. Some sensors that will be more likely to exhibit certain faults than others. While sensor class plays a role in the frequency of faults, sensor specifications are a major influence on the frequency of faults.

2.4 Sensor Network Features

Features is a general term we use to describe characteristics of the data, system, or environment that can cause faults or be used for detection of faults. To systematically define and model faults, we detail a list of features that have been commonly used and presented in the literature. From this list, we select features that are most relevant to each particular fault. These features will also be used to better understand the underlying causes for faulty behavior. While not an exhaustive list of all possible ways to describe data, it is sufficient for sensor network data in particular.

To systematize our taxonomy, we categorize features into three classes, also referred to in [MB02]: *environment features* derived from known physical constants and expected behavior of the phenomenon, *system features* derived from known component behavior and expected system behavior, and *data features*, usually statistical, calculated from incoming data. All three of these feature types are

interdependent and influence each other. For example, [SPM04] discusses how the environmental effect of rain may cause a short circuit on the sensor board that manifests itself in the data with abnormal readings.

Dependent upon the context of a feature description, *features* can be the cause of the fault, can be used to describe or identify a fault, give the context of a fault, or define the location of a fault. We will clarify how the term *feature* applies in particular contexts.

One feature that is not listed in the categories below is time scale. Modeling the expected behavior over only recent data samples, i.e. windowing, is done frequently in the literature for online detection systems. Because the duration of the fault has bearing on its detection and diagnosis, the window size for time-dependent features such as the moving average should be selected according to the sensing application. The window size may be selected from human expertise or by optimizing a specific model quality metric such as mean square error as in [NP07], though this may involve a computationally intensive search among all possibilities.

For each feature class, we provide a table defining and summarizing each feature within that class. We also provide additional details of each feature with some examples and how some can have an effect on faults or fault detection in the accompanying text.

2.4.1 Environment Features

Environment features, or context, contribute greatly to models for expected behavior and fault behavior by describing the context in which a sensor is placed. Aside from sensor location, environmental features are mostly out of the control of the sensor network operator. These features are defined in table 2.1 with

Table 2.1: Sensor Network Environment Features

Feature	**Definition**	**Examples of Features or Use**
Sensor Location	GPS location, (x,y,z) coordinates, or other system of identifying location.	Critical for use in determining spatial correlation.
Constant Environment Characteristics	Describes the context in which the sensor is deployed.	Examples: soil type, liquid environment, or sensor packaging.
Physical Certainties	These features are based upon the natural laws of science.	Can be used to define a fault. Examples: Temperature has a minimum of 0 Kelvin. Relative humidity does not exceed 100%.
Environmental Perturbations	These are contextual features are not constant throughout the deployment lifetime.	Examples: Weather patterns, rain, or irrigation events.
Environmental Models	Models of the phenomenon behavior as defined by experts and computed from the data.	Examples: Expected rate of change or micro-climate models.

examples of the feature or how the feature may be used.

Environmental features will always play a dominant role in the type and prevalence of faults because they play a significant role in determining expected behavior. This expected behavior in turn determines faults. All environmental features give context to a fault. Also, there may be uncertainty associated with some of these features, e.g. in the effects on the data by perturbations, or in the environmental models. Thus, we use confidence intervals to define the expected range of values.

2.4.1.1 Physical constants

These are constant factors that are not expected to change throughout the lifetime of the sensor deployment. This is made up of *sensor location*, *constant environment characteristics*, and *physical certainties*. As an example of a constant environment characteristic which may lead to faulty data, [SPM04] suggests that since their sensor packaging was IR transparent, a mote would heat up in direct sunlight and report higher than expected temperatures.

Physical certainties are also known as the physical range in [MB02]. An example of such a bound being exceeded is in [TPS05] where the authors removed outliers that exceeded the physical possibility of 100% relative humidity.

2.4.1.2 Environmental perturbations

Environmental perturbations can be used to explain the causes of aberrant behavior. The effect of the environment has been noted to affect sensors in both [SPM04] and [EN03]. For example, weather patterns and conditions may affect sensors in adverse ways. Rain can cause humidity sensors to get wet and create a path inside the sensor power terminals, giving abnormally large readings [SPM04].

Environmental perturbations can also be leveraged in the modeling of expected behavior. For example, in [RBB06], irrigation events that influence the concentration of chemical ions in soil are expected on a regular basis. By incorporating the prior knowledge of how the concentration should change due to irrigation, one can increase the accuracy of any type of model developed.

2.4.1.3 Environmental models

Environmental models are crucial in defining expected behavior of a phenomenon. The quality of the model in turn greatly affects performance of fault detection algorithms. For example, in the cold air drainage experiment described in [NP07], temperatures are not expected to be homogeneous at the different sensor locations. If the authors had a model of the degree to which temperatures differed between each sensor, then it would have increased the fault detection ability.

2.4.2 System Features and Specifications

We now discuss features specific to individual sensors and features involving the overall sensor network; these may influence any model developed for behavior of the sensor network. We summarize the feature definitions and their significance as related to faults in table 2.2.

First, we examine features of individual sensors before moving to features of the sensor network which we can split into two general types. Sensor hardware features describe the components and abilities of a sensor, while calibration describes the uncertainty of the mapping from input to output.

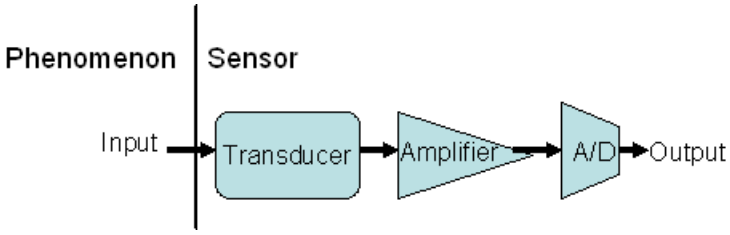

Figure 2.1: Diagram of a sensor and key components

Table 2.2: Sensor Network System Features

Feature	**Definition**	**Significance**
Transducer	The interface of sensor with the environment. Takes measurements of the phenomenon and produces a voltage output.	The reliability varies greatly dependent on sensor type. Transducer element is the component that is calibrated.
Analog-to-digital converter (ADC)	Maps the analog voltage signal into a range of discrete values.	The ADC may limit the ability to detect features above or below the maximum or minimum ADC value.
Total detection range ($R_{detection}$)	Defines the transducer input-output curve regions. This is the overall range of values for which a sensor had been tested and calibrated.	Mapping may change over time due to sensor drift (section 2.5.2.1)
Interval of confident operation ($R_{confident}$)	The range of output values that can be confidently translated into input values.	Statistically determined bounds give a user defined confidence level.
Saturated interval ($R_{saturated}$)	Complimentary to $R_{confident}$. This range of output values cannot be reliably related to one input value with low uncertainty	This range defines the environment out or range fault (section 2.5.2.4).
Sensor Age	Length of time sensor is deployed and actively monitoring.	Components can be expected to degrade over time.
Battery State	Amount of energy left in the battery relative to the minimum operating power required for sensor operation.	Low batteries can cause erratic, noisy, and/or unreliable measurements if any.
Noise	Random unwanted variation in data.	Causes uncertainty in data.
Sensor Response Hysteresis	Delay in sensor response to a change in the phenomenon.	Phenomenon may be captured incorrectly.
Sensor Network Modalities	Sensing tools that measure different but related phenomenon.	Can be leveraged to increase fault detection performance.

2.4.2.1 Hardware components

Figure 2.1 is a diagram of a typical sensor and the flow of data through major components. These features describe the location where a fault may occur. Associated with each of the components are certain static limiting features, which may be defined by specifications, that may impact resulting data. However, as the sensor user does not have access to internal signals, we will only discuss the two most pertinent components: the *transducer* at the input at and the *analog-to-digital converter* at the output.

An example of the transducer affecting sensor reliability is in ion selective electrode sensors. These sensors deployed in soil feature a chemically treated membrane that is not very robust and frequently fail in a deployment [RBB06]. As noted in table 2.2, the analog-to-digital converter limits the detection ranges, and this plays a defining role in the clipping fault in section 2.5.2.5.

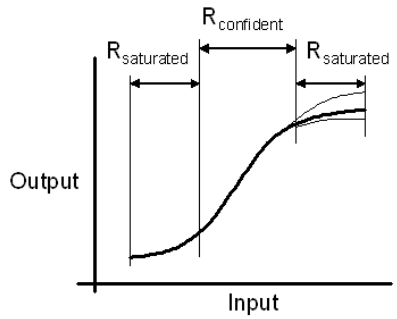

Figure 2.2: Input-Output curve of a typical sensor.

2.4.2.2 Calibration features

Calibration may be necessary to increase the accuracy of the sensor since factory calibration conditions may not always be relevant to conditions in the field. When referring to calibration, it is the transducer response that one calibrates,

assuming there is no clipping by the analog-to-digital converter. Figure 2.2 is a general input-output calibration curve, similar to that of [RSE06] and [Run06]. Calibration features are used to describe faults.

The *total detection range*, $R_{detection}$, is comprised of the *interval of confident operation*, $R_{confident}$, and *saturated interval*, $R_{saturated}$. The $R_{confident}$ is usually linear and should consist of one-to-one mappings of output values to input values. Depending on the type of sensor, there may be different degrees of variability outside the interval of confident operation. The ISE chemical sensors exhibit a "flattening" in the data outside of $R_{confident}$ [Run06], while as we will see later, the ISUS nitrate sensor will exhibit higher output variance with larger input values.

2.4.2.3 Other system features

In addition to the sensor component specific features, there are higher level features of a sensor and sensor network that may be incorporated into a fault detection system model.

Sensor age can influence the reliability of a sensor. For example, the treated filtering membrane for a chemical sensor wears out over time giving faulty data. Similarly, *battery life* is seen to give unreliable measurements in [SPM04], [RBB06], and [SGG07].

Noise can be modeled using a probability distribution, such as a Gaussian. While not always completely accurate, the Gaussian noise assumption is convenient to work with. An example of *sensor response hysteresis* affecting data quality is given in [BME03]. In an experiment measuring temperature of a heat source moving across a table, thermocouples have a slow response relative to the velocity of the heat source.

Different *sensor network modalities* can be leveraged to model sensor network behavior for fault detection. For example, humidity and temperature measurements should be correlated since the two affect one another. If the two do not correspond to the correlation model, then a fault has likely occured. The use of different modalities has been mentioned in [SPM04], [WLJ06], and [BGH05].

2.4.3 Data Features

Data features are usually statistical in nature. A confident diagnosis of any single fault may require more than one of these features to be modeled. We cannot provide a complete list of possible features and tools that can be used, but the included features are commonly exploited and simple to implement. These features are usually calculated in either the spatial or temporal domains. Data features are primarily used to describe or identify faults. We provide examples of where these features have been used in literature, and table 2.3 summarizes the usage of these features.

As discussed previously, features are commonly calculated or modeled over a window of samples. Windowing may be done over the temporal domain or over space by selecting sensors that are expected to retain similar characteristics, usually colocated or nearby sensors.

The *mean* and *variance* are commonly exploited basic statistical measures. Means and variances can be calculated in a moving average context, as in [MB02] for data smoothing. [JAF06] uses the mean across both temporal and spatial windows to correct for faulty sensor values. The variance or standard deviation is also a measure of the reliability of a sensor, since high variance is often a sign of faulty data, [SGG07].

In a sensor network, data is expected to be *correlated* in both the spatial

Table 2.3: Sensor Network Data Features

Feature	**Usage in fault modeling.**
Mean and Variance	The mean and variance can be used to determine expected behavior via regression models or correcting faulty sensor values. Variance also is a measure of reliability.
Correlation	Assumed or stated spatial or temporal correlation models are required for regression methods to have meaningful use.
Gradient	Rate of change on different scales, e.g. over 10 minutes or 24 hours etc, can be used in modeling faults.
Distance from other readings	Distance between data is used to directly or indirectly to determine if data is faulty.

domain and temporal domain for sensor networks. This correlation can be vaguely defined as in [NP07], [JAF06], and firmly defined probabilistically as in [EN04]. Spatially, [BN07], as well as the previously mentioned works, seek to exploit correlation models to improve sensor network performance.

The *gradient* is exploited in [SGG07] and [RBB06] for fault identification. The scale selection over which the gradient is calculated is a nontrivial task and will depend on the type of phenomenon being observed. If the phenomenon is slow moving, such as temperature, the scale may be longer than a highly varying phenomenon, such as wind velocity.

To use the *distance from other readings* indirectly, one would compare data with a model of expected behavior, which may be as simple as the mean from nearby sensors or recent data values as in [JAF06]. To use such a feature, one may use static thresholds as in [RBB06] or thresholds based upon an estimated probability distribution and confidence level as in [NP07].

There are many more statistical techniques, spatio-temporal and otherwise, that have been used to model sensor data, but not in the context of fault detection. Gaussian processes have been used to model the environment for sensor

placement [KGG06]. Additionally, other methods such as Kriging and variograms may prove useful in future works.

Data features are commonly employed to identify faults in fault detection algorithms. It is useful to combine data features for detection of certain faults. For example, in section 2.5.1.1 variance and gradient are given as examples for detection of outliers. As mentioned previously, the time scale over which a fault detection method evaluates data plays a critical role in determining how useful a particular data feature is effective. Also, the usefulness of a particular feature is dependent on the type of fault. The most useful features for each fault are summarized in tables 2.5 and 2.6.

2.5 Faults

With the feature list in place, we now define the most common faults observed in a sensor network. Faults carry different meanings as to their ultimate interpretation and importance. Depending on the context and sensor network application, some faults will still have informational value, while others are totally uninterpretable and the data must be discarded. We will point out examples of this grey scale interpretation of faults and summarize the impact in table 2.7.

Unless ground truth is known or given by something with high confidence, the term fault can only refer to a deviation from the expected model of the phenomenon. When defining a fault, there are two equally important approaches, and it may be easier to describe a fault using one approach over the other. Frequently there may not be a clear explanation as to the cause of a fault, e.g. outliers, and hence it may be easier to describe this fault by the characteristics of the data behavior. This is the "data-centric" view for classifying a fault and

Table 2.4: Relating system view and data view manifestations.

Data-centric fault	**System view fault**
Outlier	
Spike	Connection/Hardware Low Battery
Stuck-at	Clipping Connection/Hardware Low Battery
Noise	Low Battery Connection/Hardware Environment out of range
	Calibration

can be seen as a diagnostic approach. The second method, a "system view," is to define a physical malfunction, condition, or fault with a sensor and describe what type of features this will exhibit in the data it produces.

These two approaches are not disjoint and can overlap. A fault defined using one approach can usually be mapped, as depicted in Table 2.4, into one fault or a combination of faults defined using the other approach, and vice versa.

For each fault, we will provide examples and discuss the features that are most relevant for modeling the faults, and provide examples of how to model each fault. Where appropriate we will discuss the effect of the time scale and how human feedback can improve modeling for systems, thus reducing system supervision. Also when possible we will discuss the overlap between the system and data-centric views. In certain cases we discuss the interpretation and importance of the fault in question. As we do not seek to design or promote any particular fault detection algorithm, we only present very simple illustrative examples of how such fault models may prove useful in practice.

2.5.1 Data-centric view

We first examine faults from a data-centric view where we determine a fault based upon data from a sensor. Data-centric faults may or may not be reproducable depending on the cause.

2.5.1.1 Outliers

Outliers are one of the most commonly seen faults in sensor data. We define an outlier to be an isolated sample, in the temporal sense, or a sensor, in the spatial sense, that significantly deviates from the expected temporal or spatial models of the data which are based upon all other observations. The temporal version of an outlier has been classified as a SHORT fault and subjectively described in [RBB06] where the fault is subjectively described. Outlier detection is not new, as this issue has existed for a long time [HA04]. More recently [SLM07] has the primary focus of outlier detection in sensor networks.

We provide an example in figure 2.3 where there are clear outliers in the data. This example only considers temporal outliers, but methods described here can easily be translated to spatial outliers such as in figure 2.6(a). Figure 2.3 is humidity data in the form of raw output of the sensor (which can be converted to relative humidity percentage) [KPS03a] [NIM07]. Two of these outliers have been inserted by software declaring a communication issue (indicated by a -888) or a data-logger problem (indicated by a -999). While some of these outliers have known causes, many other outliers are completely unexpected.

To model an outlier, the most common features to consider are distance from other readings as in [SLM07] and gradient as in [RBB06]. As defined, we must first model the underlying expected behavior. For the purposes of demonstration we

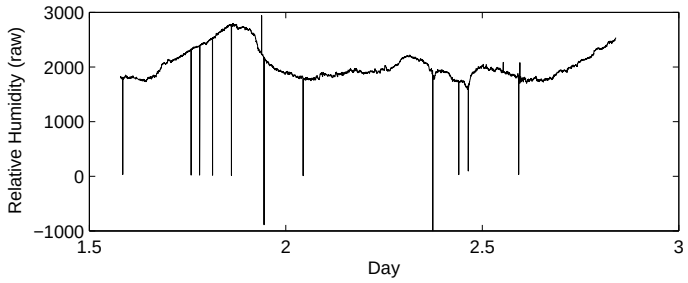

Figure 2.3: Raw humidity readings from a NIMS deployment with examples of outliers

will use simple methods of determining the expected range based upon previous data sample points.

Contextual information about the phenomenon and sensor plays a larger role in this fault since we are modeling expected behavior in an effort to identify outliers. As this is humidity data, we assume, based on an environmental model assumption, that this phenomenon does not change rapidly. One can better define this environmental model in a mathematical form to describe expected rate of change or other aspects of the data, however this is beyond the scope of this chapter. This model assumption is the basis for the window size selection and how we model the expected behavior.

We pick one particular outlier, at $(2.044, 8.469)$, to examine and model the first feature of distance. We define features to be based upon the previous 75 samples, or approximately half an hour as we do not expect humidity to change much over this time. A homogeneous data assumption allows us to define the expected model using the sample mean and variance features. We define the 95% confidence interval to be the expected range, and anything outside of this can be considered an outlier. Other possible modeling measures include the median and quartiles, regression models, and other more complex models.

After modeling the previous half hour before the sample point in question, we determine a sample mean of 1817.7 and a standard deviation of 14.923 resulting in a confidence interval of $[1787.9, 1847.6]$. The sample point being considered is compared to this, and anything outside this expected range will be marked as an outlier, e.g. $(2.044, 8.469)$.

One can apply similar techniques for developing a confidence interval for the gradient feature. By modeling the mean absolute point-to-point change or using a first order linear regression to estimate the gradient one can construct a confidence interval for the gradient and identify outliers.

The selection of the window here affects the accuracy of the very basic models developed for the expected behavior. The homogeneous assumption is less accurate as the window size is increased. On the other hand, using smaller window sizes can lower the accuracy of the model as less data is used for modeling. Developing more complex models of the expected behavior diminishes the influence of window size for outlier detection.

Outliers are most commonly not very informative, and hence can usually be discarded, e.g. [TPS05]. The effect of keeping the outlier in the data set can significantly alter the model and allow for more missed detections since any new model may be based upon faulty data.

2.5.1.2 Spikes

We define a spike to be a rate of change much greater than expected over a short period of time which may or may not return to normal afterwards. It is a combination of at least a few data samples and not one isolated data reading as is the case for outliers. It may or may not track the expected behavior of the phenomenon. While it may not always be a fault, it is anomalous behavior and

thus should be flagged for further investigation.

As [MB02] suggests, determination of spikes must be based on environmental context and models of the physical phenomenon. For example, light data in figure 2.12 can experience sudden and large changes in gradient, however in this context, this cannot always be judged to be a fault since light is a phenomenon that can give large gradients. By contrast, in the example that follows in this section, a spike is not expected to occur in this soil concentration application.

Good models, improved by human knowledge, of the phenomenon will allow for proper distinction in cases of uncertainty. Similarly, context and environmental models will dictate the time scale judged to be "a short period of time."

We look at an example from a deployment in Bangladesh as described in [RBB06] and [RSE06]. Figure 2.4 is the concentration of ammonium reported at one sensor location. There are two examples that we define as spikes. The first example occurs at the time frame 1.3805 to 1.3875 days over the four data samples and returns to normal behavior. The second example occurs between 7.8607 to 9.511 days and persists for a while.

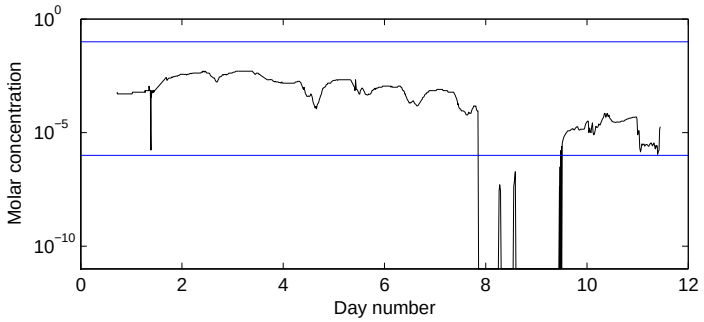

Figure 2.4: Concentration of ammonium reported in a deployment in Bangladesh. The horizontal lines indicate the range for which this sensor has been calibrated and measured, $R_{detection}$.

By definition, the primary feature for modeling is temporal gradient. Other data features that may be useful for detection are mean and temporal correlation. We will first discuss temporal gradient.

One method of modeling a spike is to determine an expected range for the gradient by modeling local rate of change across a window size using a regression or another model. Then, one can construct a confidence interval about this range similar to that of the outlier case. A spike can then be modeled as having a gradient larger than the confidence interval.

For an example, we use the first spike between time frame 1.3805 to 1.3875 days. We use a first order regression to model the expected gradient of the log of the data to be 7.0518 using data from the previous hour. The beginning of the spike itself has a gradient of -729.11, which is outside of any reasonable confidence interval around the expected gradient. Hence, if one were to generate a model for a spike, one would create a set of data that has a gradient much higher than expected.

Next, we look at temporal correlation. If one has an assumption that sensor values are expected to be correlated to some degree, as is usually the case in sensor data, then this feature may prove useful. That is, if we expect some linear correlation, one can calculate the correlation for the data. In the data prior to the 7.8607 spike, the correlation coefficient is 0.46536. However, as we expect, there is a drastic drop in correlation to -0.44338 once the spike is introduced into the data which signals that there is an anomaly.

Additionally, [MB02] uses the mean data feature and calculates a moving average to smooth data. A spike would then be defined by having the residue between the data and the moving average exceeding a defined threshold or confidence interval.

2.5.1.3 "Stuck-at" fault

A "stuck-at" fault is defined as a series of data values that experiences zero or almost zero variation for a period of time greater than expected. The zero variation must also be counter to the expected behavior of the phenomenon. The sensor may or may not return to normal operating behavior after the fault. It may follow either an unexpected jump or unexpected rate of change. The data around such a fault must exhibit some variation or noise for one to detect this fault since variation is the distinguishing characteristic of the fault.

While similar to the "CONSTANT" fault in [SGG07] and [RSE06], we differ in that the value in which the sensor may be stuck may be within or outside the range of expected values. In cases where the stuck at value is within the expected range, spatial correlation can be leveraged to identify whether the stuck sensor is faulty or functioning appropriately.

By definition, the primary feature to consider modeling is variance. Spatial correlation can also be considered especially when the stuck-at fault occurs inside the range of expected values for the phenomenon.

Human input can initially define the length of time, i.e. time scale, for which a sensor is stuck before it is considered to be a "stuck at" fault based on the sensing context and the expected variability of the readings. If little variability is expected, there should be greater tolerance for having very little variation for a greater period of time. With further development, this can be incorporated into a model and the human involvement can be reduced.

Figure 2.5 shows the chlorophyll concentrations from two buoys in a deployment at Lake Fulmor monitoring the marine environment [NAM06]. This data exhibits little variation after two unexpected changes in gradient. The flat tops

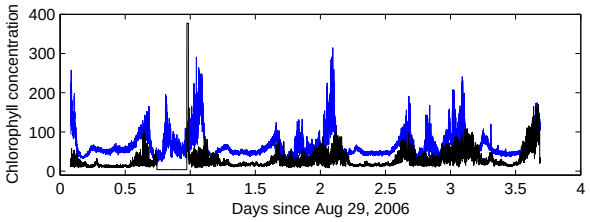

(a) Nodes 102 and 107

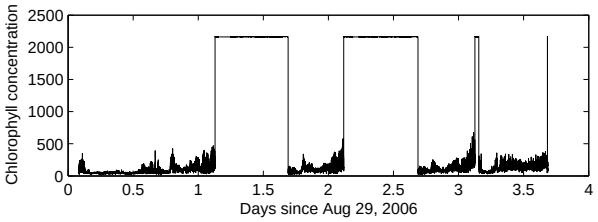

(b) Node 103

Figure 2.5: Chlorophyll concentrations from NAMOS nodes 102, 103, and 107.

of the chlorophyll concentration for node 103 in figure 2.5(b) indicate that there has likely been a stuck at fault. Furthermore, there is little or no variation at those samples near that value. For example, we calculate the variance of the data in a half day window preceding the first "stuck-at" instance to be approximately 4712. The variance of the entire first "stuck-at" instance is approximately 1.7. While this is not 0, further analysis of the data shows that there are large pockets of time during this instance where the variance is zero, and the only variation is that the sensor values vary only slightly outside these pockets. Similarly, for sensor node 107 in figure 2.5(a), the period between days 0.74 and 0.974 has an overall variance of 0.000007, with large pockets of 0 variance. The data prior to this period has an overall variance of 85.3.

To ensure that only the sensor is behaving in such a manner and it is not the phenomenon, especially in cases where precision is low and the fault occurs within the expected range, spatial correlation can be leveraged to increase confidence in detection. If there is a model indicating there should be correlation between two

sensor locations for the data or variances, then spatial correlation can be used to determine whether or not a "stuck-at" fault is actually a fault. In figure 2.5(a) we can see that sensor 102 does not exhibit the fault that sensor 107 has. Since the two sensors are expected to be correlated, which is the case for times outside of the fault, we can reasonably conclude that sensor 107's data is faulty.

Alternatively, light data in figure 2.12 exhibits a "stuck-at" fault within the expected range of the phenomenon indicating clipping. However, high spatial correlation among the sensors suggests that this is normal behavior, and the sensor is not actually malfunctioning.

Data from a "stuck-at" fault may not always be thrown away as sometimes the data may still provide some information concerning the phenomenon. In the case of sensor clipping in the light data, the "stuck-at" fault still identifies that the light is at least greater than or equal to the reported value. However in the NAMOS data presented in this section, data may be discarded as there is no useful interpretation.

2.5.1.4 High noise or variance

While noise is common and expected in sensor data, an unusually high amount of noise may be a sign of a sensor problem. Unusually high noise may be due to a hardware failure or low batteries, as in sections 2.5.2.2 and 2.5.2.3. We define a noise fault to be sensor data exhibiting an unexpectedly high amount of variation. The data may or may not track the overall trends of the expected behavior. This fault is also presented in [SGG07], but we emphasize that the noise must be beyond the expected variation of the phenomenon and sensor data.

As defined, the primary feature of interest is the variance. Spatial correlation of data and/or the moments of the data also may also be useful in judging the

nature of the fault.

We provide examples of a high noise fault from data collected from the cold air drainage deployment. In figure 2.6(a) we plot data from three nearby sensors from a cold air drainage deployment in March 2006 [CAD07]. One sensor is clearly faulty and has a considerable amount of noise in addition to the spatial outlier behavior. Also in the cold air drainage data of figure 2.6(b), there is one sensor that has a high amount of noise, yet still tracks the data. Unlike figure 2.6(a), this data tracks the expected behavior of the phenomenon.

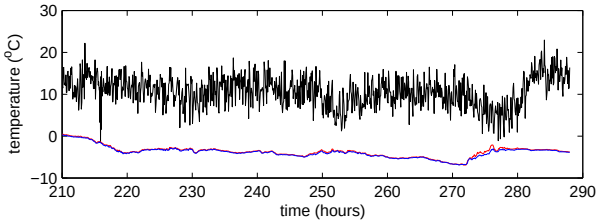

(a) CAD data from three nearby sensors

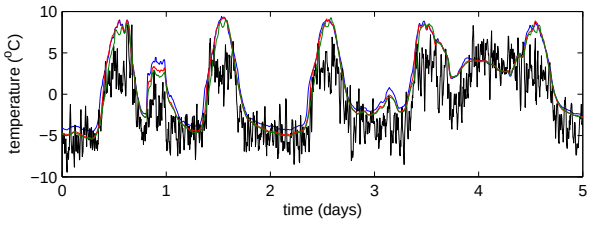

(b) CAD data with one noisy sensor tracking three others

Figure 2.6: Cold air drainage temperature data from two different time periods.

The initial selection of proper window size within which to model data and calculate the variance is dependent on modeling assumptions. If modeling similar to the regression model in [NP07] were used to estimate the variance around the expected value, then a larger window size may prove to be more accurate in estimating the sensor variance. However, if sensor variance is directly computed, a large window may produce an artificially high variance due to natural variations

in the phenomenon, e.g. diurnal patterns in the figure 2.6(b).

The expected variance of the sensor readings is given by either a data sheet of the sensor, model of other similar sensors, environmental understanding, or past behavior of the sensor in question. If the environment is expected to have a high variance, then this may not be considered a fault.

In the case of the cold air drainage data, an expected range for the variance can be based upon the other sensors. The variance of a sensor experiencing a noise fault should exceed this expected behavior.

Correlation across sensors of the moments (2nd or higher) of the data or variance features may also be leveraged to increase detection for data expected to have high variability. If a particular sensor has unexpected variability, and another nearby sensor also has high variability on the same scale, then it is less likely that a fault occurred. However, if there is no correlation in variability then it is more likely that a fault has occurred.

Examining the data in figure 2.6(a), we perform a rough estimate of the variance over an approximately 2 hour moving window. With this we examine the correlation, or covariance structure of the variance. Taking the overall pairwise linear correlation between each sensor, we find that the correlation between the two reliable sensors' variances is 0.6 indicating that these two sensors are correlated. The pairwise correlations of the variances between the reliable sensors and the faulty sensors are 0.1 and 0.2 indicating that the faulty sensor variance is not similar to the other sensors' variances.

Noisy data may still provide information regarding the phenomenon at a lower confidence level. Therefore, if the noisy data tracks the expected behavior as is the case in figure 2.6(b), then it should not necessarily be discarded. Data from figure 2.6(a) may be discarded as this is also a case of a spatial outlier.

2.5.2 System-centric view

We give general reasons for a sensor failure and detail how a sensor might behave with a certain fault with examples from real world deployments. Also, monitoring certain aspects of the hardware, such as battery life, may aid in understanding when a fault may occur.

2.5.2.1 Calibration Fault

Calibration problems can be a root cause of faulty data in many cases. Many papers cite the difficulty in calibration, especially while the sensor network is deployed [BGH05] [BME03] [BN07] [RSE06]. The result of calibration errors is that one gets a lower accuracy of sensor measurements but not necessarily lower precision. We discuss three different types of calibration errors which are named in the previously cited works:

- Offset fault - Sensor data values are offset from the true phenomenon by a constant amount. The data still exhibits normal patterns over an extended period of time.
- Gain fault - The rate of change of the measured data does not match with expectations over an extended period of time. That is, whenever the phenomenon changes by any amount, Δ, then the sensor reports a change of $G * \Delta$, where G is a positive real value.
- Drift Fault - Throughout a deployment of a sensor, sometimes performance may drift away from the original calibration formulas. That is, the offset or gain parameters may change over time.

Because these errors may be combined in several ways, calibration errors can manifest themselves in many different ways. In many cases, this makes detection and modeling of general calibration errors difficult without human input or ground truth. Even with human input, when lacking ground truth it may be difficult to differentiate between mis-calibration and natural phenomenon variations.

While calibration errors are defined relative to ground truth, without ground truth, calibration faults can only be determined relative to an expected model. This model can be a predefined model, a model generated from correlated sensors, or a combination of both. The predefined model is based upon environmental context which may include micro-climate models. Spatial correlation is important for generating the expected model when lacking ground truth, as is exploited in [BME03] and to some extent [BN07].

We present an example of what can be considered a calibration fault in figure 2.7 presented in [RSE06]. One of three sensors monitoring carbon dioxide concentration at various levels within the soil exhibits unusual sensor readings when compared to the other sensors.

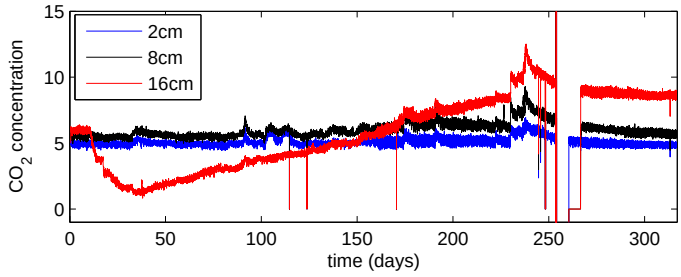

Figure 2.7: CO_2 soil concentration at three different depths at a deployment in James Reserve. The sensor at 16cm has some calibration issues.

The sensor at 16cm is clearly not measuring what is expected for the majority of the time, however while accuracy has changed, precision has not. There are

also some similarities with the other sensors and exhibits. For example there is a common spike in all three sensors prior to day 200. There is also a drift fault, since the offset changes with respect to time. Also, eventually the sensor returns to normal operation.

The data of figure 2.12 in section 2.5.2.5, presents another example of calibration error. While not as serious as the previous example, the lowest value of the "floors" differ when it is expected they report the same values. Hence, this slight difference is a sign of what is likely an offset fault.

Faulty data due to calibration issues still provides useful insight about the phenomenon and should not be readily discarded. If a proper calibration formula were to be developed, it is possible that the data may be corrected with acceptable confidence.

2.5.2.2 Connection or hardware failures

Frequently sensors may fail due to hardware problems such as poor connections. This is a general feature category since it is not possible to characterize all possible sensor failure modes. Typically, hardware failures require either replacement or repair of a sensor. This is one of the more common issues that may arise in a sensor deployment and has been cited as a cause of sensor failures in [SPM04], [RBB06], and [SGG07].

A connection or hardware fault will often manifest itself by reporting unusually high or unusually low sensor readings. These readings can even occur outside of the feasible environmental range. For example humidity outliers were discarded when the relative humidity exceeded physical possibilities in [TPS05].

One cause of hardware faults is weather or environment conditions. [SPM04] cites water contact with temperature and humidity sensors causing a short circuit

path between the power terminals as the cause for abnormally large or small readings. Including weather conditions in a model for the probability of failure can increase the likelihood of fault detection when an environmental event occurs, e.g. rain.

In another NAMOS deployment, thermistors failed due to prolonged exposure to water which created a bad connection within the sensor. Two sensors are

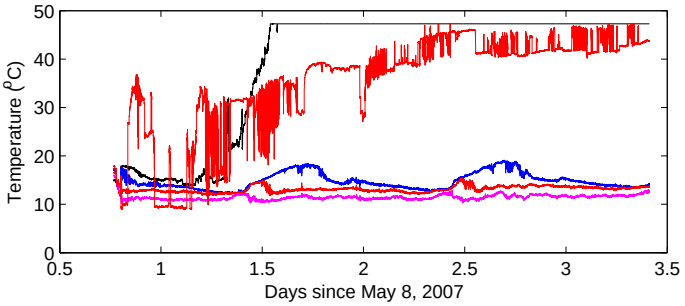

Figure 2.8: Temperatures at buoy 103 for May 2007 deployment of NAMOS sensors in Lake Fulmor.

giving anomalous and likely faulty data in figure 2.8. These faults are due to bad connections in the thermistors. There are several other sensors recording reasonable values, but the two faulty sensors are clearly out of any reasonable range as defined by an environmental and data model.

The fault behavior from connection or hardware faults are often sensor dependent. The datalogger may have software to choose to report certain values if something is out of the range of the data logger. For example, for the NIMS humidity data set in figure 2.3, the datalogger will report a -999 when it receives a value out of the range. However, in the NAMOS example given here, the sensors will continue to sample even as the values seem to be clipped by the range of either the thermistor or the ADC.

Hardware may also fail in other ways beyond electrical malfunctions. For

example, the ion-selective electrode sensors used in soil deployments are often prone to failures [RSE06]. A chemically treated membrane filtering the ion of interest in the sensor is prone to failure when deployed in the field. There may also be interference from other ions present that cause data to be inaccurate [Run06].

Human interaction plays a very important role when diagnosing an unknown hardware issue. Since it is not possible to detail every way a sensor can fail, a person's ability to investigate and provide an explanation for a fault is invaluable. Once a fault is diagnosed, its behavior recorded and incorporated in a future automated expert diagnosis tool, the future role of a person is reduced.

Once a hardware fault is detected, then it may be best to discard the data. Since the sensor is not performing as it was designed, the data it reports is likely not usable.

2.5.2.3 Low battery

Another reason for faulty or noisy data is a low battery voltage, a primary feature of the system as stated in section 2.4.2.3. Battery life is an important measure of sensor health [SPM04] [RSE06] [TPS05]. Low battery levels are not only an indication of how long a sensor will last as it can also influence sensor readings in various ways and cause less reliable or faulty data.

An example provided in [RBB06] illustrates one possible outcome of a low battery; readings from a sensor with low batteries may experience a noise fault, as in section 2.5.1.4. When a weak battery is replaced, the variance of the data samples dramatically decreases by more than threefold. Also in the cold air drainage data in figure 2.6(b), it is likely that the noisy sensor is due to a low battery. While the data still tracks the expected behavior, the noise is much

greater than expected.

Another way a battery may affect sensor data samples is that sensors may begin to report unreasonable readings. There may be an unexpected change in gradient as in the following example. At another NAMOS deployment, one buoy's battery was old and hence it did not have as much capacity. In figure 2.9 there is a drop in temperature in the last hours before the sensors stopped reporting, which is a spike fault as described in 2.5.1.2. We can also see that

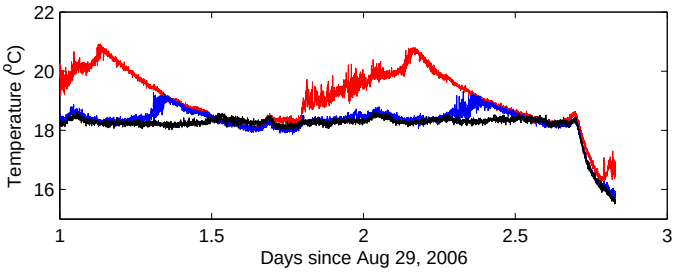

Figure 2.9: Readings from three termistors at buoy 112 for an August 2007 deployment of NAMOS sensors in Lake Fulmor. Sensors values drop significantly as batteries fail, other thermistors behave similarly.

sensors may also exhibit a "stuck-at" fault following a spike when the battery level falls too much. From the Intel Lab at Berkeley data set [Int04], we plot in figure 2.10 two nearby motes' reported temperature values and the battery voltage. Both sensors begin to fail at approximately the same voltages indicating that failure is a likely due to insufficient power. Once battery voltages drop below this value, the temperature sensors exhibit a spike, with excessive gradient, and then remain "stuck-at" one particular value for the rest of the deployment. This is also exemplified in [TPS05] where sensors' battery failures correlated with most of the outliers in the data. When the battery voltage level was less than 2.4V or greater than 3V, behavior similar to that of figure 2.10 manifested itself.

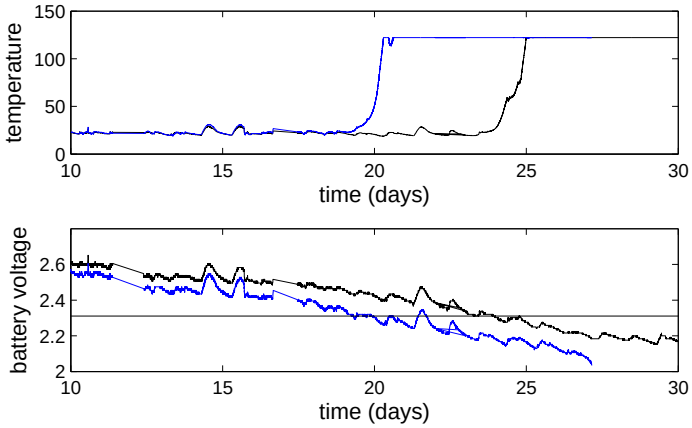

Figure 2.10: Temperature readings and battery voltages from two nearby motes in the Intel-Berkeley Lab data. The horizontal line provides an approximate voltage level at which both sensors begin to fail.

Battery supply can affect system performance significantly by either adding noise or giving faulty data depending on the type of sensor. In some cases, it may be worthwhile to keep the data, as in figure 2.6(b), as the data still retains information about the phenomenon. More often, data might be uninterpretable and must be discarded as is the case for the data in figures 2.10 and 2.9.

2.5.2.4 Environment out of range

There may be cases in which the environment lies outside of the sensitivity range of the transducer. The manifestation of this issue influenced by the calibration feature of the sensor was discussed in section 2.4.2.2.

We present two examples of common behavior when the environment is out of the range of the transducer. In the deployment of chemical sensors mentioned in [RBB06], one chloride sensor reported concentrations outside of the total detection range, figure 2.11(a). The entire range for which the sensor was measured

to have sensitivity is denoted by the horizontal lines. At the extremes, the data experiences a flattening. The sensor readings end up being predominantly outside of this range. While there are still some slight diurnal patterns, the values remain outside of the measured sensitivity range, and hence there is little confidence in these data values.

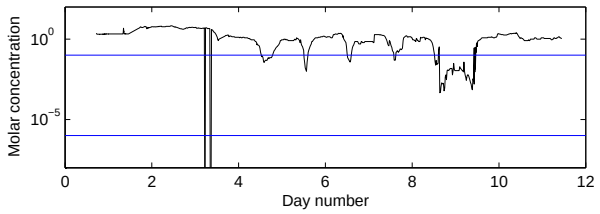

(a) Chloride chemical sensor in Bangladesh.

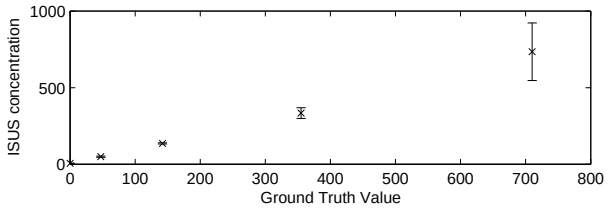

(b) ISUS sensor with increasing variance as the true concentration grows. The error bars are twice the standard deviation.

Figure 2.11: Two examples of environment exceeding the sensitivity range of the transducer.

In figure 2.11(b), a MBARI ISUS nitrate sensor was tested with various solutions of known concentrations for calibration purposes. Several samples were taken with each concentration and the error bars around the average reading in figure 2.11(b) reflect the confidence in each measurement. At high concentration levels, the ISUS nitrate sensor experiences large fluctuations in readings.

2.5.2.5 Clipping

Clipping is exhibited when a sensor seems to have maxed out, and is usually caused by the environment exceeding the limits of the analog to digital converter, R_{ADC}. This type of error mentioned in the context of light sensors in [SPM04] where the sensors saturated at the maximum ADC value and 0. While this is not exactly a sensor fault as the sensor is only operating within its designed parameters, there is reduced confidence for the data when the sensor reaches its maximum.

This fault usually manifests itself as a "stuck-at" fault for consecutive values at the extremes of the data range. Hence, the important features for detection and modeling to examine are the same as described in section 2.5.1.3. Also, this fault may follow a sudden change in gradient at the extreme values of the data range.

As we will see, by considering the context and values of the fault, one can identify the "stuck-at" fault to be clipping. Figure 2.12 shows light data from two motes along the same wall at the Intel Lab at Berkeley deployment.

In the middle of each day, the maximum value at which the sensor peaks is 1847.36 for both sensors and does not move beyond. Any variation in the data does not exceed this value. Following a sudden change in gradient to 0, this data behaves as a "stuck-at" fault. Since these two sensors, as well as other collocated sensors, behave similarly, by taking advantage of an expectation of spatial correlation, one can reasonably conclude that the cause is clipping. Thus the environment in this case has exceeded either the $R_{detection}$ or R_{ADC}.

The inference that the environment exceeded the upper limit of the sensor is based upon the underlying environmental assumptions made. We have made

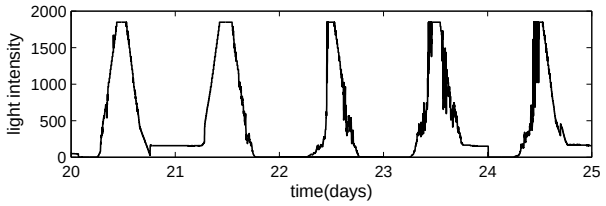

(a) Node 24

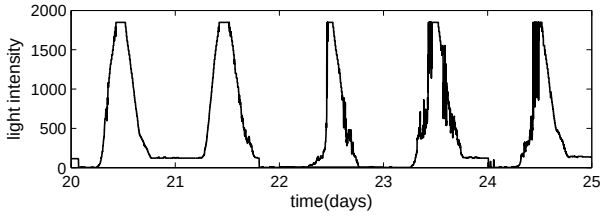

(b) Node 32

Figure 2.12: Data from two of the light sensors deployed at the Intel Research Berkeley lab.

the reasonable assumptions that light in the lab exceeds 1847.36 and that there should be variations in the light scale during the time of clipping.

These assumptions on the environmental model and spatial correlation may change depending on the context affecting the detection of this fault. For example, examining the lowest light values of figure 2.12(a), the values are not consistently the same, so it is more difficult to conclude clipping occurred. Additionally, there is a lower bound for light intensity, so light may not actually drop below measurable limits. Spatial correlation also does not provide a clear cut conclusion either. The data from node 32 does not have the same minimum values as node 24, likely due to a slight calibration error; this adds to uncertainty in a conclusion of clipping.

As mentioned in section 2.5.1.3, clipped data may still provide reduced informational value for interpretation by the scientists. Hence, data exhibiting such behavior should not be discarded.

Table 2.5: Taxonomy of data view faults: Definitions and possible causes.

Fault	**Definition**	**Indications and Possible Causes**
Outlier	Isolated data point or sensor unexpectedly distant from models.	The *distance* from other readings is beyond expectations. The *gradient* changes greatly when the outlier is included. Causes are often unknown unless software inserted by datalogger.
Spike	Multiple data points with a much greater than expected rate of change.	A sudden change in *gradient* which is greater than expected. Little temporal *correlation* between historical data and the spike. Frequent causes include battery failure and other hardware or connection failures.
"Stuck-at"	Sensor values experience zero variation for an unexpected length of time.	*Variance* is close to zero or zero. Spatial *correlation* can be leveraged to determine whether or not in-range stuck-at values are faults. Frequently the cause of this fault is a sensor hardware malfunction.
High Noise or Variance	Sensor values experience unexpectedly high variation or *noise*	*Variance* is higher than expected or historical models suggest. Spatial *correlation* can be used to judge whether or not variation is due to the environment. This may be due to a hardware failure, environment out of range, or a weakening in battery supply.

Table 2.6: Taxonomy of system view faults: Definitions and possible causes.

Fault	**Definition**	**Indications and Possible Causes**
Calibration	Sensor reports values that are offset from the ground truth.	Calibration error and sensor *drift* is the primary cause of this fault. A sensor may be *offset* or have a different *gain* from the truth. The amount of each may *drift* with time.
Connection or Hardware	A malfunction in the sensor hardware which causes inaccurate data reporting	Behavior is hardware dependent. Common features include unusually low or high data values, frequently exceeding expected range. *Environmental perturbations* and *sensor age* may indicate higher probabilities of failure. Other causes include a short circuit or a loose wire connection.
Low Battery	Battery voltage drops to the point where the sensor can no longer confidently report data.	*Battery state* is an indicator for system performance. Common behaviors include an unexpected *gradient* followed by either lack of data, or zero *variance*. There may also be excessive *noise*.
Environment out of Range	The environment exceeds the sensitivity range of the transducer.	There may be much higher noise or a flattening of the data. It may also be a sign of improper calibration.
Clipping	The sensor maxes out at the limits of the ADC	The data exhibits a "ceiling" or a "floor" at the data extremes. This is due to the environment exceeding the range of the ADC.

2.5.3 Confounding factors

There may also be confounding factors that influence sensor readings. For example temperature may influence chemical sensors, there may be interfering ions in the chemical sensors. As in figure 2.10, we see that the battery level actually fluctuates with respect to temperature. The result of this is that these factors may influence sensor behavior and the fault likelihood.

Sensor faults can have multiple contributing factors, and other sensing modalities within the network may be leveraged to detect faults. For example, temperature and humidity are usually well related and can be combined to detect faults. As suggested earlier in section 2.4.2.3, one may incorporate relevant modality features when modeling data or faults.

Also multiple faults may occur at the same time, for example, a battery fault can cause a spike and a stuck at fault at the same time. A falling battery voltage will also cause calibration issues and cause the sensor to drift.

Finally, tables 2.5 and 2.6 gives an overview of the faults their relevant features. While not specifically stated, environmental context plays a role in each one of the faults to determine the expected behavior of the sensor data. Tables 2.5 and 2.6 also provides possible causes that lead to particular faults. Table 2.7 summarizes the practical impact and duration of these faults.

2.6 Concluding remarks

We have provided a list of features which are commonly used for modeling sensor data and sensor data faults. With this, we provided a list of commonly exhibited sensor data faults which one can then use to test a specific fault detection system. There are many interactions between features and faults which make fault

Table 2.7: Duration and Impact of faults

Fault	**Duration**	**Impact of fault**
Outlier	Randomly occurring and instantaneous.	It may significantly skew the *mean*, *variance*, *gradient*, and other data features if not detected. It does not offer any useful information value and can be discarded.
Spike	Fault consists of more than one point. May or may not be temporary.	Spikes generally do not hold any informational value and should be discarded. This results in a loss of sensor data yield.
"Stuck-at"	Fault consists of more than one point. May or may not be temporary.	If cause is environment out of range or clipping, still holds informational value and data can be interpreted at lower fidelity. Otherwise data can be discarded.
High Noise or Variance	Fault consists of more than one point. Usually not temporary.	If the noisy data tracks other sensors, then the data still offers value and should not be discarded.
Calibration	Fault remains throughout the deployment.	Data should not be discarded. Uncalibrated data can still provide insight. A proper calibration formula can correct the data.
Connection or Hardware	Permanent once it occurs.	Data is meaningless as sensor is not performing as designed. Should be discarded.
Low Battery	Permanent until battery replacement or recharge.	Commonly, a battery failure results in useless data which should be discarded. The exception is if sensor behavior at low voltage gives added noise, then there may still be informational value.
Environment out of Range	Sensor returns to normal operation after environment returns to within range.	Still holds some information content. At minimum, indicates environment exceeds the sensor sensitivity range.
Clipping	Sensor returns to normal operation after environment returns to within range.	Still holds some information content. Indicates data exceeds the upper or lower ADC values.

detection so difficult. However, we have presented a systematic way of looking at sensor data faults which could ease the next step of fault detection.

With this understanding of many possible faults, one can then develop more context-specific diagnosis systems. In the following chapters we detail a method to detect some of the faults presented here. Some of the faults presented here will be injected into simulated data sets to test the efficacy of our algorithms.

CHAPTER 3

Bayesian maximum a posteriori selection of agreeing sensors for fault detection

3.1 Introduction

With the firm understanding of faults and how they behave given in the previous chapter, we can now focus on the problem of how to detect faults and faulty sensors. Our goal is to identify problems within the sensor network and determine the degree of confidence we have in our collected data.

We first present an overall design methodology upon which we develop our data fault detection techniques. As noted in chapter 2, in the absence of ground truth, data faults are judged by how well they conform to the expected model. In order to design and develop a successful sensor data fault detection system, there are several issues presented in table 3.1 that must be resolved.

Table 3.1: Data Fault Detection System Design Principles

We must model or restrict ourselves to a model of the phenomenon we are sensing.
Based upon this model, we must determine the expected behavior of the data using available data.
We must determine when sensor data conforms to the expected behavior of the network or phenomenon.
We must remedy problems or classify behavior as either acceptable or faulty and update our models.

With these problems resolved, we can then take our updated models and reapply our mechanism of determining expected behavior and conformal sensor behavior in a cyclical manner.

We approach this problem using an online detection system where data is tagged immediately. The main benefit of online detection can trigger quick and immediate human involvement if there is anomalous behavior. However, this also limits the complexity of the modeling that is done which impacts the final performance of the system.

We break this problem down into two distinct phases. First, we use a method similar to that of agreement problems combined with Bayesian maximum a posteriori (MAP) selection in order to determine a subset of sensors that are used to represent the expected behavior of the phenomenon. In the second step, we judge whether or not sensors are faulty based upon the model developed from this subset.

An overview of the approach with all of the major steps is given in figure 3.1. The notes in italics in the figure indicate where some of the issues in the design of a fault detection system listed in table 3.1 are resolved.

We select a Bayesian approach because this allows for the inclusion of background and prior knowledge in the decision of our selection. Updates are conveniently performed using the posterior probability from the previous decision as a prior probability for our next decision.

We look at two sets of data, a simulated data set and a real world data set. The simulated data set allows us to judge our algorithm's effectiveness when all of our assumptions hold true. The second set of data comes from a set of temperature sensors deployed throughout a valley and will show the real world performance of this system.

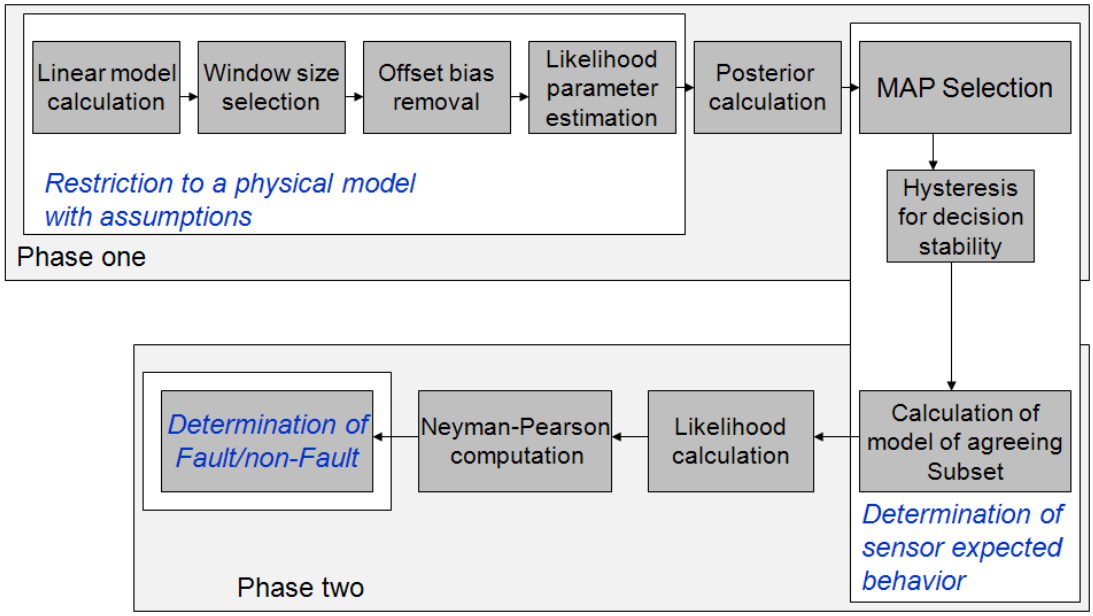

Figure 3.1: System flow of the MAP selection method

3.2 Prior work

We have already discussed in depth the problem of data faults in sensor networks and the necessity of their detection in chapter 2. We now discuss the types of approaches used in the existing literature and their merits or limitations instead of how the faults are modeled. An overview of some types of issues and approaches encountered in the information fusion domain is provided in [Rog04].

In the process control domain, [Mar90] has the goal of developing a control system that is tolerant to device failures. The authors devise an interval based averaging algorithm using "abstract" sensors where no more than a given number of sensors may fail. [PIK91] and [PIR94] extend this approach to spatially distributed sensor networks that detect and measure a certain phenomenon using clusters of redundant sensors for fault tolerant integration of readings. In our specific application, the lack of high spatial redundancy in sensors presents

a challenge to such systems.

For the application of event detection, in [CSR04] faulty nodes are assumed to send inconsistent and arbitrary values to the decision maker. The authors compare value fusion and decision fusion using the false alarm and detection probabilities as performance metrics. We will also use these metrics in our work to judge the performance of our detection system in the application of environmental monitoring.

Additional work tries to correct faulty data using models developed from the data. In [EN03], Bayesian updating for the distribution of an individual sensor's readings using prior distributions is employed. However, the prior knowledge of the phenomenon that is to provide the prior distribution is not given in detail, and the method does not explicitly take advantage of any spatial or temporal modeling. [EN04] uses spatio-temporal correlations to learn contextual information statistically. This contextual information is used in a Bayesian framework to detect faults.

[JAF06] uses a basic approach by dividing samples into temporal granules and co-located sensors into spatial granules and averaging within these granules to get an expected value. [MPD04] uses linear autoregressive models to characterize data for error correction, targeting transient "soft" failures. With these linear models, the authors develop a predictive error correction technique using current data to decide past data. In [BME03] the authors use correlated sensors in order to calibrate sensors. However, the method does not account for faults in sensors.

[CKS06] develops a distributed algorithm for faulty sensor identification. The basis of their method is majority voting, where each sensor has at least three neighboring nodes. However, the system model used is a network model that consists of a large, dense, randomly deployed sensor network. This is not the

type of network model we focus on.

Our solution involves a type of agreement, or consensus, problem in that we judge other sensors based on whether they agree with a model given by the majority of sensors. There are several types of consensus problems, a brief overview of which is given in [Fis83]. Also, [KI04] uses a Bayesian approach combined with the consensus, although their sensor network problem is to detect interesting events with a differing fault characterization.

An extension to consensus problems are reputation systems [RZF00]. An example of reputation systems in mobile distributed networks can be seen in [BL04] and [ML05]. One can view a fault as a negative interaction in a reputation system, and we can see reputation systems applied in sensor networks in [GS04].

3.3 Problem Formulation

Here we assume a system as depicted in figure 3.2 where sensor data is forwarded to a fusion center which then processes the data to determine reliable sensors. We define a set of K sensors to be taking measurements in a smoothly varying field across space.

When examining sensor data without knowledge of ground truth, one seeks to determine faults based upon the comparison of sensor data trends and relative offsets. We construct a framework to determine faults and initially only consider data trends when determining non-faulty sensors. We then examine the effect of including sensor offsets. The case of considering sensor offsets requires an additional assumption on the data set discussed in section 3.4.2. While these features may be correlated, we begin by assuming that these features are independent.

To employ sensor trends, we assume that the data from non-faulty sensors

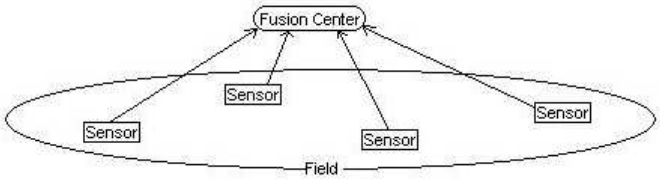

Figure 3.2: Sensor Network

behave with some smoothness in time. That is, we assume that data from non-faulty sensors can be modeled locally with a linear model. While we could select a higher order polynomial model, we choose to use a first order approximation for simplicity. Also, we assume that there are no large gaps in time where data points are not forwarded to the fusion center, so that we have sufficient data to model with. We currently do not handle this type of fault. Since the field is smooth, we expect that all sensors will move with similar trends. So, when there is an increase in temperature at one location there should be a similar increase in temperature at another sensor location. We consider a Gaussian noise model for sensor noise for simplicity, and the actual temperature or phenomenon being measured is also expected to behave smoothly without any sharp spikes.

Our goal is to detect sensors that behave outside of the norm relative to other sensors. We approach the problem by picking a subset of sensors that is capable of representing the trends in the data. Then all sensors are compared to a model developed from this subset of agreeing sensors. This set is determined using a Bayesian detection approach where we base decisions on a posterior probability, i.e. the probability that a subset of sensors is the correct set given the data.

In order to have a guaranteed consensus decision, it is required that there be a minimum of $\frac{K}{2}$ sensors in our agreeing subset. If a smaller minimum were to be considered, then there may be cases where we have two clusters of agreeing

sensors, yet the clusters as a whole disagree. In this case we would not know what cluster of agreeing sensors to trust. Thus, we assume that in our sensor system we have at least $\frac{K}{2}$ sensors that are not faulty at any given time. We also assume that all good sensors are correlated and that all faulty sensors do not behave as an entirely separate correlated process. We limit subsets under consideration to size $\frac{K}{2}$ allowing for situations where half of the sensor network is allowed to be faulty.

We seek to determine which subset contains the sensors that best match each other given the data and a list of subsets. We can frame our problem as a simple maximum a-posteriori probability (MAP) problem. This selects the subset of sensors that gives the best posterior probability of being the same.

We represent a subset of sensors by a vector $\vec{\phi}$ with length K, where $\phi_i \in \{0, 1\}$, and the binary values $\{0, 1\}$ represent exclusion and inclusion in the set respectively. The posterior probability is $P(\vec{\phi}|\vec{D}, \xi)$ where $\vec{D}$ is data and ξ is other background information. We can exhaustively search all possible $\vec{\phi}$ allowed by the restrictions described above; this problem is stated as the maximum a posteriori probability problem:

$$\hat{\vec{\phi}} = \arg\max_{all\vec{\phi}}(P(\vec{\phi}|\vec{D}, \xi)) \tag{3.1}$$

Additionally, we assume that sensor faults are relatively persistent. That is, a sensor fault lasts at least as long as our model estimation depth, M, which is described in further detail in the following section.

3.4 Implementation

In a MAP problem, we require the evaluation of the posterior probability of a hypothesis given a set of data. In our case the hypotheses are the possible $\vec{\phi}$. We

use Bayes' rule, as introduced in chapter 1, with modifications for notation:

$$P(\vec{\phi}|\vec{D},\xi) = \frac{f(\vec{D}|\vec{\phi},\xi)P(\vec{\phi}|\xi)}{f(\vec{D}|\xi)} \tag{3.2}$$

Also, we use linear autoregressive models as introduced in section 1.1.4 extensively to model data.

3.4.1 Finding the posterior probability

The prior probability distribution, $P(\vec{\phi}|\xi)$, is updated with the posterior distribution, $P(\vec{\phi}|\vec{D},\xi)$, evaluated in the previous iteration of the algorithm. Initially, we set the prior probability distribution to be uniform, as this makes no initial assumptions on the reliability of the sensors; all sensors are equally likely to be faulty. Also, recall $f(\vec{D}|\xi)$ can be decomposed into $\sum_{all\,\vec{\phi}} f(\vec{D}|\vec{\phi},\xi)P(\vec{\phi}|\xi)$. Thus, we need only be concerned with the calculation of the likelihood function, $f(\vec{D}|\vec{\phi},\xi)$. Before we discuss the final calculation of the likelihood function, we must account for a few issues.

3.4.1.1 Sample window size

In a sensor network data will usually arrive serially. So, we use M to define the total number of samples across all sensors we use to develop our models. That means if there are K sensors, assuming there is no missing data, then there are $P = \frac{M}{K}$ data points for each sensor within the window M. Or, if data is missing, then we have for each sensor P_i samples such that $\sum_{i=1}^{K} P_i = M$. The choice of the sample window, M, is a factor in the ability for the linear model to interpolate data and also plays a factor in the calculation of the covariance matrix, Λ. A window size M that is too large can make predictions inaccurate since the data may not be linear when considering large window sizes. A window that is too

small may be inaccurate as well because the line may be only following the noise. We want a line to model individual sensors that minimizes the error of the data points involved and the next point relative to a predicted value from the model. We can adaptively select M based on how well the data fits a linear model.

With each iteration of the algorithm, i.e. when new data arrives, we derive for each sensor, i, a linear model for a particular M. We then extrapolate one future point with this model, and we determine the mean square error for this particular M and sensor i with respect to the actual data points measured. Across all sensors $i \in 1 \ldots K$, we consider the sensor with the maximum mean square error. Finally, across all M such that $M_{min} \leq M \leq M_{max}$, we choose the M that has the smallest maximum mean square error. More formally, we choose an M for the following problem

$$\min_{M} \max_{i} \frac{1}{P+1} \sum_{j=1}^{P+1} (\widehat{x_i^M}(t_k) - x_i^M(t_k))^2$$

The estimate for point $j = P + 1$ is included in order to consider the predictive error for the model. $\widehat{x_i^M}(t)$ is the least squares linear model for the data $x_i^M(t_k)$ where $k = 1, \ldots, P$, the P points for sensor i within the past M total samples. This can be calculated by solving the following least squares regression problem for the parameters a and b:

$$\begin{bmatrix} x_i^M(t_1) \\ \vdots \\ x_i^M(t_P) \end{bmatrix} = \begin{bmatrix} t_1 & 1 \\ \vdots & \vdots \\ t_P & 1 \end{bmatrix} \begin{bmatrix} a \\ b \end{bmatrix} \tag{3.3}$$

The resulting model is $\widehat{x_i^M}(t) = a * t + b$.

In our implementation, we choose M_{min} such that $P \geq 3$ in order to avoid a linear fit with just two points giving zero error. We choose M_{max} based on the maximum time before we want to make a decision on the data. We consider

step sizes of length 5 when choosing M for easier computation, i.e., we consider $\{M|M = M_{min} + 5q \text{ where } q = 1, \ldots, \frac{M_{max}-M_{min}}{5}\}$. Dependent on user needs, different sized steps can be considered.

3.4.2 Accounting for offset data

Absent a strong model of the phenomenon of interest, in order to remove offsets in sensor data, we apply a simplistic method. Using the linear model developed for each sensor from the past M samples, we simply subtract the bias, i.e. y-intercept, of each model from the data points for the corresponding sensors. In effect, we are "grounding" the sensor data for the current M sample window.

Under the data trends only test, there are cases in which sensors follow the general trend of data yet have significantly large offsets, this may often signal calibration errors or other issues. By imposing a new assumption on the data that all sensor data is clustered and measuring similar data values, we eliminate this possibility and increase our detection rate. In order to combine the consideration of both trend and offset, we can apply the detection algorithm that we use for data trends to data values where we remove the trend from the data set instead of the offset. This leaves only the consideration of the distance between data from different sensors.

Thus when considering only data offsets for fault detection, we take the trend as calculated from the model developed for each sensor and subtract the trend from the sensor data for the corresponding sensors and time. By doing so, we can consider only the distance of data for a particular sensor from the model of expected sensor behavior. We can then apply our algorithm to this data and combine the results from both trend and offset into an overall detection decision. If a sensor is marked as faulty in either case, then it is marked as faulty overall.

3.4.2.1 Likelihood function

The likelihood function, $f(\vec{D}|\vec{\phi},\xi)$, may be based upon several factors. We only consider the noise factor, although there may be other background information, ξ, that may affect the likelihood or measurements, $\vec{D}$. We consider a joint Gaussian distribution, since sensors are unlikely to have completely independent readings; for a given $\vec{\phi}$ being considered in our MAP problem, we have:

$$f(\vec{D_\phi}|\vec{\phi},\xi) = \frac{1}{(2\pi)^{\frac{\vec{1}^T\vec{\phi}}{2}}|\Lambda_\phi|^{\frac{1}{2}}} e^{-\frac{1}{2}(\vec{D_\phi}-\vec{\mu_\phi})^T\Lambda_\phi^{-1}(\vec{D_\phi}-\vec{\mu_\phi})} \tag{3.4}$$

For each subset, $\vec{\phi}$, we only include values for sensors included in that subset. For example, if $\vec{\phi} = [1\ 0\ 1\ 0]^T$, then $\vec{\mu_\phi}$ is a vector containing only the expected values of sensors 1 and 3.

With our assumption of local linearity due to a smoothly varying field, we can use a least squares regression to derive all of our linear models.

Incoming sensor data is not synchronized to regularly defined intervals, and data points may be occasionally dropped. So, we use a linear model, also for simplicity, for each individual sensor based upon recent data and interpolate the data based upon this model. With these models, we can calculate the expected value vector and covariance matrix and evaluate the likelihood function.

We first seek to determine the expected value, $\mu_i(t)$, for sensor i at any time t as derived from a linear model derived from the previous M total samples excluding the samples from sensor i. This allows us to judge each individual sensor relative to the collective group without the possibility of self influence.

Let $x(t_n)$ represent the data point measured at time t_n, where n is the n^{th} sample out of the M total samples in our window; this does not discriminate among sensors. Then denote $x_{(i^-)}(t_n)$ as $x(t_n)$ without the samples from sensor i; there are only $(M - P_i)$ data values when we discuss $x_{(i^-)}$. We can re-index

our time such that $x_{(i^-)}(t_m)$ represents the m^{th} sample out of the $(M - P_i)$ data values in $x_{(i^-)}$. So, our expected value for a particular sensor, $\mu_i(t)$, is derived from $x_{(i^-)}$. The value for $\mu_i(t)$ will be given by $\mu_i(t) = a * t + b$, and is determined by solving for a and b in a least squares regression problem similar to that of equation 3.3. We use $x_{(i^-)}(t_j)$ in place of $x_i^M(t_j)$ with $j = 1, \ldots, (M - P_i)$.

With our Gaussian noise model, we now need to estimate the covariance matrix, Λ, using data and models developed from the past M samples. We can estimate the components of Λ as:

$$\Lambda_{ij} = \frac{1}{M} \sum_{k=1}^{M} (x_i(t_k) - \mu_i(t_k))(x_j(t_k) - \mu_j(t_k))$$

Recall, we have already calculated models of the data for each individual sensor for our M, $\widehat{x_i^M}(t)$, which we will refer to now as $\widehat{x_i}(t)$ since our M is fixed. $x_i(t_k)$ is defined to be the actual data measured or, if a measurement is unavailable, $x_i(t_k)$ estimated from the model $\widehat{x_i}(t_k)$. Also, $\mu_i(t_k)$ is the expected value of $x_i(t_k)$ as discussed earlier.

Once we have this distribution, we can plug in our data into equation 3.4 to find our likelihood value. Recall, the likelihood function for each possible ϕ is the standard multivariate Gaussian with mean μ_ϕ and covariance Λ_ϕ. For the covariance, Λ_ϕ, we have our estimated Λ with the rows or columns removed as indicated by ϕ. We use the data vector $\vec{D}_\phi$ with interpolated readings from our linear model $\widehat{x_i}(t)$ for missing samples in evaluating the likelihood.

Now we have our likelihood values. We can plug the likelihood value into equation 3.2 to determine the posterior probability for a particular $\vec{\phi}$. We now can consider and apply our MAP selection criterion, equation 3.1, to select a $\hat{\vec{\phi}}$.

3.4.3 Rapid changes in selection

One other issue in the selection of the agreeing subset is ensuring the stability of decisions. That is, there may be iterations where the MAP selection of the optimal subset will change from a long established subset $\vec{\phi_n}$ to subset $\vec{\phi_m}$. And after only a brief moment, the MAP selection will return from subset $\vec{\phi_m}$ back to $\vec{\phi_n}$. We want to avoid this "hiccup" as we would like decisions of faulty sensors to be as consistent as possible. While it is unlikely that a "hiccup" would alter many decisions as sensors in set $\vec{\phi_m}$ and not $\vec{\phi_n}$ are likely reliable as well, to avoid any difficulty in evaluating sensor faults, we would like to avoid this situation.

We include a small lag of length L in our decisions of the agreeing subset of sensors in order to eliminate this issue. If there is a quick jump from $\vec{\phi_i}$ to another subset and back, then the lag in our decision will allow us to ignore this. Thus the original agreeing subset is assumed to be correct. The depth of the lag, L, is dependent on the lengths of jumps the user wants to avoid. We choose $L = 3$ in our implementation.

To do this, we compare our new decision of $\vec{\phi_m}$ with the previous L selections made by our MAP problem, $\{\vec{\phi_l} \mid l = 1 \dots L\}$. Note that these $\vec{\phi_l}$, are only our MAP selected subsets, and not the final decisions made on our agreeing subset after this part of the algorithm. If among these L samples, $\vec{\phi_m} \neq \vec{\phi_l} \ \forall \ l = 1 \dots L$, then we choose $\vec{\phi_1}$ to be our agreeing subset.

3.4.4 Determining faulty sensors

For the second phase of our algorithm, once we have decided on what subset of sensors we believe to be a good representation of the data or data trends, we can determine whether sensors are faulty or non-faulty. In order to do so, we use

the likelihood that a sensor's data is correct given a sensor subset. This metric is the natural extension to the Bayesian approach we used in determining our agreeing set. We evaluate the likelihood function, $f(\vec{D}|\vec{\phi},\xi)$, and normalize all of the likelihoods.

Using all of the data from each sensor in the agreeing subset, we can determine the expected behavior with one linear model. We take the data from the sensors in our subset, denoted by, $x_{\hat{\phi}}(t_n)$, and derive one linear model $\hat{x}(t)$ using all of our data. We calculate $\hat{x}(t)$ using equation 3.3 where we have $x_{\hat{\phi}}(t_n)$ in place of $x_i^M(t_j)$. And we take $n = 1, \ldots, N$ where N is the number of data points in $x_{\hat{\phi}}(t_n)$. This $\hat{x}(t)$ gives us the expected value in our likelihood function. The variance for our likelihood can be estimated by calculating $\frac{1}{N-1}\sum_{n=1}^{N}(x_{\hat{\phi}}(t_n) - \hat{x}(t_n))^2$.

We can then evaluate the likelihood of data for each sensor, including sensors in the agreeing set, given this composite model. We use a moving average of the likelihood probability to smooth out wild variations and more clearly see the trend of a particular sensor. Since we considered the previous M samples in modeling, we use the previous M likelihood values for averaging and developing statistics on the likelihood.

In making a final decision on each sensor, we try to maximize the probability that a faulty sensor is correctly detected, i.e. P_D, while keeping the probability that a non-faulty sensor is marked as faulty below a given value, i.e. P_{FA}. That is, we use a simple Neyman-Pearson test to select faulty sensors at each iteration of our algorithm. We assume that the likelihood moving average is approximately Gaussian in distribution for the sensors in the agreeing subset [MW95]. This assumption is made to simplify our calculations. We then calculate the average of the mean and variance of the likelihood values for each sensor. We use these statistics in evaluating the Neyman-Pearson test.

Note that, since we use a composite model developed from the agreeing subset, there is a possibility that a sensor in the agreeing subset may be incorrectly flagged. However in our simulated conditions with all of our assumptions true, this case very rarely occurs. In our experiments, we set our threshold to be $P_{FA} = 0.05$.

3.5 Results

We first look at data that was simulated, so we know all data conditions and assumptions. We simulate a set of four temperature sensors taking data measurements as seen in the top plot in figure 3.3. We generate sinusoidal data to simulate rising and falling data values and we include one persistently faulty noisy sensor. Each sensor has a slightly different amplitude and offset associated with its data. We also add additive Gaussian noise to each sensor. We note that sensor node 4 is the faulty sensor and is also noisier.

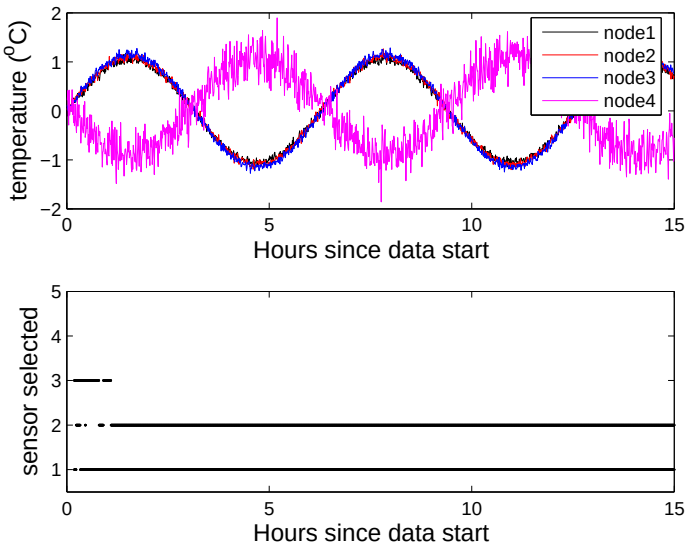

Figure 3.3: Simulated sensor data and sensors included in the agreeing subset

Also in figure 3.3 we see what sensors are included in the agreeing sensor set. We confirm that the faulty sensor is never included in the agreeing sensor set. This agreeing set is then used to develop the likelihood values for each sensor and final decisions are made on each sensor. We can see the likelihood moving average for each sensor in the top plot of figure 3.4. Sensor 4 has its likelihood moving predominantly along the lower axis. In the bottom plot of figure 3.4, we see which sensors are marked as faulty after our final decisions.

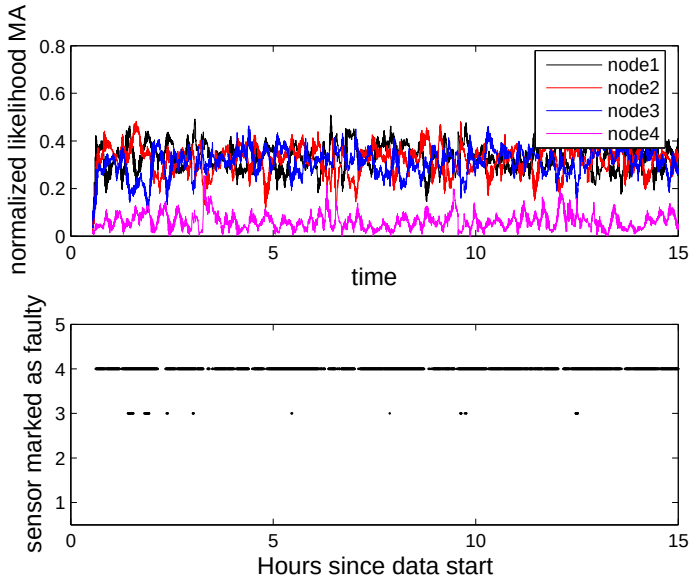

Figure 3.4: Moving average for likelihood and Faulty sensor decisions based upon trend

To judge our success, we examine the proportion of time instances that we correctly and incorrectly identified faulty sensors. Looking at Table 3.2, we see that the faulty sensor is detected 82.0% of the time when we only consider data trends. Some of the missed detection is attributed to moments in time when both the model and the faulty sensor have the same general trend with a significantly large offset as described in section 3.4.2, e.g. at the peaks of the sinusoids.

Table 3.2: Results for Simulated Data: Proportion of sensors marked as faulty

Sensor	**Considering trend only**	**Considering trend and offset**
1	0	0
2	0	0.0089
3	0.0189	0.0234
4	0.8201	0.9934

The false flagging of each good sensor remained under our previously mentioned threshold of $P_{FA} = 0.05$ which is as expected.

We see that when we add consideration of sensor offsets, we have a dramatically increased detection rate of 99.3%. With this increase in detection, our individual false detection rate also increased slightly, however the overall performance was still good.

Now, we apply our algorithm to data from four temperature sensors that are close to each other deployed in a valley [CAD07]. The first plot in figure 3.5 shows the data that was collected from the deployed sensors. We see that there is a clearly faulty sensor, sensor 4, and the other sensors have data that generally move together. The data is more variable and not as regular as in the previous case.

The second plot in figure 3.5 gives the results of the likelihood plot and the final decisions made. We see that predominantly sensor 4 is marked as faulty while there is a higher rate of false detection of sensors than in the simulated case. The exact proportion of sensors marked as faulty can be seen in table 3.3.

Table 3.3 shows the correct marking for a faulty sensor occurred 75.89% of the time when considering only trends. While for individual sensors 1 and 3 we remain under P_{FA}, sensor 2 does not. As this sensor is not, for the most part, in the agreeing subset and not involved in the model development, we expect

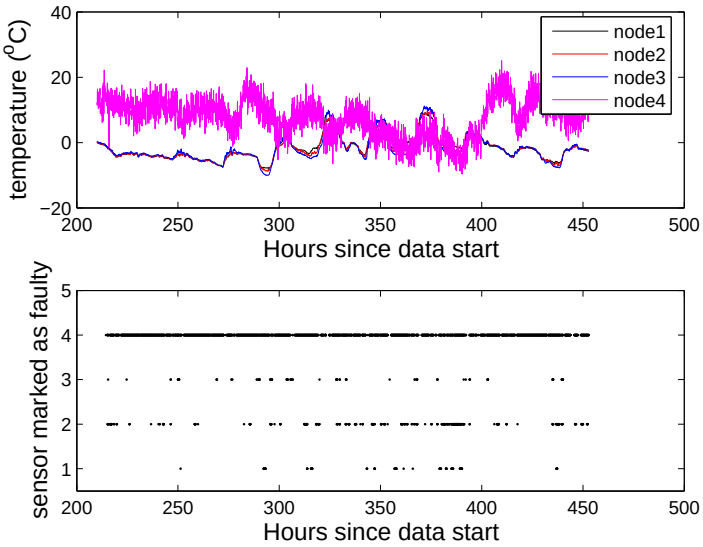

Figure 3.5: Sensor data collected from deployed sensors and sensors marked as faulty based upon trend

Table 3.3: Results for Actual Data: Proportion of sensors marked as faulty

Sensor	**Considering trend only**	**Considering trend and offset**
1	0.0186	0.0297
2	0.0796	0.1478
3	0.0194	0.0803
4	0.7589	0.9793

that it might be marked as faulty more often. The total $P_{FA} = 0.1176$ exceeds the design parameter P_{FA} indicating that under real world conditions, some of our assumptions are flawed. The Gaussian assumption on the distribution of the likelihood for non-faulty sensors may not be accurate since the P_{FA} is higher than a expected. The detection of the faulty sensor was only slightly lower than the detection rate in our simulated data set indicating that the probability distribution for the likelihood for faulty sensors is close but not the same in both data sets.

In our first attempt at detecting faults when including offsets, detection rate jumps to 97.9%, at the cost of a high false detection rate. This is due to the new restriction of having similar data values as discussed in section 3.4.2 suggesting that in the future, we must detail a better model of the data and a fault model for sensors.

3.6 Conclusions

In this chapter, we have introduced a Bayesian MAP formulation of a sensor network data fault detection system. Using a this approach we can determine a set of sensors from which to develop a model of the proper data behavior, and then based upon this, we determine faulty sensors. This technique provides us with an initial framework for flagging sensors that need immediate repairs while the sensor network is deployed.

While the system is capable of successfully selecting a good subset of sensors, the final detection results have much room for improvement. Detection rate is not very good while false detection rates commonly exceeds the design specifications. The main handicaps to this system are the inaccuracies of the assumptions and the poor modeling of the phenomenon. In the next chapter we will adjust several assumptions and focus on how to better model the phenomenon using hierarchical Bayesian space-time modeling. Using a simplified tagging method, we will compare the performance of the improved modeling method with a linear modeling technique similar to the one used in this chapter.

CHAPTER 4

Detection of data faults in sensor networks using hierarchical Bayesian space-time modeling

4.1 Introduction

As seen in the previous chapter, the modeling of sensor data plays a crucial role developing an effective fault detection algorithm. The choice of using linear autoregressive modeling required several assumptions on how sensor data is expected to behave. Frequently, many of these assumptions proved to be invalid or not very accurate, and inevitably this hamstrung the performance of the fault detection system. In this chapter we introduce a new modeling technique that is more capable of representing different trends in the data.

We utilize the hierarchical Bayesian space-time (HBST) modeling found in [WBC98] and apply it to the problem of fault detection. While HBST modeling is much more complex than techniques such as linear autoregressive (AR) modeling, we validate its use in fault detection by applying HBST modeling to both simulated data and real data collected from two different experiments. Using a simplistic technique for tagging questionable data we compare the performance of the two modeling techniques. While not perfect, HBST modeling is more accurate and robust than linear AR modeling to unmodeled dynamics.

Bayesian techniques are not new in the fault detection application as discussed

in chapter 3 as well as [EN03] and [EN04]. However none of the Bayesian fault detection methods are used to directly model the data and learn the parameters of the data model. We will show that the use of HBST modeling improves the performance of the system.

We will use the modeling framework for hierarchical Bayesian space-time models presented in [WBC98] which is used to model space-time data "ubiquitous in the environmental sciences." This introduces better spatial and temporal modeling than has been previously utilized in sensor network data fault detection. To get around the issue of the complexity and computational costs involved with Bayesian modeling, we will show how such modeling can be used in a "semi-realtime" fault detection scheme to improve fault detection results.

In section 4.2, we discuss some preliminaries before defining our HBST model. We define the system setup and assumptions for which we develop our approach. We also detail how we synchronize sensor network data for use in spatial statistics tools using a binning approach. Section 4.3 first presents the model used in [WBC98]. Then, we adapt this model for its new application to fault detection and detail specific assumptions on the model structure. In section 4.4 we discuss how we determine the parameters of this HBST model using Bayesian estimation with Markov Chain Monte Carlo (MCMC) methods and Gibbs sampling. Section 4.5 explains how a "semi-realtime" detection scheme would work and presents the simple fault tagging method that we use to compare HBST modeling with linear AR models.

Results are presented in section 4.6, where we apply HBST and linear AR modeling to simulated data and real data. The results show that HBST modeling in comparison to linear AR modeling excels at reducing false detection while maintaining good detection rates. Further discussion about the advantages and

disadvantages of HBST modeling for use in fault detection is in section 4.7. Following the conclusion (section 4.8), we include an appendix in section 4.9 where full conditional distributions for use in the Gibbs sampler are derived.

4.2 System model and setup

The sensor network system setup, context, and application significantly influences how one should model the target phenomenon. For demonstrative purposes, we will model temperature data as this is one of the most common measurements. We will apply our method to two sets of real world data to show its versatility. The first set is from the same experiment as the data in chapter 3 and measures cold air drainage across a canyon in James Reserve, California. The second set of data is temperature at the surface of Lake Fulmor, in the James Reserve. In both of these scenarios, sensors are deployed in a close to linear manner, therefore the spatial dimension we will use will consist of only one axis.

As is currently done in most sensor deployments and in keeping with chapter 3, all sensor data is forwarded to a central fusion center without modification. We assume that corrupted or missing data communication packets are simply unavailable data points which have no bearing on data faults. The fusion center will perform relevant modeling computations and make decisions regarding faults of individual sensors.

Additionally, as noted in chapter 3, real world data from all sensors are not usually synchronized so the data arriving to the fusion center cannot be easily vectorized. Most common space-time statistical tools assume that samples occur at regularly defined time intervals in a synchronized manner so that they may be easily placed in vectors at each time instant. In order to adapt real world data

to such a scheme we "bin" the data by time instances for each sensor.

For one sensor, examining the regularly defined time instant at time t_i, we look at the interval surrounding this which is of the size r, where r is the difference between time instances t_i and t_{i+1}. If within the interval $t_i - \frac{r}{2}$ and $t_i + \frac{r}{2}$ there is one sensor value for this sensor then the output at time t_i for this sensor is exactly this sensor value. If there are multiple sensor values within this interval, then the output at time t_i is the mean of all these values. However, if there is no data point, then a line between the two nearest surrounding data points is used to interpolate all values in between.

Note that in chapter 3 we use a linear AR model based off of a large window to interpolate missing data points. This may be inaccurate at times if the model itself is inaccurate. However, here we are just "filling in the blanks" in between two points. This proves to be an accurate method of estimation given that the following assumption hold.

We require the data to be sufficiently sampled such that linear interpolation in between data points provides a good approximation. This primarily means that there are no large gaps in sensor data, otherwise interpolation will fail to effectively capture data. We have observed this to be the case in our data.

To show that this process is effective, we examined the energy difference between a binned data set and the original data by calculating the area under the curve of the two sets. We tested the cold air drainage data from day to day. On average, the percentage difference between the areas is insignificant. For example, we pick one node to illustrate. Over the course of four days, the average day to day difference in area was an insignificant 0.27%. Visually there is little difference from the original data set and the binned set, as shown in Figure 4.1.

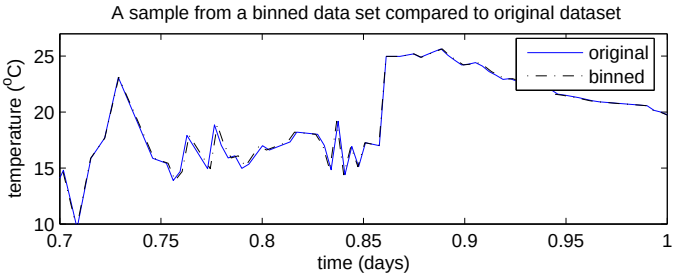

Figure 4.1: Sample data and a binned version. This figure focuses on a small portion of the data to show that binning has no real effect on any analysis.

4.3 Hierarchical Bayesian Space-Time Model

We first provide an overview of the method presented in [WBC98], as the adaptation of this approach for fault detection is the basis of our work. [WBC98] details a flexible hierarchical model for space-time data using a multi-stage approach. We use this approach as a guideline to model sensor network data for the purposes of fault detection and make modifications to fit our needs. The flexibility, robustness, and systematic approach of this method makes it suitable for fault detection. Also its direct application to modeling climate data is ideal for the environmental monitoring that sensor networks perform.

In [WBC98], the hierarchical space-time model consists of five stages of modeling. In the first stage, a statistical measurement error model is defined. Assuming $Y(s,t)$ is the process for sensor s at a location l_s and time t, then the observed (measured) data $Z(s,t)$ is distributed by some error distribution $P(Z(s,t)|Y(s,t),\theta_1)$ where θ_1 is a collection of parameters for the distribution. The next stage models the process Y. Based on the relevant processes of interest in [WBC98], Y consists of several components. These components are a site-specific mean $\mu(s)$, a large-scale temporal model with site specific parameters $M(t;\beta(s))$, a short-time scale dynamic process $X(s,t)$, and a zero mean random

variable that models noise $\gamma(s,t)$. The specification of the joint distribution of $\gamma(s,t)$ is simplified to avoid modeling a $ST \times ST$ covariance matrix. The hierarchical approach allows this since other modeled features of $Y(s,t)$ will explain the space-time structure, X(s,t).

The third stage defines these spatial structures and dynamics for the Y process. In the example presented in [WBC98], μ is defined to be a Markov random field, and X is modeled as a one step space-time autoregressive moving average. We will deviate from these assumptions in our own modeling. The fourth stage defines the prior distributions on the model parameters. The fifth stage defines hyperprior distributions on the prior parameters of the fourth stage. With simplifications made in our modeling, we do not define any hyperprior distributions.

[WBC98] presents an example in which this approach is applied to monthly averaged maximum temperature data in the midwestern United States. For the application of sensor data fault detection we make several adjustments and deviate from the example presented. Also, because of the type of system as well as the much smaller scale we are observing, we detail further restrictions on the data when defining our model.

Given at time t a set of observations from S sensors, Z_t is a $S \times 1$ vector of the observations. We begin by modeling the measurement process, Z_t as simply the phenomenon process with additive noise, ϵ_Z.

$$Z_t = Y_t + \epsilon_Z$$

Assuming the measurements $Z_t(s) \forall\, s = 1, \ldots, S$ are all independent and the noise is normal, then we represent Z_t as:

$$Z_t | \{Y_t, \sigma_Z^2\} \sim \mathcal{N}(Y_t, \sigma_Z^2 \mathbf{I}) \tag{4.1}$$

This is a departure from the example presented in [WBC98] where the m obser-

vations in Z_t are mapped to a state vector of S grid locations Y_t using a $m \times S$ matrix $\mathbf{K}$. This allows for some predictive ability, but in for our experiments these predictions at unobserved locations were not close to accurate. Also, as discussed later in this section, we do not restrict our model to a regular lattice.

The phenomenon process can be modeled as a combination of three main components and the noise component ϵ_Y. This noise component requires the assumption that the noise $\gamma(s,t)$ is normal and independent and identically distributed for all Y_t.

$$Y_t = \mu + M_t + X_t + \epsilon_Y$$

As in [WBC98] we will assume that all $Y_t(s)$ are normally distributed and conditionally independent such that:

$$Y_t|\{\mu, M_t, X_t, \sigma_Y^2\} \sim \mathcal{N}(\mu + M_t + X_t, \sigma_Y^2\mathbf{I}) \tag{4.2}$$

The spatial structures and dynamics consist of site specific means μ, a "long term" trend M_t, and a time dynamic process X_t accounting for day to day variations.

We make several departures from [WBC98] in how these spatial structures are modeled and defined in order to decrease complexity and also to better match our system. Instead of defining a Markov random field, in order to decrease run time, we first define the site specific mean to be a simple first order spatial regression:

$$\mu(s) = \mu_1 + \mu_2 l_s$$

where l_s is the physical position of sensor s. μ_1 in this case is the overall mean of the phenomenon and μ_2 represents small corrections according to spatial trends. If there is no strong spatial trend, or the trend is not linear along s then μ_2 will tend to zero and the site specific means will tend to the overall phenomenon mean at μ_1. This will make the system more robust when a linear model is not accurate.

These two parameters of μ are modeled as independent normal random variables with fixed and specified priors.

$$\mu_1 \sim \mathcal{N}(\bar{\mu_1}, \sigma^2_{\mu_1}) \tag{4.3}$$

$$\mu_2 \sim \mathcal{N}(\bar{\mu_2}, \sigma^2_{\mu_2}) \tag{4.4}$$

We model the "long term" trend as a daily harmonic with spatially varying amplitudes and phases with an additional linear trend:

$$M_t(s) = (f_1 + f_2 l_s)\cos(\omega t) + (g_1 + g_2 l_s)\sin(\omega t) + h_1 t$$

where $\omega = 2\pi$ for a daily harmonic (when t is defined in units of days). f_1,f_2,g_1,g_2 define how the harmonic varies spatially. We add the h_1 term to account for the day to day weather trend over the modeling window; this is different from [WBC98] as their long term trend is annual which has no year to year trend.

We assume all of the parameters in M_t to be independent normal random variables with fixed and specified priors.

$$f_1 \sim \mathcal{N}(\bar{f_1}, \sigma^2_{f_1}) \tag{4.5}$$

$$f_2 \sim \mathcal{N}(\bar{f_2}, \sigma^2_{f_2}) \tag{4.6}$$

$$g_1 \sim \mathcal{N}(\bar{g_1}, \sigma^2_{g_1}) \tag{4.7}$$

$$g_2 \sim \mathcal{N}(\bar{g_2}, \sigma^2_{g_2}) \tag{4.8}$$

$$h_1 \sim \mathcal{N}(\bar{h_1}, \sigma^2_{h_1}) \tag{4.9}$$

We model the time dynamic term as a "diagonal" vector autoregressive process:

$$X_t = \mathbf{H}X_{t-1} + \epsilon_X \tag{4.10}$$

where

$$\mathbf{H} = a\mathbf{I}$$

giving

$$X_t|\{X_{t-1}, \mathbf{H}, \sigma_X\} \sim \mathcal{N}(\mathbf{H}X_{t-1}, \sigma_X^2\mathbf{I}) \tag{4.11}$$

We assume that a is the same for all locations and it is normally distributed:

$$a \sim \mathcal{N}(\bar{a}, \sigma_a^2) \tag{4.12}$$

Note that the description for X_t is much simpler than in [WBC98] in order to decrease run time and speed convergence of the Gibbs sampler. We will discuss the simulation using Gibbs sampling in section 4.4. Adding off-diagonals and allowing elements in $\mathbf{H}$ to vary quickly transforms equation 4.10 into a space-time autoregressive moving average (STARMA) model, see [Cre93]. This increases complexity and the resultant model is over-parameterized and sensitive to the initial conditions in our case. Using such a model also requires us to restrict sensors to be fixed, assigned, or translated to points in a regularly spaced lattice position which is not generally true or possible in our sensor network applications.

We specify the variances of the X, Y and Z processes to have an inverse gamma distribution, which is the conjugate prior to the normal distribution:

$$\sigma_Z^2 \sim \Gamma^{-1}(\alpha_Z, \beta_Z) \tag{4.13}$$

$$\sigma_Y^2 \sim \Gamma^{-1}(\alpha_Y, \beta_Y) \tag{4.14}$$

$$\sigma_X^2 \sim \Gamma^{-1}(\alpha_X, \beta_X) \tag{4.15}$$

The prior parameters of these inverse gamma distributions are fixed and specified.

When defining our model we used prior information regarding the type of phenomenon we are expecting to measure. In general, one should seek to maximize the use of available prior information regarding the phenomenon of interest in determining the structure and parameters in a HBST model. This improves the accuracy of the model and may also reduce the complexity of the model.

Note that the prior distribution choices were made for ease in analytically deriving the conditional distributions. Alternative prior distributions can be used but may affect the complexity in the derivations of the conditional distributions for use in the Gibbs sampler as discussed in the following section.

4.4 Model simulation

Once this model has been established and given the data collected over a period of time, we determine the parameters of this model using Bayesian estimation. To do this we use Markov chain Monte Carlo methods, and more specifically the Gibbs sampler, for stochastic simulation [GCS04]. As discussed in chapter 1, instead of drawing samples of all the parameters from one massive and difficult to calculate joint distribution, Gibbs sampling draws subsets of parameters conditioned on the value of the other parameters. This allows for quicker computation and simple derivations of conditional distributions. The derivations of the conditional distributions for our model for the Gibbs sampler are provided in section 4.9.

Choices need to be made for the starting point values and the length of the simulation to run. As is required when using Gibbs samplers to ensure convergence to the true distribution, we tested on several real world data sets with a few initial pilot simulations using different starting value sets. One of the starting value sets was the estimated means of the parameters from exploratory analysis while other starting sets were dispersed throughout the target posterior density space. Visual assessment of convergence was seen to appear by 4000 iterations for all cases. Thus for use in our algorithm, the parameters were estimated using a single long simulation (10000 iterations) with the estimated mean value starting sets. We discard the first half of the data where the sequence is converging.

An additional issue with the Gibbs sampler is the fact that each sampling iteration is dependent on the previous iteration. To regain some independence in the posterior distribution samples, we thin the sampling sequence by keeping only every 50th iteration and discarding the rest. This value was found to be sufficient in providing independent samples. More information on discarding and thinning sections of a Gibbs sampling run can be found in [GCS04].

The final result of the simulation is a number of random draws for each of the parameters as well as the X_t and Y_t dynamic processes. With these, we can then apply a fault detection method.

4.5 Fault detection

The primary weakness of HBST modeling is that the posterior simulation of the model parameters using MCMC techniques and Gibbs sampling is computationally expensive. Thus, we seek to minimize the frequency that we calculate parameters by specifying a semi-realtime detection system. By having this semi-realtime system, we can exploit the capabilities of HBST modeling while minimizing the impact of the high computation cost. Instead of performing calculations with each new incoming data value as is done in systems such as the ones in chapter 3, [KPS03b], and [MPD04], calculations are to be performed at regular time intervals at a time scale larger than the sensing intervals.

That is, sensor data integrity audits occur much less frequently than sensor samples are taken. For example, while the sensor data used in this chapter measures the phenomenon on a scale of every 5 minutes, we will audit sensors every one day. This also reflects logistical realities, in that it is unlikely for sensor replacement to be on the sensing time scale in the environmental sensing

context, e.g. a person would likely wait for the next day to replace a sensor that failed while they were sleeping that night. Also it is common for a sensor to temporarily report questionable data and then return to normal [NRC08]. Therefore, by having the audit occur at larger intervals, a sensor that returns to normal operating conditions will not be as frequently tagged.

To test the abilities of HBST modeling, our goal is to tag data from sensors which are believed to be behaving outside of the modeled behavior. With this tagging, one can use the results in a more complex memory based method for fault identification. For example, the rate at which a sensor is tagged may be thresholded and identified as cooperative or non-cooperative and used in the reputation based framework as described in [GS04]. Alternatively, the tag rate may be used as a prior in a Bayesian decision method to select a subset of trusted sensors such as in chapter 3. Going further, a Bayesian network [Hec95] may be implemented with the tagging rate influencing the probabilities. However all of these possibilities are beyond the scope of this chapter. When paired with more sophisticated fault detection methods, such as those in chapter 3 and [SGG07], HBST modeling can boost performance.

We use a simplistic thresholding technique based upon nearby sensors for detection. Consider a single data point for sensor s. For sensors $s+1$ and $s-1$ we calculate 95% credible intervals of the time dynamic term $X(s_{i\pm1}, t)$ using the variance, $\hat{\sigma}^2_X$. We denote $\hat{}$ to be the sample mean across all samples from the simulated posterior parameters. We add these to the site specific mean and estimated long term trend for sensor s. Effectively, we assume that time dynamic X_t for sensor s, which is without any spatial effects as those are carried in M_t and μ, is similar for surrounding sensors. This bounds the space time dynamic performance of each sensor by the adjacent sensor's worst case performance, then

adds these bounds to the site specific mean and long term trend. In this way, sensor s is assumed, at worst, to report location adjusted values of its neighboring sensors. We will see how this assumption holds in the results.

That is, if we consider sensor s at location l_s at a particular time time t, we define the lower bound and upper bounds of the expected time dynamic term to be:

$$X_l(s,t) = \min(\hat{X}(s-1,t) - 2\hat{\sigma}_X, \hat{X}(s+1,t) - 2\hat{\sigma}_X)$$

$$X_u(s,t) = \max(\hat{X}(s-1,t) + 2\hat{\sigma}_X, \hat{X}(s+1,t) + 2\hat{\sigma}_X)$$

If sensor $s+1$ or $s-1$ does not exist, meaning s is on the edge, then we ignore those $\hat{X}$ term. Then we use the estimated terms for μ_1, μ_2, f_1, f_2, g_1, g_2, and h_1 to calculate:

$$\widetilde{\mu}(s) = \hat{\mu}_1 + \hat{\mu_2} l_s$$

$$\widetilde{M}_t(s) = (\hat{f}_1 + \hat{f}_2 l_s) cos(\omega t) + (\hat{g}_1 + \hat{g}_2 l_s) sin(\omega t) + \hat{h}_1 t$$

Finally, the lower and upper bounds are:

$$Z_l(s,t) = \widetilde{\mu}(s) + \widetilde{M}_t(s) + X_l(s,t) - 2(\hat{\sigma}_Y + \hat{\sigma}_Z)$$

$$Z_u(s,t) = \widetilde{\mu}(s) + \widetilde{M}_t(s) + X_u(s,t) + 2(\hat{\sigma}_Y + \hat{\sigma}_Z)$$

We extend the bounds using the estimated standard deviations of the phenomenon and measurement processes, $(\hat{\sigma}_Y + \hat{\sigma}_Z)$, because we compare to measured data $Z(s,t)$. If $Z(s,t)$, the actual measurement from sensor s at time t, exceeds these bounds, then it is marked as faulty.

In our results we compare this approach to modeling with an analogous method without HBST modeling. The basis of the analogous method is using first order linear autoregressive (AR) models over a window of the previous data. This linear AR modeling is the same as the one used extensively in chapter 3

which we are trying to improve upon. Also of note, [MPD04] uses first order linear models to estimate sensor behavior. [JAF06] and [MB02] smooth data using a moving average window resulting in an expected mean, which is a less complex operation than the linear modeling done in the previously mentioned works.

For the comparison modeling technique, we create bounds similar to the HBST modeling case. The estimate of the standard deviation is derived from the linear AR model for each individual sensor. For sensor s, two surrounding sensors' readings and standard deviations are used to provide a lower and upper bound. Similar tagging is used to identify readings that exceed these bounds.

When using the conventional method, a decision must be made on the size of the window, W, used to calculate the linear model. This window size, as discussed in chapter 3 affects the quality of the fit to the data. For simplicity, we fix this window size to 25 samples because after trial and error this produces the best results in most cases for our simulated data set.

The linear AR tagging method can be summarized as follows. Considering sensor s reporting data $Z(s, t_i)$ at location l_s at a time t_i, we first solve the least squares regression problem similar to chapter 3 to get the local linear AR model over the current time window of size W:

$$\begin{bmatrix} Z(s,t_{i-1}) \\ \vdots \\ Z(s,t_{i-W}) \end{bmatrix} = \begin{bmatrix} t_{i-1} & 1 \\ \vdots & \vdots \\ t_{i-W} & 1 \end{bmatrix} \begin{bmatrix} p(s) \\ q(s) \end{bmatrix}$$

will give the linear AR model for all sensors:

$$\hat{Z}(s, t_i) = p(s)\, t_i + q(s)$$

We then estimate the standard deviation using this model.

$$\hat{\sigma}_Z^2(s, t_i) = \frac{1}{W-1} \sum_{j=1}^{W} (Z(s, t_{i-j}) - \hat{Z}(s, t_{i-j}))^2$$

Then we define the bounds as:

$$Z_l(s,t_i) = \min(Z(s-1,t_i) - 2\hat{\sigma}_Z(s-1,t_i), Z(s+1,t_i) - 2\hat{\sigma}_Z(s+1,t_i))$$

$$Z_u(s,t_i) = \max(Z(s-1,t_i) + 2\hat{\sigma}_Z(s-1,t_i), Z(s+1,t_i) + 2\hat{\sigma}_Z(s+1,t_i))$$

In interpreting the results, we use two measurement metrics: detection rate, and false detection rate. We expect that better modeling will decrease the false detection rate since a well modeled system will have less anomalies. Detection rates are expected to remain similar because questionable data should still be outside of the range of any reasonable model.

This simplistic way of bounding data by neighboring sensors' worst case performances has an additional drawback in the cases of edge sensors. Sensors on the edge are only influenced by one other sensor, greatly reducing the bounds. So it is expected that edge sensors have a higher false detection rate than non-edge sensors. However, as we will see in the results, since HBST modeling adjusts for spatial differences and trends, edge false detection is reduced significantly in comparison to AR modeling.

4.6 Results

To show the applicability of HBST modeling to multiple situations, we demonstrate our method using three separate data sets. One data set is artificially generated and used as a toy example to illustrate under ideal conditions the performance of our system. The second data set is the cold air drainage data set from sensors that have been deployed at James Reserve in California. The last set of data is from a series of buoys deployed at Lake Fulmor, also at James Reserve. For this last set of data, we use the temperature measurements that are at the surface of the water.

4.6.1 Simulated Data

We use simulated data to show the expected results from both HBST and AR modeling. Spatial structure is well defined and matches very well to the assumptions made in our fault tagging scheme. Simulated data also highlights some of the limitations of our simple tagging scheme for nodes on the edge of the sensing field. We show results from data with no faults as well as injected faults to show the best performance of each system.

The simulated data consists of a daily diurnal long term trend, as well as an extra harmonic that was not modeled by the HBST model we defined in section 4.3. Spatial structure was generated using a similar model to that of section 4.3, by including a spatial trend on the site specific mean and harmonic parameters. Parameters were fixed to rough estimates derived from actual data. We generated simulated data for six sensors all equally spaced. A sample from three sensors over three days is in figure 4.2. We apply the fault tagging techniques described

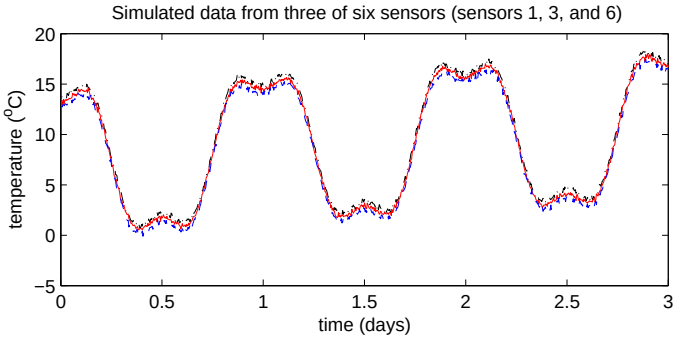

Figure 4.2: Simulated data. A sample of three days from three sensors.

in section 4.5 to get a baseline for expectations. We average the tag rates for each sensor over three days, and present the overall false detection rates in table 4.1. Also, we show the false detection rate for just the edge cases to show the increased tag rate for edge cases. As noted before, the edge cases show much

Table 4.1: False detection rates for simulated data with no faults

	HBST	**Linear AR**
Including Edge Nodes	0.2079	0.2784
Excluding Edge Nodes	0.0014	0.0041
Just Edge Nodes	0.6210	0.8270

higher false detection rates.

Examining the results of table 4.1, edge nodes have a much lower false detection rate using HBST modeling than linear AR modeling. This is expected because the HBST modeling approach is capable of modeling and correcting for spatial trends. Overall, in all cases the HBST modeling approach shows significant reductions in false detections. When including edge nodes, HBST modeling gives a 25.3% improvement over linear AR. More significantly, when edge nodes are excluded, HBST modeling gives a 64.9% improvement over linear AR.

To test detection capabilities, one day was selected to have faults injected, and we tested the detection of each fault independently. We inject two types of common faults as defined in [SGG07] and [NRC08] at arbitrary locations. In figure 4.3 we show three sensors, two with faults, and one with no faults. One sensor has a "stuck-at" fault injected, and the other has outliers. The faults were tested independently, but we show both faults in one figure for convenience.

The results for HBST modeling and linear AR modeling are shown in Figure 4.4. Outlier detection worked perfectly for both Linear AR modeling and HBST modeling. However, The HBST modeling showed a 95.9% lower false detection in comparison to linear AR modeling. One reason the HBST modeling false detection is so low is because the time dynamic uncertainty is elevated in the presence of faults, and outliers seem to affect this variance more than other faults.

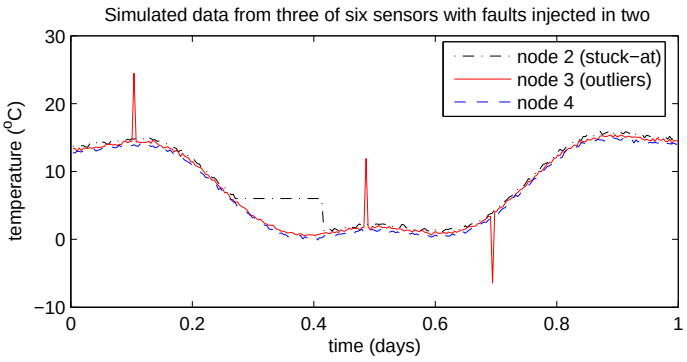

Figure 4.3: Simulated data with injected faults.

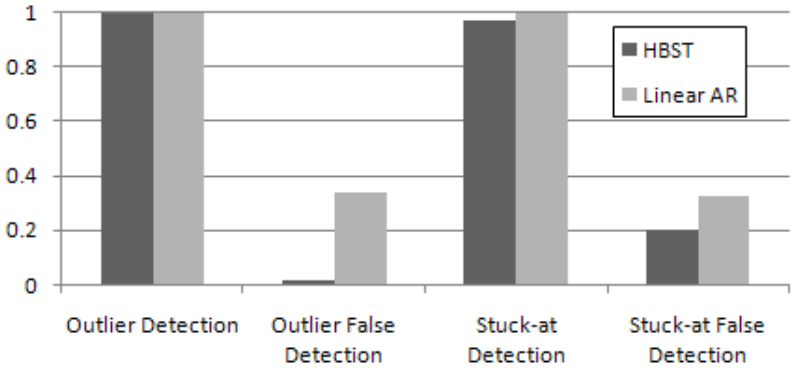

Figure 4.4: Fault detection rates for simulated data with injected faults

For the case of the stuck at fault, detection was almost equal for both cases. Although the linear AR modeling performed slightly better, the HBST modeling approach only missed one sample, which is insignificant. More significant is that HBST modeling has a 36.8% lower false detection than linear AR modeling does.

The simulated data results show that HBST modeling is superior in reducing false detection rates in all cases. Detection capability remains virtually the same. Simulated data provides us with a baseline of expected performance, and shows how the spatial modeling of HBST models is important in the edge nodes for reduction of the false detection rate.

4.6.2 Cold Air Drainage Data

Using real world data from a deployment, we examine how HBST modeling affects detection. First we examine the case where data does not exhibit any apparent errors. We examine the false detection rate of six sensors over the course of five days. Figure 4.5 shows data from the first three sensors starting on September 17, 2005. For the overall results, we look over the course of the 5 days in figure

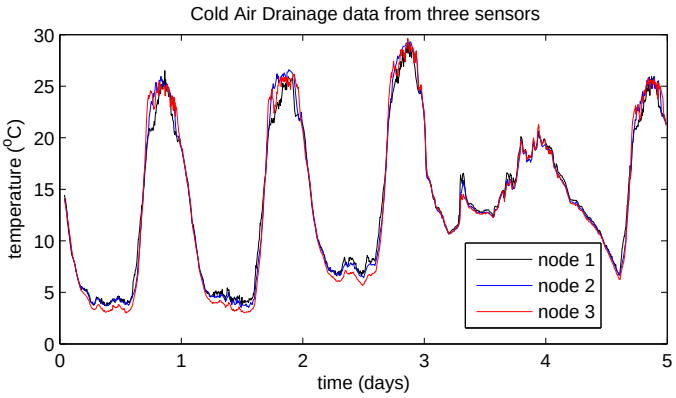

Figure 4.5: Data from three deployed sensors

4.5 and average the day to day tag rate.

The results are summarized in figure 4.6. HBST modeling gives a 42.7% lower false detection rate than linear AR modeling. Also, as expected, the edge nodes have a much higher false detection rate than the rest of the nodes. The edge cases have a false detection rate of 53.5% and 71.3% for the HBST modeling and linear AR modeling respectively. The HBST modeling is capable of reducing false detection for edge nodes due to the use of spatial means. When we exclude these values, the performance of the HBST modeling outperforms the linear AR modeling by 63.6%.

Deeper examination of the results shows that the HBST modeling tags data predominantly during the peak of the day, where the data is highly variable and

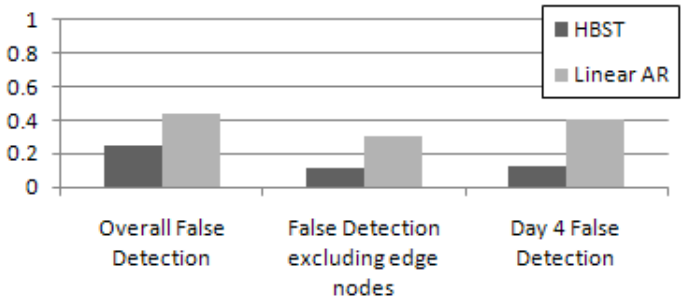

Figure 4.6: False detection rates for cold air drainage data in the absence of faults

dynamic. This is likely due to unmodeled phenomena. While our method is robust to unmodeled dynamics that are spatially correlated, these dynamics are not well correlated.

One possible cause of this is the passage of sunflecks where the sensor may be exposed to sun and shade alternatively due to the forest coverage, wind, clouds, and passage of time during the day; this causes temperature readings to rise and fall in unexpected ways. These sunflecks are highly dynamic and very difficult to model accurately. More information regarding models of sunflecks and sunlight penetration through a forest canopy can be found in [SKR89] and [RSS98]. So, it is more likely for our modeling to fail in this dynamic period.

If one were to include a model for dynamics such as sunflecks, this would undoubtedly increase the performance of the fault detection system. However, this requires much more sophistication and will likely greatly increase the computation costs of the model. This is because each sensor node is different and will have different dynamics associated with them. Also, in order to model these dynamics, information regarding the forest canopy distance from the ground and the coverage the canopy provides given the time of day and the day of the year must be obtained through more detailed measurements.

Looking across the days, we see that day 4 does not exhibit these highly variable peak temperatures, and the high temperature of the day is significantly lower than the other days. This suggests that the day may have been overcast or even rainy when sunflecks may not have existed.

If we examine only this day, then the overall false detection rate is greatly reduced when using HBST modeling. HBST modeling gives a 70.6% improvement over linear AR modeling. Linear AR modeling does not improve much since there are many correlated dynamics that are not modeled. HBST modeling is robust to unmodeled dynamics that are spatially correlated. It may be prudent to include prior knowledge in the form of daily weather patterns. If a day was noted to be overcast, then any judgments on sensor reliability may be given more weight than decisions on other days.

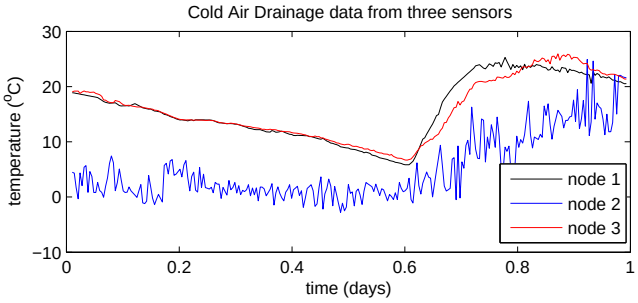

(a) Data from a faulty sensor

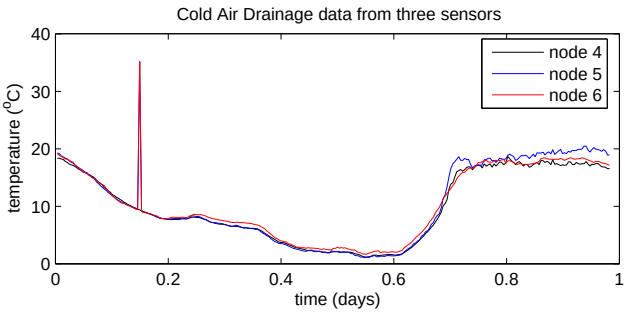

(b) Data with an outlier

Figure 4.7: Two examples of faults in real data

We now examine some examples of real data with questionable data that is assumed to be faulty. Figure 4.7(a) shows data from three sensors for one day, Sept. 25, 2005, with one sensor giving likely faulty data, with high noise and readings distant from other sensors. The other two sensors that are physically located around this sensor are also shown. Figure 4.7(b) shows data from three neighboring sensors on Sept. 16, 2005 where two independent neighboring sensors exhibit outliers at the same instant. There is no conclusive reason for why this happened, but it is important to tag such an anomaly. We test the detection rate for each fault with six sensors to model and examine the results summarized in figure 4.8. For the case of the faulty sensor in figure 4.7(a), both HBST modeling

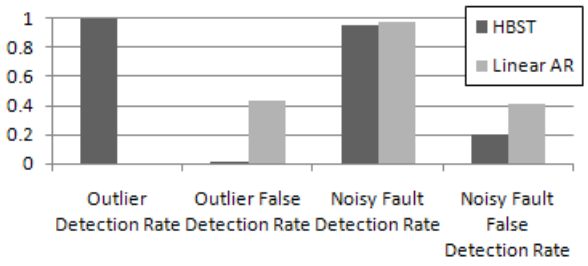

Figure 4.8: Detection and false detection rates for cold air drainage data in the presence of faults

and linear AR modeling detect the fault very well, exceeding 95% detection. However, the false detection rate for HBST modeling is 49.7% lower than linear AR modeling. For the case of the outlier fault in figure 4.7(b), HBST modeling detects the outliers perfectly while the linear AR modeling completely misses the outliers. The false detection rate is significantly lower for HBST modeling as well, giving a 96.5% lower rate.

These results show that HBST modeling is a significant improvement over linear AR modeling in both accuracy and robustness. False detection rates are

42.7% to 96.5% lower using HBST modeling in comparison to linear AR modeling. As we will see in the next set of data, this gain is not limited to one specific deployment.

4.6.3 Lake Fulmor Data

To show our method can be adapted to multiple types of deployments, we present results from a second set of real data. We use temperature data collected at the surface from sensors deployed on buoys at Lake Fulmor in James Reserve between August 28th and September 1st, 2006. Figure 4.9 shows data from three of the five sensors used in this test. Nodes 2 and 3 display likely outliers at the beginning, while node 3 shows aberrant behavior starting at approximately day 2.65. This fault at the end of the data set is due to the battery failing on this particular node.

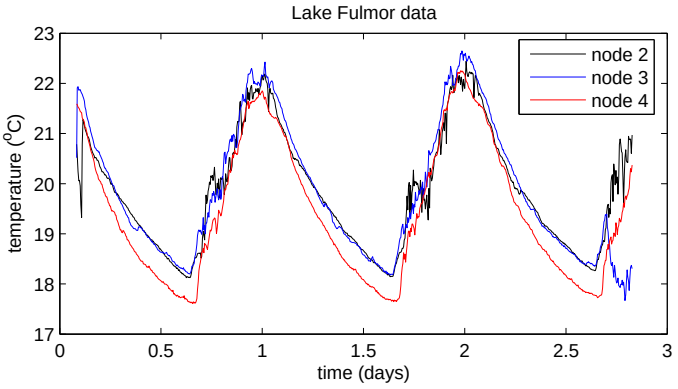

Figure 4.9: Data from three buoys at lake Fulmor

Figure 4.10 presents a summary of the results. We initially exclude the faults from modeling to test the case where faults are not present. The results are similar to the results of the cold air drainage data set of section 4.6.2. HBST modeling reduces false detections by 44.4%.

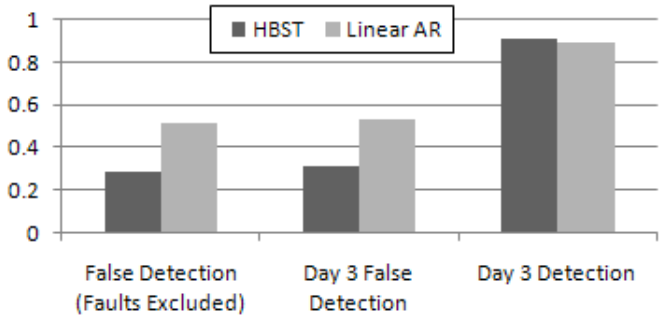

Figure 4.10: Detection and false detection for Lake Fulmor data

The linear AR modeling method is unable to capture the fault at the beginning of the data set because the fault occurs during the delay before being able to tag data that linear AR models must have when starting up. The HBST modeling does correctly identify this outlier. Focusing on the fault for node 3 at the end of the data, we see that HBST modeling outperforms linear AR modeling as expected. HBST modeling has a 41.5% lower false detection rate while having a slight 3% advantage in detection.

These results show that the new application of hierarchical Bayesian space-time modeling can produce similar, if not better, detection rates of faults, while greatly reducing the false detections which are caused by poor modeling.

4.7 Discussion

While the performance of our fault detection method has room for improvement, the overall performance of the HBST modeling is much better than the case of standard linear AR models. However, there are trade-offs in accuracy, robustness, and computation where the linear AR modeling may have an advantage. There are different opportunities where each method may be used.

The first advantage of linear AR models is that they are very simple. They are simple to understand and there are few parameters to determine given the data. This is the primary reason why they were used as the basis of the fault detection algorithm in chapter 3. On the other hand, the HBST model is much more complex with many more parameters for which we have to solve. It requires the use of posterior simulation techniques such as the Gibbs sampler used here, which in turn requires the derivation of full conditional posterior distributions.

A direct consequence of this is the computational cost. Once a window size is determined, linear AR modeling is computationally much cheaper than the HBST modeling as discussed in section 4.5. Let I be the number of iterations used in Gibbs sampling, and let W be the size of the moving window for linear AR modeling. Asymptotically the performance for the HBST modeling is $O(ITS^3)$ FLOPs while the linear AR modeling performance is $O(W^3TS)$ FLOPs. However this is not descriptive because the HBST method has much more complex calculations that are performed many more times. For the computer we used, to model and process one day's worth of data for six sensors, the conventional method takes less than a half second, while the HBST modeling takes roughly seven to eight minutes.

It may be possible to reduce the computation time of the HBST modeling approach through the use of updates to the prior distributions by tracking previously calculated parameters. This would decrease convergence time and hence decrease the overall computation cost. This is reserved for possible future directions.

The issue of window size selection in linear AR modeling may limit its computational advantage. The selection of a good window requires either good prior knowledge or retrospective analysis after acquiring a big data set. In section 4.5,

we performed several trials to determine the best window size to use for our data. Trial and error or other more systematic methods will increase the overall cost of linear AR modeling.

With linear AR modeling, human involvement may be required periodically to adjust and test different sized windows. When considering how much human involvement the HBST modeling and linear AR modeling may require in a long term deployment, the HBST modeling requires less constant supervision. HBST modeling requires high initial human involvement in the derivation of the model and distributions, but once deployed, this model is robust and requires very little involvement from day to day. On the other hand, linear AR modeling may require regular involvement throughout the deployment to tune the window sizes depending on the dynamics of each day. This may be acceptable for a one-time only short-term deployment, but it may be difficult or impractical in a long term deployment.

One usually minor disadvantage of linear AR modeling, as we have presented here, is that linear AR modeling requires at least W samples available before it can begin to work. Thus there is a delay before linear AR modeling begins tagging data. This is usually not a big deal as data from a prior day is available to begin modeling. However in the case of the Lake Fulmor data, there is no data prior to the outliers seen, and as such linear AR modeling is unable to detect this fault. It may be possible to use future samples to help predict the first few samples of the data set, but this does add some complexity to the simple linear AR modeling scheme.

The difference in accuracy of modeling can be seen in our results. Overall, the HBST modeling outperforms the linear AR modeling method. It has lower false detection rates which suggests better modeling capabilities. The linear AR

modeling outperformed in the simulated data with injected "stuck-at" and noise faults. This is likely due to the fact that HBST modeling also models uncertainty more than the linear AR modeling. If the data exhibits higher variability throughout the day, then σ_X^2 will be higher because there is less certainty. This results in larger credible intervals and lower detection rates. However, this type of uncertainty is not captured in linear AR modeling, and is apparent by the significant increase in false detection rate with real data.

Also contributing to the lack of accuracy for linear AR modeling is the fact that spatial structure is not used in modeling expected behavior. The only spatial relationship assumed is in our rudimentary tagging method. This lack of spatial modeling is most apparent in the edge cases where only one other sensor influences the tagging of an edge sensor. The HBST method is able to compensate for this and the standard linear AR modeling more than doubles the false detection rate in the edge cases.

HBST modeling is much more robust than linear AR modeling. Linear AR modeling is simple, but if data does not fit there is no correction made. However, if the model structure we assumed for μ or M_t is not accurate, the time-dynamic term, X_t will compensate for any difference between the assumed structure and the real data. The variability may increase in X_t as a result, but this will be captured in the σ_X^2 term.

It may be more useful for one to use linear AR modeling as a quick way of estimating parameters for priors in the HBST modeling. Also, HBST modeling may not be necessary in cases where sensor deployment is dense since there is likely to be less spatial variation. However, once priors are estimated or given then HBST modeling may be utilized to monitor the network. If the network is also sparsely deployed, then spatial structure is more important to estimate and

utilize in fault detection. This is where HBST modeling holds the advantage.

4.8 Conclusion

We have presented a new approach to fault detection by modifying the existing hierarchical Bayesian space-time modeling technique of [WBC98]. While it is much more complex than the first order linear AR modeling method, the results show that additional modeling greatly increases the performance of a fault detection system. It reduces the false detection rate significantly while maintaining good detection ability. In some cases, it is more capable in detecting outliers.

There are cases where our models break down, as in the case of the peak temperatures during the day time. In both linear AR modeling and HBST modeling, humans must be involved when there are unmodeled dynamics to identify whether or not the data is truly faulty. Additionally, linear AR modeling may require human involvement in the selection of window sizes. In the future, better modeling can be utilized in these cases to increase the performance.

While we have paired our modeling with a simple fault tagging system here, more complex systems that include historical behavior may produce bigger gains than we have seen with our simple system. In the following chapter, we pair this complex modeling with a modified version of the maximum a posteriori sensor subset selection method discussed in chapter 3 to realize some of these gains in system performance.

4.9 Appendix: Derivations of full conditional probability distributions

It is computationally efficient to use a Gibbs sampler to obtain draws from the joint posterior distribution. With the conditional independence assumptions afforded by the hierarchical model structure, we can easily derive the conditional distributions needed in the Gibbs sampler.

Many of the derivations are similar to those detailed in the appendix of [WBC98] with some minor changes. Here we detail the derivations for the conditional distributions which have changed due to the modeling differences we make. For completeness, we also reproduce the derivations for distributions that are mostly unchanged (aside from notation) from [WBC98], which are $p(X_t|\cdot)$, $p(\sigma_X^2|\cdot)$, and $p(\sigma_Y^2|\cdot)$.

The derivations make use of Bayes rule:

$$\begin{aligned} p(A|B) &= \frac{p(B|A)p(A)}{p(B)} \\ &\propto p(B|A)p(A) \end{aligned}$$

Also, as in [WBC98], a "completing the squares" method is extensively used in the derivations which we reproduce here. For a parameter vector θ, if the full conditional distribution is:

$$p(\theta|\cdot) \propto \exp(-\frac{1}{2}[\theta^T A\theta - 2B\theta])$$

then, after completing the square

$$\theta|\cdot \sim \mathcal{N}(A^{-1}B^T, A^{-1})$$

4.9.1 $p(Y_t|\cdot)$

From Bayes rule, we start with:

$$p(Y_t|\cdot) \propto p(Z_t|Y_t, \sigma_Z^2)\; p(Y_t|\mu, M_t, X_t, \sigma_Y^2)$$

Using the distributions for Z_t and Y_t as defined in equations 4.1 and 4.2 respectively, we get:

$$\begin{aligned} p(Y_t|\cdot) \;\; \propto \;\; & \exp\{-\frac{1}{2\sigma_Z^2}(Z_t - Y_t)^T(Z_t - Y_t)\} \\ & \times \exp\{-\frac{1}{2\sigma_Y^2}(Y_t - [\mu + M_t + X_t])^T \\ & \times (Y_t - [\mu + M_t + X_t])\} \end{aligned}$$

Define $B = \mu + M_t + X_t$.

$$\begin{aligned} p(Y_t|\cdot) \;\; \propto \;\; & \exp\{-\frac{1}{2\sigma_Z^2}(Z_t^T Z_t - Z_t^T Y_t - Y_t^T Z_t + Y_t^T Y_t) \\ & -\frac{1}{2\sigma_Y^2}(Y_t^T Y_t - Y_t^T B - B^T Y_t + B^T B)\} \end{aligned}$$

We drop the terms that do not involve Y_t as they can be extracted as constants for normalization.

$$\begin{aligned} p(Y_t|\cdot) \;\; \propto \;\; & \exp\{-\frac{1}{2}\, Y_t^T(\frac{1}{\sigma_Z^2}\mathbf{I} + \frac{1}{\sigma_Y^2}\mathbf{I})Y_t \\ & +(\frac{1}{\sigma_Z^2}Z_t^T + \frac{1}{\sigma_Y^2}B^T)Y_t\} \\ \propto \;\; & \exp\{-\frac{1}{2}(Y_t^T(\frac{1}{\sigma_Z^2}\mathbf{I} + \frac{1}{\sigma_Y^2}\mathbf{I})Y_t \\ & -2(\frac{1}{\sigma_Z^2}Z_t^T + \frac{1}{\sigma_Y^2}B^T)Y_t)\} \end{aligned}$$

Thus:

$$\begin{aligned} Y_t|\cdot \;\; \sim \;\; & \mathcal{N}((\frac{1}{\sigma_Z^2}\mathbf{I} + \frac{1}{\sigma_Y^2}\mathbf{I})^{-1}(\frac{1}{\sigma_Z^2}Z_t^T + \frac{1}{\sigma_Y^2}B^T)^T, \\ & (\frac{1}{\sigma_Z^2}\mathbf{I} + \frac{1}{\sigma_Y^2}\mathbf{I})^{-1}) \end{aligned} \tag{4.16}$$

for all $t = 1, \ldots, T$.

4.9.2 $p(\mu_1, \mu_2|\cdot)$

Define the design matrix for all sensors s, $s = 1, \ldots, S$ with positions l_s to be:

$$\mathbf{P} = \begin{bmatrix} \vdots & \vdots \\ \mathbf{1} & l_s \\ \vdots & \vdots \end{bmatrix} \tag{4.17}$$

And define

$$\mu_L = \begin{bmatrix} \mu_1 \\ \mu_2 \end{bmatrix}$$

such that $\mu = \mathbf{P}\mu_L$. Also define

$$\Sigma_\mu = \begin{bmatrix} \sigma^2_{\mu_1} & 0 \\ 0 & \sigma^2_{\mu_2} \end{bmatrix}$$

Furthermore, define $\bar{\mu_L} = [\bar{\mu_1}\ \bar{\mu_2}]^T$. From the formulations of the distributions for μ_1, μ_2, and Y_t from equations 4.3, 4.4, and 4.2 respectively:

$$\begin{aligned} p(\mu_L|\cdot) &\propto p(\mu_L|\bar{\mu_1}, \bar{\mu_2}, \sigma^2_{\mu_1}, \sigma^2_{\mu_2}) \prod_{t=1}^{T} p(Y_t|\mu, M_t, X_t, \sigma^2_y) \\ &\propto \exp\big(-\frac{1}{2}(\mu_L - \bar{\mu_L})^T \Sigma_\mu^{-1}(\mu_L - \bar{\mu_L})\big) \\ &\quad \times \exp\big(-\frac{1}{2\sigma^2_Y}\sum_{t=1}^{T}(Y_t - (\mathbf{P}\mu_L + M_t + X_t))^T \\ &\quad \times (Y_t - (\mathbf{P}\mu_L + M_t + X_t))\big) \\ &\propto \exp\big(-\frac{1}{2}(\mu_L^T(\Sigma_\mu^{-1} + \frac{1}{\sigma^2_Y}\sum_{t=1}^{T}\mathbf{P}^T\mathbf{P})\mu_L) \\ &\quad -2(\mu_L^T\Sigma_\mu^{-1} + \frac{1}{\sigma^2_Y}\sum_{t=1}^{T}(Y_t - M_t - X_t)^T\mathbf{P})\mu_L)\big) \end{aligned}$$

This gives:

$$\mu_L|\cdot \ \sim \ \mathcal{N}((\Sigma_\mu^{-1} + \frac{T}{\sigma^2_Y}\mathbf{P}^T\mathbf{P})^{-1}(\mu_L^T\Sigma_\mu^{-1}$$

$$+\frac{1}{\sigma_Y^2}\sum_{t=1}^{T}(Y_t - M_t - X_t)^T\mathbf{P}),$$
$$(\Sigma_\mu^{-1} + \frac{T}{\sigma_Y^2}\mathbf{P}^T\mathbf{P})^{-1}) \tag{4.18}$$

4.9.3 $p(f|\cdot)$, $p(g|\cdot)$, and $p(h|\cdot)$

These derivations follow closely to [WBC98] with some changes to accommodate h_1. First we define $f_L = [f_1\, f_2]^T$, and similarly define $g_L = [g_1\, g_2]^T$. Then we can write M_t as:

$$M_t = \mathbf{P}f_L\cos(\omega t) + \mathbf{P}g_L\cos(\omega t) + h_1 t\vec{\mathbf{1}}$$

where $\mathbf{P}$ is the design matrix defined in equation 4.17.

Let $\bar{f_L} = [\bar{f_1}\ \bar{f_2}]^T$ and $\bar{g_L} = [\bar{g_1}\ \bar{g_2}]^T$. Also, define $\Sigma_f = [\sigma_{f_1}^2\ \sigma_{f_2}^2]\mathbf{I}$ and $\Sigma_g = [\sigma_{g_1}^2\ \sigma_{g_2}^2]\mathbf{I}$.

We first derive $p(f_L|\cdot)$:

$$\begin{aligned}
p(f_L|\cdot) &\propto p(f_L|\bar{f_L}, \Sigma_f)\prod_{t=1}^{T} p(Y_t|\mu, X_t, f_L, g_L, h_1, \sigma_Y^2) \\
&\propto \exp(-\frac{1}{2}(f_L - \bar{f_L})^T\Sigma_f^{-1}(f_L - \bar{f_L})) \\
&\quad \times \exp\Big(-\frac{1}{2\sigma_Y^2}\sum_{t=1}^{T}[Y_t - (\mu + \mathbf{P}f_L\cos(\omega t) \\
&\quad +\mathbf{P}g_L\sin(\omega t) + h_1 t\vec{\mathbf{1}} + X_t)]^T[Y_t - (\mu \\
&\quad +\mathbf{P}f_L\cos(\omega t) + \mathbf{P}g_L\sin(\omega t) + h_1 t\vec{\mathbf{1}} + X_t)]\Big) \\
&\propto \exp\Big(-\frac{1}{2}(f_L^T(\Sigma_f^{-1} + \frac{1}{\sigma_Y^2}\sum_{t=1}^{T}\cos(\omega t)^2\mathbf{P}^T\mathbf{P}) \\
&\quad \times f_L - 2(\bar{f_L}^T\Sigma_f^{-1} + \frac{1}{\sigma_Y^2}\sum_{t=1}^{T}(Y_t - (\mu \\
&\quad +\mathbf{P}g_L\sin(\omega t) + h_1 t\vec{\mathbf{1}} + X_t))^T\mathbf{P}\cos(\omega t))f_L)\Big)
\end{aligned}$$

This gives:

$$\begin{aligned} f_L|\cdot &\sim \mathcal{N}\Big((\Sigma_f^{-1} + \frac{1}{\sigma_Y^2}\sum_{t=1}^{T}\cos(\omega t)^2\mathbf{P}^T\mathbf{P})^{-1}(\bar{f_L}^T\Sigma_f^{-1} \\ &+\frac{1}{\sigma_Y^2}\sum_{t=1}^{T}(Y_t - (\mu + \mathbf{P}g_L\sin(\omega t) + h_1 t\vec{\mathbf{1}} + X_t))^T \\ &\times\mathbf{P}\cos(\omega t))^T, (\Sigma_f^{-1} + \frac{1}{2}\sum_{t=1}^{T}\cos(\omega t)^2\mathbf{P}^T\mathbf{P})^{-1}\Big) \end{aligned}$$

Similarly for $p(g_L|\cdot)$ we have:

$$\begin{aligned} g_L|\cdot &\sim \mathcal{N}\Big((\Sigma_g^{-1} + \frac{1}{\sigma_Y^2}\sum_{t=1}^{T}\sin(\omega t)^2\mathbf{P}^T\mathbf{P})^{-1}(\bar{g_L}^T\Sigma_g^{-1} \\ &+\frac{1}{\sigma_Y^2}\sum_{t=1}^{T}(Y_t - (\mu + \mathbf{P}f_L\cos(\omega t) + h_1 t\vec{\mathbf{1}} + X_t))^T \\ &\times\mathbf{P}\sin(\omega t))^T, (\Sigma_g^{-1} + \frac{1}{2}\sum_{t=1}^{T}\sin(\omega t)^2\mathbf{P}^T\mathbf{P})^{-1}\Big) \end{aligned}$$

And finally for $p(h_1|\cdot)$ we have:

$$\begin{aligned} h_1|\cdot &\sim \mathcal{N}\Big((\frac{1}{\sigma_{h_1}^2} + \frac{S}{\sigma_Y^2}\sum_{t=1}^{T}t^2)^{-1}(\frac{\bar{h_1}}{\sigma_{h_1}^2} + \frac{1}{\sigma_Y^2}\sum_{t=1}^{T}(Y_t \\ &-(\mu + \mathbf{P}f_L\cos(\omega t) + \mathbf{P}g_L\sin(\omega t) + X_t))^T\vec{\mathbf{1}}t) \\ &, (\frac{1}{\sigma_{h_1}^2} + \frac{S}{\sigma_Y^2}\sum_{t=1}^{T}t^2)^{-1}\Big) \end{aligned}$$

Where S is the number of sensors.

4.9.4 $p(a|\cdot)$

Recall:

$$\begin{aligned} \mathbf{H}X_{t-1} &= a\mathbf{I}X_{t-1} \\ &= aX_{t-1} \end{aligned}$$

Then:

$$p(a|\cdot) \propto p(a|\bar{a}, \sigma_a^2)\prod_{t=1}^{T}p(X_t|X_{t-1}, a, \sigma_X^2)$$

$$\begin{aligned} &\propto \exp(-\frac{1}{2\sigma_a^2}(a-\bar{a})^2)\exp(-\frac{1}{2\sigma_X^2} \\ &\quad \times\sum_{t=1}^{T}(X_t - aX_{t-1})^T(X_t - aX_{t-1})) \\ &\propto \exp(-\frac{1}{2}(a^2(\frac{1}{\sigma_X^2}\sum_{t=1}^{T}X_{t-1}^T X_{t-1} + \frac{1}{\sigma_a^2}) \\ &\quad -2(\frac{1}{\sigma_X^2}\sum_{t=1}^{T}X_t^T X_{t-1} + \frac{\bar{a}}{\sigma_a^2})a)) \end{aligned}$$

Thus we have that:

$$\begin{aligned} a|\cdot \;\sim\; &\mathcal{N}\Big((\frac{1}{\sigma_X^2}\sum_{t=1}^{T}X_{t-1}^T X_{t-1} + \frac{1}{\sigma_a^2})^{-1} \\ &\times(\frac{1}{\sigma_X^2}\sum_{t=1}^{T}X_t^T X_{t-1} + \frac{\bar{a}}{\sigma_a^2}) \\ &,(\frac{1}{\sigma_X^2}\sum_{t=1}^{T}X_{t-1}^T X_{t-1} + \frac{1}{\sigma_a^2})^{-1}\Big) \end{aligned}$$

4.9.5 $p(X_t|\cdot)$

This derivation and distribution is largely unchanged from [WBC98]. We reproduce it here with the associated notation changes to fit our model.

Recall that we have assumed in equation 4.2:

$$Y_t|\{\mu, M_t, X_t, \sigma_Y^2\} \sim \mathcal{N}(\mu + M_t + X_t, \sigma_Y^2\mathbf{I})$$

And also equation 4.11 gives:

$$X_t|\{X_{t-1}, \mathbf{H}, \sigma_X\} \sim \mathcal{N}(\mathbf{H}X_{t-1}, \sigma_X^2\mathbf{I})$$

For $t = 1, \ldots, T-1$,

$$\begin{aligned} p(X_t|\cdot) \;\propto\; &p(Y_t|\mu, M_t, X_t, \sigma_Y^2)p(X_{t+1}|X_t, \mathbf{H}, \sigma_X^2) \times \\ &p(X_t|X_{t-1}, \mathbf{H}, \sigma_X^2) \end{aligned}$$

$$
\begin{aligned}
\propto \;& \exp\Big(-\frac{1}{2}\Big(\frac{1}{\sigma_Y^2}(Y_t-(\mu+M_t+X_t))^T(Y_t-(\mu+M_t+X_t))+ \\
& \frac{1}{\sigma_X^2}(X_t-\mathbf{H}X_{t-1})^T(X_t-\mathbf{H}X_{t-1})+ \\
& \frac{1}{\sigma_X^2}(X_{t+1}-\mathbf{H}X_t)^T(X_{t+1}-\mathbf{H}X_t)\Big)\Big) \\
\propto \;& \exp\Big(-\frac{1}{2}\Big(X_t^T(\frac{1}{\sigma_Y^2}\mathbf{I}+\frac{1}{\sigma_X^2}\mathbf{H}^T\mathbf{H}+\frac{1}{\sigma_X^2}\mathbf{I})X_t- \\
& 2(\frac{1}{\sigma_Y^2}(Y_t-\mu-M_t)^T+\frac{1}{\sigma_X^2}X_{t+1}^T\mathbf{H}+\frac{1}{\sigma_X^2}X_{t-1}^T\mathbf{H}^T)X_t\Big)\Big)
\end{aligned}
$$

where the initial condition X_0 is needed.

$$
X_t|\cdot \;\sim\; \mathcal{N}\Big(C^{-1}(\frac{1}{\sigma_Y^2}(Y_t-\mu-M_t)^T+\frac{1}{\sigma_X^2}X_{t+1}^T\mathbf{H}+\frac{1}{\sigma_X^2}X_{t-1}^T\mathbf{H}^T)^T, C^{-1}\Big)
$$

where $C=\frac{1}{\sigma_Y^2}\mathbf{I}+\frac{1}{\sigma_X^2}\mathbf{H}^T\mathbf{H}+\frac{1}{\sigma_X^2}\mathbf{I}$.

For $t=T$

$$
p(X_t|\cdot)\propto p(Y_T|\mu,M_T,X_T,\sigma_Y^2)p(X_T|X_{T-1},\mathbf{H},\sigma_X^2)
$$

gives

$$
\begin{aligned}
X_T|\cdot \;\sim\; & \mathcal{N}\Big((\frac{1}{\sigma_Y^2}\mathbf{I}+\frac{1}{\sigma_X^2}\mathbf{I})^{-1}(\frac{1}{\sigma_Y^2}(Y_T-\mu-M_T)^T+\frac{1}{\sigma_X^2}X_{T-1}^T\mathbf{H}^T)^T, \\
& (\frac{1}{\sigma_Y^2}\mathbf{I}+\frac{1}{\sigma_X^2}\mathbf{I})^{-1}\Big)
\end{aligned}
$$

For the initial condition X_0. Assuming that $X_0|\mu_{X_0},\Sigma_{X_0}\sim\mathcal{N}(\mu_{X_0},\Sigma_{X_0})$ will give:

$$
\begin{aligned}
X_0|\cdot \;\sim\; & \mathcal{N}\Big((\frac{1}{\sigma_X^2}\mathbf{H}^T\mathbf{H}+\Sigma_{X_0}^{-1})^{-1}(\frac{1}{\sigma_X^2}X_1^T\mathbf{H}+\mu_{X_0}\Sigma_{X_0}^{-1})^T, \\
& (\frac{1}{\sigma_X^2}\mathbf{H}^T\mathbf{H}+\Sigma_{X_0}^{-1})^{-1}\Big)
\end{aligned}
$$

4.9.6 $p(\sigma_Z^2|\cdot)$

We define the inverse gamma distribution slightly differently in our derivation than [WBC98], though this makes no difference in the final result. We use the

inverse scale parameter β whereas [WBC98] uses a normal scale parameter $\tilde{r}$ such that $\frac{1}{\beta} = \tilde{r}$.

Note that in [WBC98] m represents the number of sampling locations and S represents the number of lattice locations on a grid for which the model will be regularized to. As discussed in section 4.3, we do not use a lattice structure, so for our purposes $m = S$. Also, the $m \times S$ mapping matrix K becomes a $S \times S$ identity matrix which simplifies the derivation.

For $p(\sigma_Z^2|\cdot)$:

$$\begin{aligned}
p(\sigma_Z^2|\cdot) &\propto \prod_{t=1}^{T} p(Z_t|Y_t, \sigma_Z^2) p(\sigma_Z^2|\alpha_Z, \beta_Z) \\
&\propto \frac{1}{(\sigma_Z^2)^{\frac{ST}{2}}} \exp\Big(- \frac{1}{2\sigma_Z^2} \sum_{t=1}^{T} (Z_t - Y_t)^T (Z_t - Y_t) \Big) \times \\
&\quad \frac{\beta_Z^{\alpha_Z}}{\Gamma(\alpha_Z)} \frac{1}{(\sigma_Z^2)^{\alpha_Z+1}} \exp\Big(- \frac{\beta_Z}{\sigma_Z^2} \Big) \\
&\propto \frac{1}{(\sigma_Z^2)^{\frac{ST}{2}+\alpha_Z+1}} \exp\Big(- \frac{1}{2\sigma_Z^2} \sum_{t=1}^{T} (Z_t - Y_t)^T (Z_t - Y_t) - \frac{\beta_Z}{\sigma_Z^2} \Big) \\
&\propto \frac{1}{(\sigma_Z^2)^{\frac{ST}{2}+\alpha_Z+1}} \exp\Big(- \frac{1}{\sigma_Z^2} (\beta_Z + \frac{1}{2} \sum_{t=1}^{T} (Z_t - Y_t)^T (Z_t - Y_t)) \Big)
\end{aligned}$$

Which gives:

$$p(\sigma_Z^2|\cdot) \sim \Gamma^{-1}\Big(\frac{ST}{2} + \alpha_Z, (\beta_Z + \frac{1}{2} \sum_{t=1}^{T} (Z_t - Y_t)^T (Z_t - Y_t)) \Big)$$

4.9.7 $p(\sigma_Y^2|\cdot)$ and $p(\sigma_X^2|\cdot)$

The derivations for $p(\sigma_Y^2|\cdot)$ and $p(\sigma_X^2|\cdot)$ follow closely to that of $p(\sigma_Z^2|\cdot)$. For $p(\sigma_Y^2|\cdot)$:

$$p(\sigma_Y^2|\cdot) \propto \prod_{t=1}^{T} p(Y_t|\mu, M_t, X_t, \sigma_Y^2) p(\sigma_Y^2|\alpha_Y, \beta_Y)$$

gives

$$\sigma_Y^2|\cdot \sim \Gamma^{-1}\Big(\frac{ST}{2} + \alpha_Y, (\beta_Y + \frac{1}{2} \sum_{t=1}^{T} (Y_t - \mu - M_t - X_t)^T \times$$

$$(Y_t - \mu - M_t - X_t))\Big)$$

Similarly for $p(\sigma_X^2|\cdot)$:

$$p(\sigma_X^2|\cdot) \propto \prod_{t=1}^{T} p(X_t|\mathbf{H}, X_{t-1}, \sigma_X^2) p(\sigma_X^2|\alpha_X, \beta_X)$$

gives

$$\begin{aligned} \sigma_X^2|\cdot \quad \sim \quad & \Gamma^{-1}\Big(\frac{ST}{2} + \alpha_X, (\beta_X + \frac{1}{2}\sum_{t=1}^{T}(X_t - \mathbf{H}X_{t-1})^T \times \\ & (X_t - \mathbf{H}X_{t-1}))\Big) \end{aligned}$$

CHAPTER 5

End to end implementation of Bayesian sensor selection combined with hierarchical Bayesian space-time modeling

5.1 Introduction

In chapter 3 we first introduced a method to select the most similar sensors based on the Bayesian maximum a posteriori (MAP) criterion. However, the first order linear autoregressive (AR) models that we used to estimate the expected behavior of the data were not accurate and reduced the effectiveness of the final fault detection scheme. Chapter 4 introduces a more accurate hierarchical Bayesian space-time (HBST) modeling technique to model sensor data. This technique was shown to be much more accurate and reduced the false detection rate significantly when compared to the linear AR modeling method. However the fault detection scheme was overly simplistic and suffered from some drawbacks.

In this chapter we seek to resolve the deficiencies of the two methods presented in both chapters by combining the two components into one end-to-end system. In pairing the MAP selection method with the HBST modeling, we can remove several artificial assumptions and decisions made in chapters 3 and 4. Recalling the design principles presented chapter 3 in table 3.1, we better model the phenomenon being sensed using the HBST modeling instead of restricting

the phenomenon to being a "smoothly" varying field. With a better model, we can also more accurately determine the expected behavior of the phenomenon. Consequently, we can better determine whether or not the data is faulty.

This chapter is organized as follows. In section 5.2, we first discuss the assumptions that we make and how some may differ from previous chapters. In section 5.3, we introduce the end-to-end Bayesian implementation of our fault detection system which is broken up into two phases. We also discuss several issues that are resolved by combining the MAP selection method with HBST modeling. We then apply our method to the three datasets used in chapter 4 to see the effectiveness of this end-to-end Bayesian system. The results presented in section 5.4 show that this system can be effective in some situations, but when an environment is under-sampled and the model is inaccurate, then this system has trouble.

5.2 System and Assumptions

In this chapter we still assume the same system setup as previous chapters. As in section 2.3.1 and figure 3.2, all of the data from S sensors is forwarded to the fusion center where data processing and fault analysis occurs. Corrupted or missing data communication packets are ignored and treated as unavailable.

Since we now use HBST modeling to model the phenomenon, we can refine or remove some of the vague assumptions placed on the phenomenon in chapter 3. In the MAP selection algorithm, the phenomenon was assumed to be smoothly varying across both space and time. The temporal smoothness was to allow for the use of local first order linear autoregressive models. The spatial smoothness assumption was to allow for comparison of just data trends between sensors.

With the HBST modeling presented in chapter 4, both of these assumptions are refined to fit our defined models in section 4.3.

Sensor measurements are assumed to include normal additive noise as well as the phenomenon process. The phenomenon process itself is composed of several components in addition to normal additive noise. The phenomenon is assumed to have a long term diurnal trend with an additional day to day linear trend. Each sensor has a site specific mean that is assumed to have a spatial linear trend. The phenomenon also has a time dynamic term which is assumed to be a diagonal vector autoregressive process.

Additionally, the detection algorithm in chapter 3 assumes that faults are relatively persistent, lasting at least as long as the defined model estimation window length. Since we no longer do such a windowing operation, this assumption is effectively removed, and faults can be very short. This allows for the possibility of single point outlier detection, which is one of the most common faults. Finally, chapter 3 assumes that a minimum of $\frac{S}{2}$ sensors must not be faulty at any given time. In this chapter, we increase this to be a minimum of $\lfloor \frac{S}{2} \rfloor + 1$ to avoid any confusion and to have a firm majority of sensors in the agreeing subset.

Also, since we use HBST modeling, we use the binning technique introduced in 4.2 to have synchronous data. This requires that we must make the same assumptions. We require that there are no large data gaps, linear interpolation between data is effective when there is a missing point, and the actual process variation where there is a missing point is low. This method is more accurate than linear interpolation over a window, which is done in chapter 3

5.3 End-to-end Bayesian implementation

We first introduce the end-to-end Bayesian implementation, and then we will discuss how this system improves upon the previous systems. Similar to the MAP selection system in chapter 3, we divide the system into the same two phases. The first phase will use the MAP criterion to determine a set of agreeing subsets. The second phase will make a final determination as to whether certain data is faulty or not. An overview of this process and its major steps is presented in figure 5.1. In the figure, we have also noted in italics the major design issues first introduced in table 3.1.

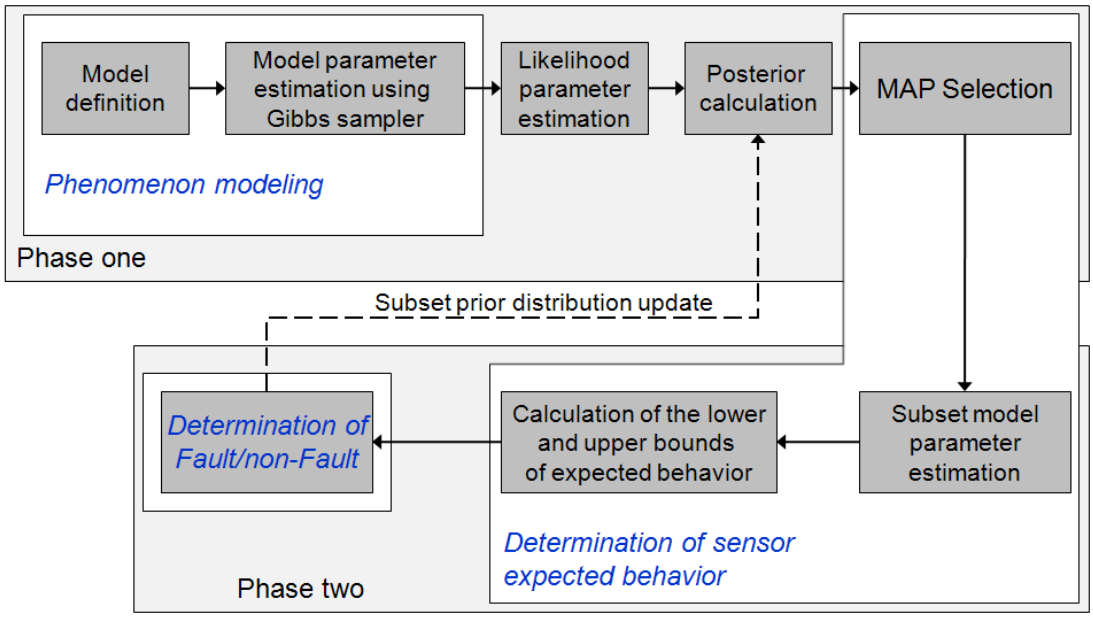

Figure 5.1: Flow of the end-to-end Bayesian fault detection system

5.3.1 Phase One

We begin the first phase by modeling data from all of the sensors over the course of the modeling window of size T, which is usually one day in our case. We use

the HBST modeling approach developed in chapter 4. The measurement process Z_t is the phenomenon process with additive normal noise:

$$Z_t|\{Y_t, \sigma_Z^2\} \sim \mathcal{N}(Y_t, \sigma_Z^2\mathbf{I})$$

The phenomenon process consists of a site specific mean, $\mu(s)$, which has a first order linear trend in space, a daily harmonic with an additional linear day-to-day linear trend in time, $M_t(s)$, a time dynamic "diagonal" vector autoregressive process X, and some additive normal noise with variance σ_Y^2. This gives

$$Y_t|\{\mu, M_t, X_t, \sigma_Y^2\} \sim \mathcal{N}(\mu + M_t + X_t, \sigma_Y^2\mathbf{I})$$

For further details on how each one of these subcomponents are modeled, refer to section 4.2. By using the Gibbs sampler we will have samples from distributions for each of the parameters in the model.

Once we have the parameters of this model, we can then begin the selection of the subset of agreeing sensors. For this step, we use the time dynamic term X_t as the basis of our decision. This is similar to the MAP selection system approach of chapter 3 where the data offsets are removed before the calculation of the likelihood. The time dynamic term removes all modeled trends, and only leaves unmodeled time dynamics to compare. This assumes that we have captured all of the space-time processes in our HBST model, resulting in the assumption that all time dynamic variations should be the same for each location.

As in section 4.5, we let the symbol $\hat{}$ represent the sample mean across all samples for the simulated posterior parameters. The first task is to estimate the covariance of this $\hat{X}$ term. Note that in our model, we modeled the vector autoregressive noise term to be independent spatial white noise for simplicity and simulation convergence reasons. However, here we no longer hold that X_t has no

instantaneous spatial interaction, correcting for this deficiency. So, we first must determine the expected mean before we can estimate the covariance for $\hat{X}$.

We use a similar approach to that of section 3.4.2.1 where the mean for sensor s is determined by all other sensors excluding s. That is, for sensor $s = 1, \ldots, S$ at time $t = 1, \ldots, T$ we define the mean to be:

$$\bar{X}_t(s) = \frac{1}{S-1}\Big(\sum_{r=1}^{s-1} \hat{X}_t(r) + \sum_{r=s+1}^{S} \hat{X}_t(r)\Big)$$

With this mean, we estimate the components of the covariance, Λ for $\hat{X}$ as:

$$\Lambda_{nm} = \frac{1}{T}\sum_{t=1}^{T}(\hat{X}_t(n) - \bar{X}_t(n))(\hat{X}_t(m) - \bar{X}_t(m))$$

Following a similar approach as the MAP selection method in chapter 3, we evaluate the likelihood for all size $\lfloor \frac{S}{2} \rfloor + 1$ subsets, ϕ. We define the covariance for the subset ϕ, Λ_ϕ to be Λ with the appropriate rows and columns removed as indicated by ϕ. Similarly, the mean $\bar{X}_{t,\phi}$ and data $\hat{X}_{t,\phi}$, has the appropriate values of the vector removed indicated by ϕ. For each subset, we calculate the likelihood $f(\hat{X}_t(s)|\phi)$ to be:

$$f(\hat{X}_t(s)|\phi) = \frac{1}{(2\pi)^{\frac{K}{2}}|\Lambda_\phi|^{\frac{1}{2}}} \exp\Big(-\frac{1}{2}(\hat{X}_{t,\phi} - \bar{X}_{t,\phi})^T \Lambda_\phi^{-1}(\hat{X}_{t,\phi} - \bar{X}_{t,\phi})\Big)$$

K is the number of subsets in consideration.

In order to calculate the maximum a posteriori criterion, $P(\phi|\hat{X}_t)$, at time instant t, we only need the prior probabilities $P(\phi)$. Initially, this can be set to be a uniform distribution indicating that there is no prior knowledge as to whether one sensor or subset is better than the others. This distribution is then updated each successive day we model according to the results of the fault detection in the second phase of the end-to-end system. Given the prior and the likelihood, the MAP criterion for a time instant t can be computed in a similar fashion as

chapter 3:

$$P(\phi|\hat{X}_t) = \frac{f(\hat{X}_t(s)|\phi)P(\phi)}{\sum_{all\,\phi} f(\hat{X}_t(s)|\phi)P(\phi)}$$

Finally, to select the overall best subset, $\tilde{\phi}$, used to develop a model of expected behavior, we average over all $t = 1, \ldots, T$ this posterior value and select the maximum:

$$\tilde{\phi} = \arg\max_{all\,\phi} \mathbf{E}_t[P(\phi|\hat{X}_t)]$$

5.3.2 Phase Two

We can now use the agreeing subset of sensors, $\tilde{\phi}$, to develop the model of expected behavior for all sensors. Using just the sensors included in $\tilde{\phi}$, we reapply our HBST modeling technique to obtain new samples from the distributions for the model parameters. The new parameters based off of this subset, are averaged across all of the Gibbs sampling draws to produce the mean of all distributions, $\tilde{X}_t$, $\tilde{\sigma}_X^2$, $\tilde{\sigma}_Y^2$, $\tilde{\sigma}_Z^2$, $\tilde{\mu}_1$, $\tilde{\mu}_2$, $\tilde{f}_1$, $\tilde{f}_2$, $\tilde{g}_1$, $\tilde{g}_2$, and $\tilde{h}_1$.

For the determination of a data fault, we modify the fault detection method presented in section 4.5. We determine the bounds of the process $Z_l(s,t)$ and $Z_u(s,t)$ and compare the actual data to these bounds.

To do this, we first determine the limits on the time dynamic term at a time t using the estimates of $\tilde{X}_t$ for the sensors in the subset $\tilde{\phi}$. Instead of using just two neighboring sensors to calculate the bounds, as is done in section 4.5, we use all sensors in the agreeing subset. Thus, the lower and upper bounds of the time dynamic term are:

$$X_l(s,t) = \min_{all\,n \in \tilde{\phi}} (\tilde{X}_t(n) - 2\tilde{\sigma}_X)$$

$$X_u(s,t) = \max_{all\,n \in \tilde{\phi}} (\tilde{X}_t(n) + 2\tilde{\sigma}_X)$$

And following from section 4.5, for the each sensor s at location l_s, we estimate the following:

$$\widetilde{\mu}(s) = \tilde{\mu}_1 + \tilde{\mu}_2 l_s$$

$$\widetilde{M}_t(s) = (\tilde{f}_1 + \tilde{f}_2 l_s)cos(\omega t) + (\tilde{g}_1 + \tilde{g}_2 l_s)sin(\omega t) + \tilde{h}_1 t$$

where $\omega = 2\pi$. Finally, the lower and upper bounds are:

$$Z_l(s,t) = \widetilde{\mu}(s) + \widetilde{M}_t(s) + X_l(s,t) - 2(\tilde{\sigma}_Y + \tilde{\sigma}_Z)$$

$$Z_u(s,t) = \widetilde{\mu}(s) + \widetilde{M}_t(s) + X_u(s,t) + 2(\tilde{\sigma}_Y + \tilde{\sigma}_Z)$$

With the bounds calculated, we then compare the data $Z_t(s)$ to see if it is within the bounds. If data is not within the bounds, they are tagged as being faulty.

Once all of the data is tagged, we can then update the prior distribution of the subsets for the next day's posterior calculation using the proportion of data for each sensor not tagged as being faulty. This is a slight alteration of the process in chapter 3 where the priors are updated using the previous iteration's subset posterior probabilities. Here, we changed it because using the actual results of how frequently a sensor is not tagged is a better indicator of a set's probability of agreeing.

The prior distribution update occurs as follows. Given the vector of data with the rates that each individual sensor has been tagged, τ, it is simple to calculate the percent of samples that are correct for each sensor: $\mathbf{1} - \tau$. We can normalize this into the probability that each sensor should be included in the agreeing subset:

$$\eta_i = \frac{1 - \tau_i}{\sum_{all\, j}(1 - \tau_j)}$$

To determine the next day's subset prior we simply apply these probabilities to each set and normalize them:

$$P(\phi) = \frac{\phi^T \eta}{\sum_{all\,\phi} \phi^T \eta}$$

5.3.3 Issues resolved

With the integration of HBST modeling with a MAP subset selection scheme, several problems with the schemes in chapters 3 and 4 are easily resolved. In the MAP selection method of chapter 3, there are several simplifications that can be made because these problems do not arise when HBST modeling is used. This is evident when comparing the system flow in figure 3.1 with the end-to-end system in figure 5.1.

The first issue of the MAP selection system was the selection of a window size over which to model the data. Since we now analyze data on a much larger time scale than the sensing intervals, for reasons explained in section 4.5, this issue no longer exists. We no longer need to test multiple sizes and hence this step is no longer necessary in our end-to-end system.

Similarly, following the selection of the agreeing subset in chapter 3, we introduced a lag before changing our agreeing subset in order to have some stability in decisions from sample to sample. However, since we are no longer working on the sensing interval time scale, a decision is made after data from an entire day is evaluated. Because of this, decision instability is not an issue anymore, and the hysteresis step for the subset decision can and should be removed.

Also, since the phenomenon was assumed to behave smoothly in space in chapter 3, we first removed the bias associated with any linear model, effectively comparing only the slopes between sensors. However, since we now use HBST

modeling, the bias and other behaviors are all included in the model. Thus, the offset bias removal step of figure 3.1 can be removed.

By using a MAP subset selection in conjunction with HBST, we improve on a couple of issues with the system in chapter 4. Since we find a subset of agreeing sensors with which we base the expected phenomenon behavior, contrary to chapter 4, faulty sensors are never involved with any fault decisions.

Also, one of the main issues with the simple fault detection scheme described in section 4.5 is that edge sensors see significantly higher false detection rates. This is due to the fact that only one sensor defines the bounds for an edge sensor instead of two. However, now that we have a whole subset of sensors that are trusted, there are multiple sensors defining the bounds, reducing the false detection significantly. Note though, for cases where an edge sensor is not in the agreeing subset, this sensor still may have slightly higher false detection than the other sensors just because it is on the edge.

If one were to consider two and three dimensional sensor deployments, the fraction of nodes which are on the edge increases. Thus, use of a system as proposed here that employs a larger subset of the sensors to judge the edge sensors becomes even more important.

5.4 Results

To show the gains that we get from having an end-to-end Bayesian system, we apply our method to the same three datasets presented in chapter 4. Since we have already shown that HBST is superior to linear modeling in section 4.6, we only compare the end-to-end Bayesian system with the HBST modeling fault detection system results.

5.4.1 Simulated Data

The first data set is the same set of simulated data as in section 4.6 figure 4.2. We use simulated data to test the system under ideal and well defined conditions. Data from six sensors over three days exhibit a site specific mean, diurnal harmonics, a long term trend, and an additional unmodeled harmonic. Table 5.1 summarizes the results when there are no faults.

Table 5.1: False detection rates for simulated data with no faults

	End-to-end	**HBST**
Overall	0	0.2079
Excluding Edge Nodes	0	0.0014
Just Edge Nodes	0	0.6210

The end-to-end Bayesian system makes no errors in false detections. In each of the days, the agreeing subset consisted of the four middle nodes while neither edge sensor ever was in the agreeing subset. This is expected behavior because edge nodes agree the least with rest of the sensors. Even though these nodes were not in the agreeing set, there is still a lack of any false detection with these nodes indicating that the added sensors in the decision helped reduce the false detection rates.

We next compare the the performance of our method when there are faults included in the data. We use the data depicted in figure 4.3 where two types of faults have been injected. As in section 4.6, the faults were tested independently of each other. After applying the end-to-end Bayesian system to this data, we obtain results that are summarized in figure 5.2.

The detection success rate for the two detection systems is the same for both fault types indicating that we have not lost any detection capabilities using the end-to-end Bayesian system. At the same time, the false detection rate has

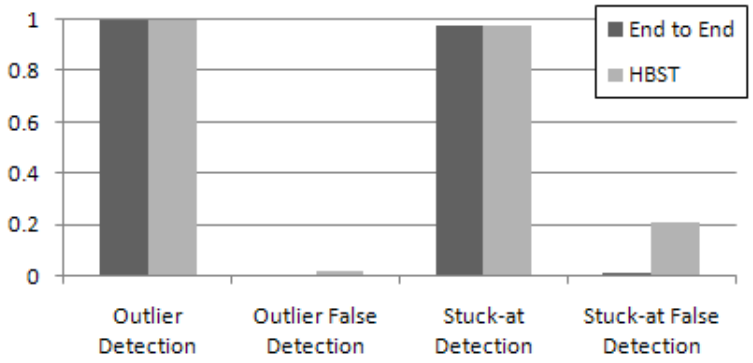

Figure 5.2: Fault detection rates for simulated data with injected faults

significantly dropped. There were no false detections in the case of the outlier, and the stuck-at fault case saw a 96.3% reduction in the false detection rate. Also, we note that when there were faults, the selection of the best agreeing subset always excluded the sensors containing the fault. These results show that the end-to-end Bayesian system is capable of detecting faults with a very low false detection rate.

5.4.2 Cold Air Drainage Data

Now, we examine the application of the end-to-end Bayesian system to real data. The results for the cold air drainage data depicted in figure 4.5 where no faults are present are summarized in figure 5.3 .

We see that there is a significant difference in the overall false detection rate over the course of the five days. The end-to-end Bayesian system reduces the false detection rate from 25.2% for the HBST modeling system down to 1.8%. This is a 92.9% decrease.

Looking further, dropping the edge nodes from consideration to get the HBST modeling system's best overall performance, the HBST still has a 11.0% overall

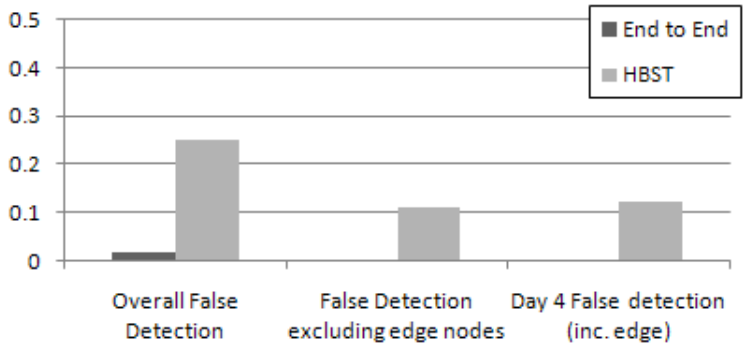

Figure 5.3: Fault detection rates for cold air drainage data with no faults

false detection rate. Alternatively, when we disregard the edge nodes the end-to-end Bayesian system has no false detection over the course of five days. Also, in days 4 and 5 an edge node was included in the agreeing subset. This resulted in no false detection for the included edge node and no increase in false detection for any middle node.

Examining the results for just day 4 where the HBST modeling system performs its best, we see that the end-to-end Bayesian system performance gives a 99.0% decrease in false detection rate. The end-to-end Bayesian system drops the false detection from 11.9% down to 0.1%.

The results for this non-faulty cold air drainage data show that the end-to-end Bayesian system is very capable of reducing false detection, even when there are many unmodeled dynamics such as sunflecks as discussed in section 4.6.2. Through the use of more sensors in developing a model of expected behavior, these unmodeled dynamics end up being averaged out leading to lower false detection rates. If the goal is to detect such phenomena, then increasing the spatial sampling density is required to detect these small scale dynamics.

To ensure that this false detection reduction does not come at the expense

of a decrease in detection rate, we apply the end-to-end Bayesian system to the two faults depicted in figure 4.7. The fault in figure 4.7(a) shows one sensor with high noise that is not tracking the data. The fault in figure 4.7(b) has two outliers occurring simultaneously in two sensors. The results for this data are summarized in figure 5.4.

Figure 5.4: Fault detection rates for cold air drainage data with faults

We see that both systems are very capable of detecting the faults. In both cases, the outliers from sensors 5 and 6 were detected perfectly even though they occurred at the same time, but the end-to-end Bayesian system had no false detections while the HBST modeling system had a false detection rate of 1.5%.

When examining the data with the noisy sensor, we see that both the end-to-end Bayesian system and the HBST modeling system were able to detect the faulty sensor very well. The end-to-end Bayesian system was slightly better at detection with 96.5% detection versus 95.8% detection with the HBST modeling system.

However, the biggest improvement was in the reduction of false detections in the presence of the noisy data of figure 4.7(a). The end-to-end Bayesian system improved on the HBST modeling system performance by 88.7%, reducing the false

detection rate down to 2.3%. Note that all of the false detection for the end-to-end system was in sensor 1, with an individual rate of 11.6% false detection. This is expected because it is an edge sensor and since sensor 2 is faulty, the closest sensor in the agreeing subset is sensor 3. This is much improved in comparison to the HBST modeling system result. For the HBST modeling system, most (but not all) of the false detection was also in sensor 1, but the rate of false detection in this individual sensor was 97.9%. This is due to the fact that the only sensor involved in judging sensor 1 is the faulty sensor 2 in the HBST modeling system.

The results of the application of the end-to-end Bayesian system to the cold air drainage, both non-faulty and faulty, indicate that this approach can be an effective way of determining sensor network data faults. This system is capable of effectively detecting data faults while maintaining low false detection rates.

5.4.3 Lake Fulmor Data

We now apply the end-to-end Bayesian system to the data from five nodes deployed across a lake presented in section 4.6.3 figure 4.9. The results of this are presented in figure 5.5.

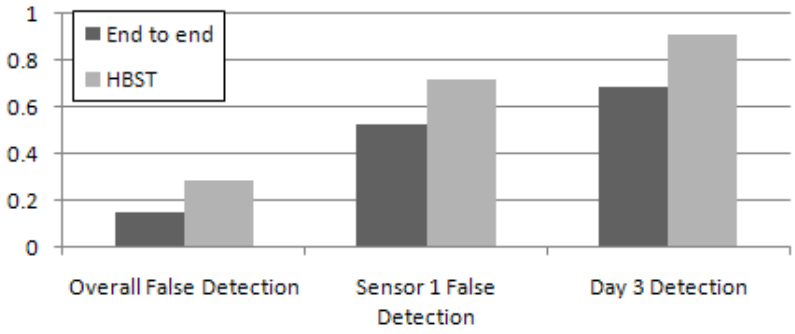

Figure 5.5: Detection rates for Lake Fulmor Data

The end-to-end Bayesian system has decreased the overall false detection in comparison to the HBST modeling system. The higher overall false detection in HBST modeling is also linked to the higher detection rate, partially explaining the degraded detection performance. Also, we note that the false detection rate for sensor 1 is very high for both end-to-end Bayesian and HBST modeling systems.

Closer examination of the data reveals that the temperatures do not behave in a consistent clear spatially linear trend. To illustrate this point, figure 5.6 shows sensors 1 and 4 from the original data dataset used in section 4.6.3. Sensor 1 clearly goes between being approximately $\frac{2}{3}^{\circ}$C warmer than sensor 4 to the same or even $\frac{1}{2}^{\circ}$C cooler than sensor 4.

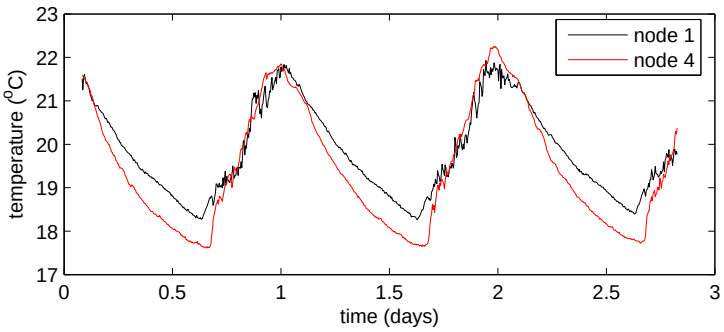

Figure 5.6: Data from two nodes in the Lake Fulmor data showing a inconsistent spatial trend

This behavior suggests that the phenomenon is incorrectly modeled. The linear spatial trend in the data is inconsistent, so it may be more useful to consider a higher order model for this data. However, the type and form of this model is unclear and not easily determined from the given data because of the low deployment density. This suggests the need for a second experiment with higher deployment densities to better derive a spatial model of the phenomenon. The main effect of this inaccurate spatial model is an increase in false detection

coupled with a decrease in detection.

Sensor 1 is the most egregious of sensors causing the data to exhibit this non-linear behavior. If we reapply the end-to-end Bayesian system to the data disregarding sensor 1 we get significantly different results. With just sensors 2 through 4, the detection rate of the fault rises from 68.6% to 71.4%. The false detections for all sensors have all dropped to zero. The increase in detection and decrease in false detection indicates that the four sensors behave in a much more spatially linear manner.

The results of the application of the end-to-end Bayesian system to the Lake Fulmor data give mixed results. While overall fault detection rates dropped even in comparison to the HBST modeling system, this also resulted in a drop in detection rate.

These results also emphasize that a higher deployment density is required to accurately model a phenomenon that has high variability. The relatively low deployment density was sufficient to model the temperature field for cold air drainage experiment in section 5.4.2 due to the low spatial variability. Meanwhile, the deployment density for the Lake Fulmor experiment was not high enough to capture the higher spatial variability of the phenomenon.

5.4.4 Effect of Prior Distribution

To show the effect of having the prior distribution updated by the final tagged proportion, we also tested the Lake Fulmor data without the prior distribution updating that was described in section 5.3.2. Table 5.2 show the sensors included in the agreeing subset when we exclude and include the use of the calculated prior distribution updates.

Examination of the results show that on the third day, sensor 1 is included

Table 5.2: Sensors included in the agreeing subset with and without prior distributions being used.

Day	No Priors	Using Priors
1	2,4,5	2,4,5
2	2,3,4	2,3,4
3	1,4,5	2,4,5

in the agreeing subset. This is the sensor that does not follow the linear spatial trend. This sensor also exhibited a 75.7% tag rate on day 2 which is very high and suggests that this sensor should not be in an agreeing subset. Additionally, when we excluded the use of prior distributions, the detection rate of the fault in day three drops to 22.9%.

These results show that the inclusion and updating of prior distributions in the manner presented in section 5.3.2 is effective and crucial to the success of our algorithm. It ensures the exclusion of faulty sensors from the agreeing subset, and because of this it improves the accuracy of the fault detection system.

5.5 Conclusion

We have shown the effectiveness of an end-to-end Bayesian modeling system using a MAP sensor subset selection combined with HBST modeling. By combining elements of the approaches in chapters 3 and 4, several issues hurting detection performance are resolved.

However, we also see that accurate modeling is still very important as evidenced in the Lake Fulmor data of section 5.4.3. In the future, we seek to include an update to the model definition in figure 5.1 and incorporate this into an iterative design for a sensor network deployment. This design update may include increasing deployment density to allow for better modeling of phenomena with

high variability. In future work, one can further include Bayesian elements in this system by using Bayesian decisions in the selection of the models used in specific situations.

CHAPTER 6

Conclusion

We have presented a comprehensive look at the types of data faults facing sensor network users and developers. For sensor networks to be used in environmental monitoring, it is usually uncommon to have a thorough in-depth validation phase, and the equipment used is not robust against environmental factors that can cause sensor failures. Thus, having an understanding of what types of faults can occur and why they occur is important in detecting and diagnosing sensor problems.

While the methods we have presented to detect these data faults are effective in many cases, these methods still require heavy human involvement. The sensor networks currently in use generally are not deployed in high density or redundancy. As such, accurate models of the system and phenomenon are vitally important to the success of a fault detection system in an under-deployed network.

In cases where there is a lack of specific prior knowledge of the phenomenon, as in chapter 3, loose assumptions can be made, and a general modeling method such as linear autoregressive modeling is a practical technique to use. Regardless of what underlying modeling technique is used, the lack of a well crafted model limits the performance of a fault detection system. In such cases, human oversight may be necessary throughout the deployment to ensure the overall accuracy of the results and to adjust parameters in the model such as window size.

But when more prior information is available, maximizing its use will improve the accuracy of a fault detection system significantly. For example, the HBST modeling techniques used in chapters 4 and 5 assumes the phenomenon has behaviors such as diurnal patterns and spatial trends. This information proves to help in greatly increasing fault detection performance. However, since HBST modeling is a less generic tool than linear AR modeling, it cannot be utilized in every situation without tuning, as seen in the case for the Lake Fulmor data in chapter 5. The definition and tuning of the models must be done by a human prior to the deployment of a sensor network. While the constant human oversight required in the general modeling case is reduced, it cannot be eliminated since model updates may still be necessary for changing environmental conditions.

The lack of an extensive and involved validation procedure will always mean some level of human monitoring of the sensor network is necessary. And, as sensor networks evolve, there will be newer phenomena to measure that require modeling which also requires human expertise. A goal of a general fault detection system in this context should not to be completely exclude human involvement, rather it should be to minimize the involvement at steady state (during deployment) and concentrating human interaction into ensuring an accurate model definition, as we have done here.

6.1 Future Work

The inescapable need for human involvement suggests that we should develop iterative experiments and update sensor network deployments. With each experiment, new fault modes may be exposed, and models may be updated to reflect this. Further, phenomenon models can also be tuned for each experiment. Hence, we will seek to add a model analysis and update phase in between deployments

or in the system flow in figure 5.1.

There are also several additional issues that have not been resolved in our end-to-end Bayesian data fault detection system and are reserved as directions for the future. The first issue is that the selection of the best agreeing subset requires an enumeration of all possible subsets of a given size. However, this can be time consuming, costly, and possibly infeasible if the number of nodes involved increases significantly. While we avoid this problem by breaking down a large set of sensors into smaller more related groupings to consider, it may be necessary at one point to consider all sensors in a large deployment.

To resolve this, one could consider searching for a good subset of sensors instead of the absolute best subset of agreeing sensors. In this case, a costly search over each possible subset can be avoided in favor of a search until a subset that is good enough is found. However, this raises several new questions. How does one define what is good enough in a systematic manner? What kind of criterion or metric should be used to measure how good a set is? When searching among subsets, how does one determine whether or not the subset selected is a local maximum while there are other significantly better choices? Both of these suggest the use of selection heuristics such as a greedy algorithm, which leads to the question of the selection and effectiveness of the type of heuristic used.

Related to this issue of the selection of the best subset versus a good subset is the flexibility of set size. By restricting the size of the subset to a simple majority, there are likely to be several other good sensors that are left out of the modeling of expected behavior. Thus, we are discarding possibly useful information when modeling. To avoid this, flexibility in the subset size to allow for larger subsets should be considered. However, this increases the number of subsets of to consider significantly.

A possible solution to this is to have a promotion and demotion algorithm to add and subtract sensors from the agreeing subset. When a sensor is exhibiting questionable behavior, it is demoted from this good subset. However, if a sensor is behaving better, it can be added to the agreeing subset. This allows for a flexible, self-updating, computationally inexpensive way of adding and subtracting sensors in an agreeing subset. There are problems with this approach though. Depending on the false detection rate, how much faulty behavior is enough to remove it from the good subset? One may also envision the case where slowly many faulty sensors take over the agreeing subset while good sensors are slowly demoted out of the subset.

Also, as noted in chapter 2, faulty data may still provide usable information. Additionally, when sensors are excluded from an agreeing subset due to transient faults, they still have useful information. The incorporation of this data can be used to improve modeling and the performance of a fault detection system.

Finally, the contributions of this thesis can be utilized in a modular fault detection system that can be adapted to any sensing application. The goal of this overriding modular scheme is to be able to simply plug in parameter adjusted tools and analysis modules as required given the type of phenomenon being measured and the type of sensor being used. We have provided several underlying foundations upon which to build this system. For example, the HBST modeling module has already been applied to two different deployments. We have also provided a method for selecting a subset of agreeing sensors that has been paired with two different modeling approaches. The fault taxonomy presented here lays the groundwork for a fault diagnosis module. Such a modular fault detection system will ideally be effective, flexible, and easy to use for any situation.

Furthermore, in a modular fault detection system it is necessary to develop

diagnostic tools to judge the performance of each component. If the overall fault detection system is consistently giving incorrect results then it is important to quickly and easily determine the module or component that is failing. For example, predictive posterior checks and other techniques can be used to ensure model accuracy in the HBST model [SS03] [SS05].

References

[BBM03] J.-L. Bertrand-Krajewski, J.-P. Bardin, M. Mourad, and Y. Branger. "Accounting for sensor calibration, concentration heterogeneity, measurement and sampling uncertainties in monitoring urban drainage systems." *Water Science & Technology*, **47**(2):95–102, 2003.

[BGH05] Phil Buonadonna, David Gay, Joseph M. Hellerstein, Wei Hong, and Samuel Madden. "TASK: Sensor Network in a Box." Technical Report IRB-TR-04-021, Intel Research Berkeley, January 2005.

[BL04] Sonja Buchegger and Jean-Yves Le Boudec. "A robust reputation system for P2P and Mobile Ad-Hoc Networks." In *Proceedings of P2PEcon 2004*, Harvard University, Cambridge, MA, June 2004.

[BME03] Vladimir Bychkovskiy, Seapahn Megerian, Deborah Estrin, and Miodrag Potkonjak. "A Collaborative Approach to In-Place Sensor Calibration." In *Proceedings of the 2nd International Workshop on Information Processing in Sensor Networks (IPSN '03)*, Palo Alto, CA, USA, April 2003.

[BN07] Laura Balzano and Robert Nowak. "Blind Calibration in Sensor Networks." In *Information Processing in Sensor Networks (IPSN)*, April 2007.

[CAD07] CAD. "Cold Air Drainage.", 2006–2007. Data sets available: *http://sensorbase.org*.

[CES04] David Culler, Deborah Estrin, and Mani Srivastava. "Guest Editors' Introduction: Overview of Sensor Networks." *Computer*, **37**(8):41–49, August 2004.

[CKS06] Jinran Chen, Shubha Kher, and Arun Somani. "Distributed Fault Detection of Wireless Sensor Networks." In *Workshop on Dependability Issues in Wireless Ad-hoc Networks and Sensor Networks (DIWANS)*, September 2006.

[Cre93] Noel A. C. Cressie. *Statistics for Spatial Data*. Wiley-Interscience, 1993.

[CSR04] Thomas Clouqueur, Kewal K. Saluja, and Parameswaran Ramanathan. "Fault tolerance in collaborative sensor networks for target detection." *IEEE Transactions on Computers*, **53**(3):320–333, March 2004.

[CT91] Thomas M. Cover and Joy A. Thomas. *Elements of Information Theory*. Wiley-Interscience, 1991.

[CYH07] Gong Chen, Nathan Yau, Mark Hansen, and Deborah Estrin. "Sharing Sensor Network Data." Technical Report 71, CENS, March 2007.

[DGM04] Amol Deshpande, Carlos Guestrin, Samuel R. Madden, Joseph M. Hellerstein, and Wei Hong. "Model-Driven Data Acquisition in Sensor Networks." In *Proc. of Very Large Databases*, 2004.

[DPK04] A. Durresi, V. Paruchuri, R. Kannan, and S.S. Iyengar. "A lightweight protocol for data integrity in sensor networks." In *Intelligent Sensors, Sensor Networks and Information Processing Conference, 2004.*, pp. 73–77, Dec. 2004.

[EGP01] D. Estrin, L. Girod, G. Pottie, and M. Srivastava. "Instrumenting the world with wireless sensor networks." In *Proc. International Conference on Acoustics, Speech, and Signal Processing (ICASSP 2001)*, June 2001.

[EN03] Eiman Elnahrawy and Badri Nath. "Cleaning and querying noisy sensors." In *Proc. of International Workshop on Wireless Sensor Networks and Applications (WSNA)*, 2003.

[EN04] Eiman Elnahrawy and Badri Nath. "Context aware sensors." In *Proc. of the First European Workshop on Wireless Sensor Networks (EWSN 2004)*, January 2004.

[Fis83] Michael J. Fischer. "The Consensus Problem in Unreliable Distributed Systems (A Brief Survey)." In *Fundamentals of Computation Theory*, pp. 127–140, 1983.

[GBT07] Jayant Gupchup, Randal Burns, Andreas Terzis, and Alex Szalay. "Model-Based Event Detection in Wireless Sensor Networks." In *Proc. of Workshop on Data Sharing and Interoperability on the World-Wide Sensor Web (DSI)*, 2007.

[GCS04] Andrew Gelman, Jon B. Carlin, Hal S. Stern, and Donald B. Rubin. *Bayesian Data Analysis*. Chapman & Hall/CRC, second edition, 2004.

[GS04] Saurabh Ganeriwal and Mani B. Srivastava. "Reputation-based Framework for High Integrity Sensor Networks." In *ACM workshop on Security in Ad-hoc & Sensor Networks (SASN) 2004*, October 2004.

[HA04] Victoria Hodge and Jim Austin. "A Survey of Outlier Detection Methodologies." *Artificial Intelligence Review*, **22**(2):85–12, 2004.

[Hec95] David Heckerman. "A Tutorial on Learning with Bayesian Networks." Technical Report MSR-TR-95-06, Microsoft Research, March 1995.

[Int04] Intel. "Intel Lab at Berkeley data set, nodes 2 and 35.", 2004. Data set available: *http://berkeley.intelresearch.net/labdata/*.

[Ise05] Rolf Isermann. *Fault-Diagnosis Systems: An Introduction from Fault Detection to Fault Tolerance*. Springer, 2005.

[JAF06] Shawn R. Jeffery, Gustavo Alonso, Michael J. Franklin, Wei Hong, and Jennifer Widom. "Declarative Support for Sensor Data Cleaning." In *4th International Conference on Pervasive Computing*, 2006.

[KGG06] Andreas Krause, Carlos Guestrin, Anupam Gupta, and Jon Kleinberg. "Near-optimal Sensor Placements: Maximizing Information while Minimizing Communication Cost." In *Fifth International Conference on Information Processing in Sensor Networks (IPSN'06)*, April 2006.

[KI04] Bhaskar Krishnamachari and Sitharama Iyengar. "Distributed Bayesian Algorithms for Fault-Tolerant Event Region Detection in Wireless Sensor Networks." *IEEE Transactions on Computers*, **53**(3):241–250, March 2004.

[KPS03a] William J. Kaiser, Gregory J. Pottie, Mani Srivastava, Gaurav S. Sukhatme, John Villasenor, and Deborah Estrin. "Networked Infomechanical Systems (NIMS) for Ambient Intelligence." Technical Report 31, CENS, December 2003.

[KPS03b] Farinaz Koushanfar, Miodrag Potkonjak, and Alberto Sangiovanni-Vincentelli. "On-line Fault Detection of Sensor Measurements." In *Proc. of IEEE Sensors*, 2003.

[Lau05] Alan J. Laub. *Matrix Analysis for Scientists & Engineers*. Society for Industrial and Applied Mathematics, 2005.

[Mar90] Keith Marzullo. "Tolerating failures of continuous-valued sensors." *ACM Transactions on Computer Systems*, **8**(4):284–304, 1990.

[MB02] M. Mourad and J.-L. Bertrand-Krajewski. "A method for automatic validation of long time series of data in urban hydrology." *Water Science & Technology*, **45**(4–5):263–270, 2002.

[ML05] Joechen Mundinger and Jean-Yves Le Boudec. "Analysis of a Robust Reputation System for Self-Organized Networks." *European Transactions on Communication*, **16**(5):375–384, 2005.

[MPD04] Shoubhik Mukhopadhyay, Debashis Panigrahi, and Sujit Dey. "Model Based Error Correction for Wireless Sensor Networks." In *Proc. Sensor and Ad Hoc Communications and Networks SECON 2004.*, pp. 575–584, Oct 2004.

[MW95] Robert N. McDonough and Anthony D. Whalen. *Detection of Signals in Noise*. Academic Press, 1995.

[NAM06] NAMOS. "NAMOS: Networked Aquatic Microbial Observing System.", 2006. Data set available: *http://www-robotics.usc.edu/ namos/*.

[NIM07] NIMS. "NIMS: Networked Infomechanical Systems.", 2007. Data set available: *http://sensorbase.org*.

[NP07] Kevin Ni and Greg Pottie. "Bayesian Selection of Non-Faulty Sensors." In *IEEE International Symposium on Information Theory*, June 2007.

[NRC08] Kevin Ni, Nithya Ramanathan, Mohamed Nabil Hajj Chehade, Laura Balzano, Sheela Nair, Sadaf Zahedi, Greg Pottie, Mark Hansen, and Mani Srivastava. "Sensor Network Data Fault Types." *ACM Transactions on Sensor Networks*, accepted for publication 2008.

[PIK91] Lakshman Prasad, S. Sitharama Iyengar, R. L. Kashyap, and Rabinder N. Madan. "Functional Characterization of Fault Tolerant Integration in Distributed Sensor Networks." *IEEE Transactions on Systems, Man, and Cybernetics*, **21**(5):1082–1087, Sept./Oct. 1991.

[PIR94] L. Prasad, S. S. Iyengar, R. L. Rao, and R. L. Kashyap. "Fault-tolerant sensor integration using multiresolution decomposition." *Physical Review E*, **49**(4):3452–3461, April 1994.

[PK00] G. J. Pottie and W. J. Kaiser. "Wireless Integrated Network Sensors." *Communications of the ACM*, **43**(5):51–58, May 2000.

[RBB06] Nithya Ramanathan, Laura Balzano, Marci Burt, Deborah Estrin, Tom Harmon, Charlie Harvey, Jenny Jay, Eddie Kohler, Sarah Rothenberg, and Mani Srivastava. "Rapid Deployment with Confidence: Calibration and Fault Detection in Environmental Sensor Networks." Technical Report 62, CENS, April 2006.

[Rog04] Galina Rogova. "Reliability in Information Fusion: Literature Survey." In *7th International Conference on Information Fusion*, 2004.

[RSE06] Nithya Ramanathan, Tom Schoellhammer, Deborah Estrin, Mark Hansen, Tom Harmon, Eddie Kohler, and Mani Srivastava. "The Final Frontier: Embedding Networked Sensors in the Soil." Technical Report 68, CENS, November 2006.

[RSS98] J. Ross, M. Sulev, and P. Saarelaid. "Statistical treatment of the PAR variability and its application to willow coppice." *Agricultural and Forest Meteorology*, **91**(1-2):1–21, 1998.

[Run06] Chris C. Rundle. "A Beginner's Guide to Ion-Selective Electrode Measurements.", 2006.

[RZF00] Paul Resnick, Richard Zechauser, Eric Friedman, and Ko Kuwabara. "Reputation Systems." *Communications of the ACM*, **43**(12):45–48, 2000.

[SGG07] Abhishek Sharma, Leana Golubchik, and Ramesh Govindan. "On the Prevalence of Sensor Faults in Real-World Deployments." In *IEEE Communications Society Conference on Sensor, Mesh and Ad Hoc Communications and Networks (SECON)*, June 2007.

[SKR89] W.K. Smith, A. K. Knapp, and W. A. Reiners. "Penumbral effects on sunlight penetration in plant communities." *Ecology*, **70**(6):1603–1609, 1989.

[SLM07] Bo Sheng, Qun Li, Weizhen Mao, and Wen Jin. "Outlier Detection in Sensor Networks." In *Proc. of 8th ACM International Symposium on Mobile Ad Hoc Networking and Computing (MobiHoc)*, September 2007.

[SMP04] Robert Szewczyk, Alan Mainwaring, Joseph Polastre, John Anderson, and David Culler. "An Analysis of a Large Scale Habitat Monitoring Application." In *2nd International Conference on Embedded Networked Sensor Systems (SenSys)*, November 2004.

[SP04] Elaine Shi and Adrian Perrig. "Designing Secure Sensor Networks." *IEEE Wireless Communications Magazine*, **11**(6), December 2004.

[SPM04] Robert Szewczyk, Joseph Polastre, Alan Mainwaring, and David Culler. "Lessons From A Sensor Network Expedition." In *Proc. of the 1st European Workshop on Sensor Networks (EWSN)*, January 2004.

[SS03] Sandip Sinharay and Hal S. Stern. "Posterior predictive model checking in hierarchical models." *Journal of Statistical Planning and Inference*, **111**(1-2), February 2003.

[SS05] Hal S. Stern and Sandip Sinharay. "Bayesian Model Checking and Model Diagnostics." In Dipak Dey and C.R. Rao, editors, *Bayesian Thinking: Modeling and Computation, Handbook of Statistics Vol. 25*, pp. 171–192. Elsevier, 2005.

[TPS05] Gilman Tolle, Joseph Polastre, Robert Szewczyk, David Culler, Neil Turner, Kevin Tu, Stephen Burgess, Todd Dawson, Phil Buonadonna, David Gay, and Wei Hong. "A macroscope in the redwoods." In *Proc. 3rd international conference on Embedded networked sensor systems (SenSys '05)*, 2005.

[Vog04] Harald Vogt. "Integrity Preservation for Communication in Sensor Networks." Technical Report 434, ETH Zrich, Institute for Pervasive Computing, February 2004.

[WBC98] Christopher K. Wikle, L. Mark Berliner, and Noel Cressie. "Hierarchical Bayesian Space-Time Models." *Environmental and Ecological Statistics*, **5**(2):117–154, February 1998.

[WLJ06] Geoff Werner-Allen, Konrad Lorincz, Jeff Johnson, Jonathan Lees, and Matt Welsh. "Fidelity and Yield in a Volcano Monitoring Sensor Network." In *7th USENIX Symposium on Operating System Design and Implementation*, November 2006.